

AD-760 563

DUAL DIAMETER ROLLER BEARING - 3.5  
MILLION DN-600F

John Rumberger, et al

Franklin Institute Research Laboratories

Prepared for:

Air Force Aero Propulsion Laboratory

May 1973

DISTRIBUTED BY:

**NTIS**

National Technical Information Service  
U. S. DEPARTMENT OF COMMERCE  
5285 Port Royal Road, Springfield Va. 22151

AFAPL-TR-73-23

AD 760563

DUAL DIAMETER ROLLER  
BEARING - 3.5 MILLION DN-600°F

John Rumbarger  
Edmund Filetti  
James Dunfee  
David Gubernick

Franklin Institute Research Laboratory

TECHNICAL REPORT AFAPL-TR-73-23

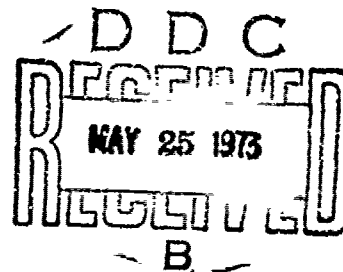
May 1973

Approved for public release:  
distribution unlimited

Reproduced by  
NATIONAL TECHNICAL  
INFORMATION SERVICE  
U.S. Department of Commerce  
Springfield VA 22151

Air Force Aero Propulsion Laboratory  
Air Force Systems Command  
Wright-Patterson Air Force Base, Ohio

Details of illustrations in  
this document may be better  
studied on microfiche



UNCLASSIFIED

Security Classification

## DOCUMENT CONTROL DATA - R &amp; D

Security classification of title, body of abstract and indexing annotation must be entered when the overall report is classified

1. ORIGINATING ACTIVITY (Corporate author) The Franklin Institute 20th & The Parkway Philadelphia, Pa. 19103		2a. REPORT SECURITY CLASSIFICATION UNCLASSIFIED	
		2b. GROUP N/A	
3. REPORT TITLE  DUAL DIAMETER ROLLER BEARING - 3.5 MILLION DN-600°F			
4. DESCRIPTIVE NOTES (Type of report and inclusive dates) Final Report, June 23, 1971 - December 31, 1972			
5. AUTHOR(S) (First name, middle initial, last name) John Rumberger                      Edmund Filetti James Dunfee                      David Gubernick			
6. REPORT DATE May 1973		7a. TOTAL NO OF PAGES 173	7b. NO OF REFS 11
8a. CONTRACT OR GRANT NO F-33615-71-C-1883 b. PROJECT NO 3048		9a. ORIGINATOR'S REPORT NUMBER(S)  F-C3132	
c. Task No. 304806 d.		9b. OTHER REPORT NO(S) (Any other numbers that may be assigned this report)  AFAPL-TR-73-23	
10. DISTRIBUTION STATEMENT  Approval for public release: distribution unlimited			
11. SUPPLEMENTARY NOTES Details of illustrations in this document may be better studied on microfiche		12. SPONSORING MILITARY ACTIVITY Air Force Aero Propulsion Laboratory Air Force Systems Command Wright-Patterson Air Force Base, Ohio	
13. ABSTRACT  Five gas turbine engine mainshaft roller bearing configurations were investigated for capability of sustained performance at DN values (Bore in mm x Speed in RPM) from 2 million to 3.5 million and normal operating temperatures to 600°F. A unique Dual Diameter Roller was selected for the final analysis of stress and lubrication parameters, design and fabrication. A 140 mm Bore Dual Diameter Roller Bearing operated successfully for 30 min. continuous operation at 25,000 RPM (3.5 million DN) with stabilized outer race temperatures above 525°F. Lubrication was with Polyphenyl Ether 5P4E in an air environment.			

UNCLASSIFIED

Security Classification

UNCLASSIFIED

Security Classification

KEY WORDS	LINK A		LINK B		LINK C	
	ROLE	WT	ROLE	WT	ROLE	WT
Elastohydrodynamic Lubrication						
Dual Diameter Roller						
Polyphenyl Ether						
MIL-L-7808						
3.5 Million DN						
600°F						

ib

DUAL DIAMETER ROLLER  
BEARING - 3.5 MILLION DN-600°F

John Rumbarger  
Edmund Filetti  
James Dunfee  
David Gubernick

Approved for public release:  
distribution unlimited

## FOREWORD

This report was prepared by the Franklin Institute Research Laboratories, 20th and Benjamin Franklin Parkway, Philadelphia, Pa. 19103 under USAF Contract F-33615-71-C-1883. The work was administered under the direction of the Air Force Aero Propulsion Laboratory, with Mr. John Jenkins and Mr. M. R. Chasman (AFAPL/SFL) acting as project engineers.

This report covers work conducted from 23 June 1971 - 31 December 1972.

The Franklin Institute Research Laboratories was prime contractor and performed all of the analysis and design. The prototype test bearings were manufactured by the Bower Bearing Div., Federal-Mogul Corp., Detroit, Mich. The prototype testing was accomplished by subcontractor Midwest Aero Industries Div., Pure Carbon Company, Saint Mary's, Pa. The testing was under the direction of Mr. Donald Moyer of MAIC.

Publication of this report does not constitute Air Force Approval of the report's findings or conclusions. It is published only for the exchange and stimulation of ideas.

HOWARD F. JONES, CHIEF  
Lubrication Branch  
Fuels and Lubrication Division

## ABSTRACT

Five gas turbine engine mainshaft roller bearing configurations were investigated for capability of sustained performance at DN values (Bore in mm x Speed in RPM) from 2 million to 3.5 million and normal operating temperatures to 600°F. A unique Dual Diameter Roller was selected for the final analysis of stress and lubrication parameters, design and fabrication. A 140 mm Bore Dual Diameter Roller Bearing operated successfully for 30 min. continuous operation at 25,000 RPM (3.5 million DN) with stabilized outer race temperatures above 525°F. Lubrication was with Polyphenyl Ether 5P4E in an air environment.

## CONTENTS

<i>Section</i>	<i>Title</i>	<i>Page</i>
I	INTRODUCTION. . . . .	1
II	SELECTION OF PRELIMINARY CONFIGURATION. . . . .	4
	1. Candidate Bearing Configurations. . . . .	4
	2. Load Life Parametric Study. . . . .	13
	3. Cage-Slip and Horsepower Loss Study . . . . .	17
	4. Series Hybrid Bearing . . . . .	21
	5. Selection of Dual Diameter Roller Bearing . . . . .	26
III	LUBRICANT SELECTION . . . . .	27
IV	DUAL DIAMETER BEARING ANALYSIS AND DESIGN . . . . .	32
	1. Design Considerations . . . . .	32
	2. Inner Race Stresses . . . . .	35
	3. Lubrication . . . . .	36
	4. Performance Analysis. . . . .	40
	5. EHD Parameters. . . . .	48
	6. Design Drawings . . . . .	48
V	DUAL DIAMETER BEARING FABRICATION . . . . .	57
VI	DUAL DIAMETER BEARING TESTS . . . . .	65
	1. Test Rig . . . . .	65
	2. MIL-L-7808, Test Bearing A1 . . . . .	69
	3. 5P4E, Test Bearing A1 . . . . .	69
	4. 5P4E, Test Bearing C3 . . . . .	82
VII	CONCLUSIONS . . . . .	87
	APPENDIX I - TEST LOGS. . . . .	88

CONTENTS (CONT'D.)

<i>Section</i>	<i>Title</i>	<i>Page</i>
	APPENDIX II - GAS TURBINE ENGINE MAINSHAFT ROLLER BEARING-SYSTEMS ANALYSIS . . . . .	111
VIII	REFERENCES . . . . .	175

## FIGURES

<i>Figure No.</i>	<i>Title</i>	<i>Page</i>
1(a)	Solid Rollers - Inner Land Riding Cage. . . . .	5
1(b)	Solid Rollers - Outer Land Riding Cage. . . . .	6
1(c)	Hollow Roller Concept . . . . .	7
1(d)	Series Hybrid Bearing . . . . .	9
2	Dual Diameter Roller Bearing Configuration. . . . .	10
3	Kinematics of Dual Diam. Roller . . . . .	11
4	Relative Kinematics of Two Diameter Roller. . . . .	12
5	Bearing Life vs. Roller Diam. (Hollow Rollers). . . . .	15
6	Bearing Life vs. Roller Diam. (Dual Diam. Rollers). . . . .	16
7	Cage Slip % vs. Radial Load . . . . .	20
8	Cage Speed in RPM vs. Radial Load . . . . .	22
9	HP Loss vs. Speed . . . . .	23
10	Friction Loss vs. Speed Ratio, MIL-L-7808 Oil . . . . .	25
11	Bearing Life with 5P4E Lubricant. . . . .	30
12	Inner Race Maximum Tangential Stress Vs. Shaft Speed . . . . .	34
13	Finite Element Analysis of Inner Race Tangential Stresses at $4.0 \times 10^6$ DN . . . . .	37
14	Thermal Nodes and Methods of Lubrication. . . . .	39
15	Effect of Oil Flow Upon Outlet Temperature and Bearing Power Loss. . . . .	42
16	Dual Diameter Roller Bearing Frictional Horsepower Losses . . . . .	46

## FIGURES

<i>Figure No.</i>	<i>Title</i>	<i>Page</i>
17	Two-Diameter Roller Bearing Assembly . . . . .	52
18	Inner Ring, Two Diameter Roller Bearing . . . . .	53
19	Outer Ring, Two Diameter Roller Bearing. . . . .	54
20	Two Diameter Roller. . . . .	55
21	Cage, Two Diameter Roller Bearing. . . . .	55
22	Dual Diameter Roller Bearing Assembly. . . . .	58
23	Bearing No. C3 Inner Race Circularity. . . . .	60
24	Bearing No. C3 Inner Raceway Contour . . . . .	61
25	Bearing No. C3 Outer Race Circularity. . . . .	62
26	Bearing No. C3 Outer Raceway Contour . . . . .	63
27	Typical Dual-Diameter Roller Crown Profile Traces. . . . .	64
28	Dual Diameter Roller Bearing Test Stand. . . . .	66
29	Dual Diameter Roller Bearing Instrumentation . . . . .	67
30	Cross Section of Dual Diameter Bearing Test. . . . .	68
31	Test Bearing No. 1, $\Delta T$ vs. Speed, MIL-L-7808 G . . . . .	71
32	Test Bearing No. 1, $\Delta T$ vs. Speed, Polyphenyl Ether, 5P4E . . . . .	74
33	Test Bearing No. 1, Inner Race Failure . . . . .	75
34	Test Bearing No. 1, Outer Race Cage Roller Assembly Failure. . . . .	76
35	Failed Rollers . . . . .	77
36	Test Bearing No. 1, Outer Ring Failure . . . . .	78

## FIGURES

<i>Figure No.</i>	<i>Title</i>	<i>Page</i>
37	Test Bearing No. 1 Cage Failure . . . . .	79
38	Test Bearing No. 2 $\Delta T$ vs. Speed, Polyphenyl Ether, 5P4E . . . . .	84
39	Second Dual Diameter Test Bearing . . . . .	85

# TABLES

<i>Table No.</i>	<i>Title</i>	<i>Page</i>
I	Bearing Operating Requirements . . . . .	2
II	Duty Cycle at $4.0 \times 10^6$ DN . . . . .	14
III	Schedule of Computer Runs. . . . .	18
IV	Summary of Computer Results. . . . .	19
V	Summary of Test Results. . . . .	28
VI	Properties of Test Lubricants. . . . .	29
VII	Lubricant Properties Used in the Analysis. . . . .	31
VIII	Properties of M-50 Hardened to RC-60 Per VASCO Technical Bulletin . . . . .	35
IX	Inner Race Tangential Stress (ksi) . . . . .	38
X	Effect of Oil Flow Rate on Bearing Performance . . . . .	41
XI	Oil Flow Rate vs. Speed (DN) . . . . .	41
XII	Summary of Performance Analysis Computer Runs. . . . .	43
XIII	Summary of Temperature Profiles for Dual Diameter Roller Bearing . . . . .	45
XIV	Summary of Cage Analysis . . . . .	47
XV	Traction Values - Outer Race Contact - Unloaded Rollers. . . . .	49
XVI	Traction Values - Outer Race Contact - Maximum Loaded Rollers . . . . .	50
XVII	Traction Values - Inner Race Contact - Maximum Loaded Rollers . . . . .	51
XVIII	Summary of Test Bearing Dimensional Tolerances . . . . .	59
XIX	Data Summary Sheet First Test Bearing - MIL-L-7808 Oil . . . . .	70

## TABLES

<i>Table No.</i>	<i>Title</i>	<i>Page</i>
XX	Data Summary Sheet First Test Bearing - Polyphenyl Ether 5P4E . . . . .	73
XXI	Thermal Analysis of First Test Bearing Conditions with 5P4E. . . . .	81
XXII	Data Summary Sheet, Second Test Bearing Polyphenyl Ether 5P4E . . . . .	83

## SECTION I

### INTRODUCTION

The objective of this research program was to develop a long life, high speed roller bearing design for future high performance turbine engines. The bearing must be capable of sustained performance at DN values from  $2.0 \times 10^6$  to above  $3.5 \times 10^6$  and normal operating temperatures to 600 F while maintaining the rotating shafts within the necessary tolerance for optimum compressor and turbine performance.

The trends in turbine engine technology are toward increased rotational speed, larger bearing diameters and increased bearing temperature. It is anticipated that bearing DN requirements (bearing bore mm x rpm) will grow from the current  $2 \times 10^6$  or less to greater than  $3.5 \times 10^6$  in the 1980's. Efforts to increase bearing DN capability are currently aimed at ball bearings. Approaches being investigated for ball bearings include hollow balls and compliant races. The roller bearing has received very little attention. Efforts which have focused on roller bearings indicate that variations in roller bearing geometry such as the dual diameter roller and hollow rollers, show promise for significant increases in bearing performance. Improved ball and roller bearing capability is required for future systems.

Known current roller bearing types were investigated in order to select a preliminary configuration for further development. The selection was based on the potential of each type to meet the capabilities shown in Table I. A bearing bore of 140 mm was selected for this preliminary configuration study.

The results of the preliminary configuration study resulted in the selection of the dual diameter roller bearing concept for further consideration. This selection was based upon lower cage speeds obtained in

the dual diameter bearing which result in significantly lower mechanical losses (viscous loss due to shearing of the oil). These lower drags or losses in turn result in a lower cage slip threshold.

Table I  
BEARING OPERATING REQUIREMENTS

Normal Operating Temperature	600°F
Operating Temperature Range	-65 to +800°F
Normal Operating DN (mm x rpm)	$4.0 \times 10^6$
Operating Radial Load Range (lb.)	0 to 2000
$L_{10}$ Life, Hr. (greater than)	1000
Radial Deflection at Max. Load, (in.)	0.010
Minimum Heat Generation	

The dual diameter roller bearing configuration was subjected to a thorough analysis from which a final design was developed. A complete systems analysis incorporating the latest available elastohydrodynamic lubrication technology and including fluid drag forces and thermal effects was accomplished by means of a digital computer program (Reference 1). This analysis was used to finalize the bearing design and determine operating clearances and oil flow or lubrication requirements of the bearing. Complete detailed working drawings of the prototype test bearings are contained in the body of this report.

Six prototype dual diameter roller bearings were manufactured by the Federal-Mogul Corporation, Bower Bearings Div., Detroit, Michigan, to the drawings and specifications contained in this report. A summary of inspection data relating to dimensional quality of the test bearings is also included.

Two dual diameter prototype roller bearings were tested by the Midwest Aero Industries Div., Pure Carbon Co., St. Mary's, Pa. on a special high speed mainshaft test rig. The test bearings were operated

initially with MIL-L-7808 lubricant at 250°F oil inlet and then later with Polyphenyl Ether 5P4E lubricant at 600°F.

## SECTION II

### SELECTION OF PRELIMINARY CONFIGURATION

#### 1. CANDIDATE BEARING CONFIGURATIONS

Five basic concepts or candidate bearing configurations, as shown on Figure 1(a-d), were investigated. The reasons for considering the various configurations are listed below:

- a. Solid rollers - inner land riding cage: The inner land riding cage solid roller concept, Figure 1a, is one of the most commonly used mainshaft roller bearing designs. This design consists of an inner race with two integral shoulders to guide the roller complement. The one piece fully machined cage has close clearance and rides on an oil film in contact with the lands on the inner race. The outer race is a sleeve construction which allows complete axial freedom of the inner race and roller complement. It is common in some designs to provide coolant flow through slots under the inner race since the inner race operating temperature is approximately 50°F hotter than the outer race operating temperature. An advantage of this type of cage construction is the fact that friction in the cage to land areas will help to drive the cage at synchronous or epicyclic speed.
- b. Solid roller - outer land riding cage: This outer land riding concept, Figure 1b, is very similar to the concept above; the main difference being that the integral guiding flanges and the cage to race land guidance are on the outer race. This bearing configuration is also common in modern jet engines. The advantage of this type of construction is better retention of oil at the outer race contact (due to centrifugal forces) under momentary oil starvation. Also some engine applications are more easily assembled with this type of roller guidance. It should be noted that in this configuration the friction in the cage to land surfaces is a dissipative effect which will tend to place a drag on the cage and add to the cage slipping tendency.
- c. Hollow roller concept: The roller bearing concept is shown in Figure 1c. This concept can be applied to either an inner land riding cage or an outer land riding cage configuration. Basically the use of a hollow roller reduces the outer race to roller loading. The centrifugal force on the outer race due to

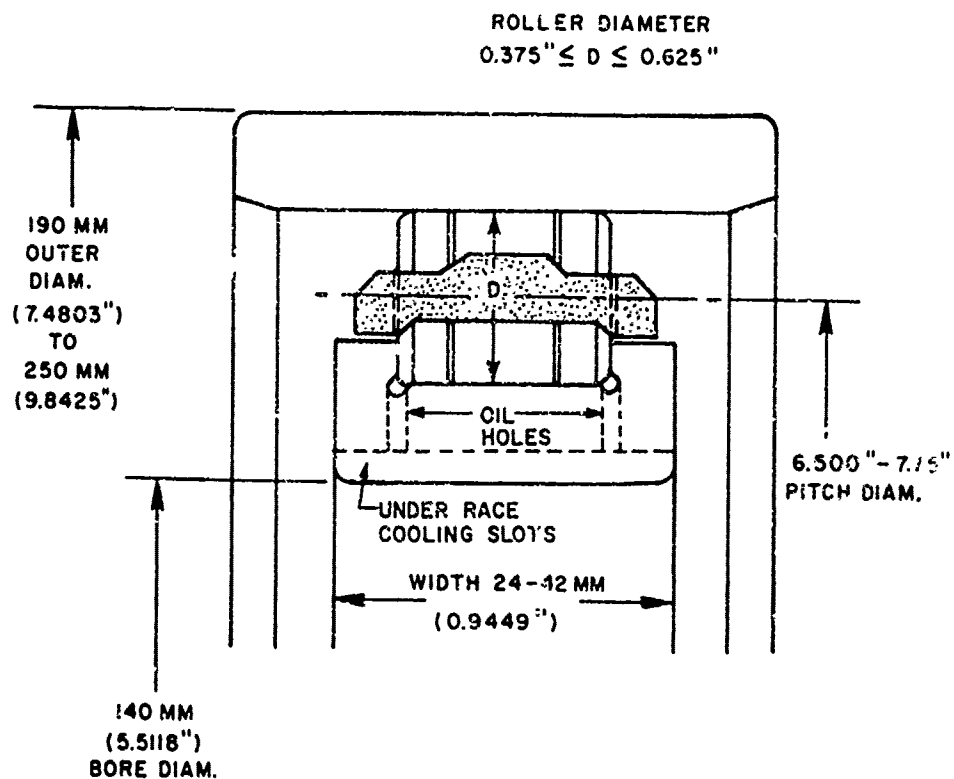


Figure 1(a). Solid Rollers - Inner Land Riding Cage

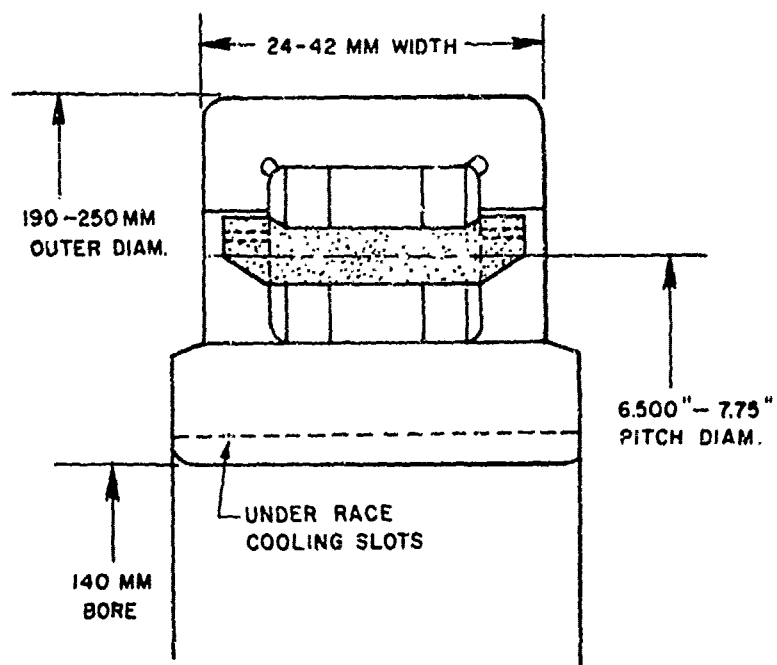
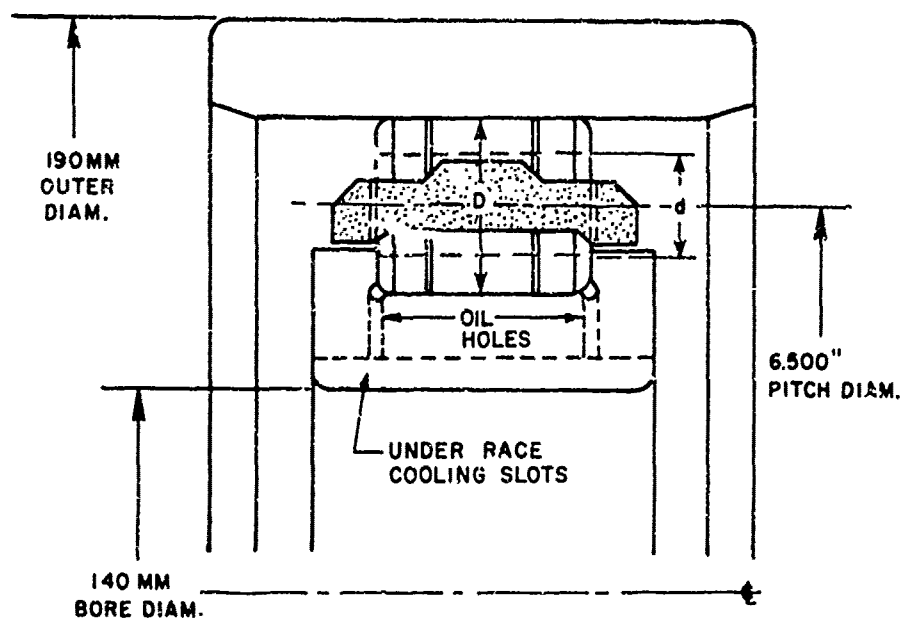


Figure 1(b). Solid Rollers - Outer Land Riding Cage



**HOLLOW ROLLER CONCEPT  
(Reduce Roll Mass)**

Figure 1(c). Hollow Roller Concept

the cage and roller complement rotative speed results in significant contact loading. Hollow rollers of less mass than solid rollers are found to be beneficial. A note of caution is indicated in that prior experience shows that too thin a wall section in the hollow rollers will lead to roller breakage due to reverse bending of the rings. Thus mass reduction must be compromised with ring bending fatigue properties. Attempts have been made in the past to use three or more oversized hollow rollers equally spaced in a solid roller complement to provide rollers which are always under load and essentially drives the cages up to cyclic speed. The effect which was analyzed in the preliminary selection of configurations was the mass reduction effect only.

- d. Series hybrid bearing: The series hybrid bearing is a relatively new concept, Figure 1d, for reducing the effective speed of rotation at the inner race of a mainshaft roller bearing. This concept consists of a rolling element bearing and an oil film journal bearing in series. The inner race of the roller bearing is separated from the outer surface of the rotating shaft by means of the hydrodynamic oil film bearing. Both bearings carry the full radial load, however, the inner race of the rolling bearing will rotate at some intermediate speed to the shaft speed resulting in a lower effective DN operating regime for the roller bearing. The speed reduction is the main advantage of this configuration. Additional under race cooling of the inner race can also be accomplished if locating oil film thrust bearing surfaces are built as pumps to supply additional coolant flow under the inner race. These locating thrust bearings to maintain the location of the inner race are not shown on Figure 1d. The main disadvantage is the obvious one of mechanical complexity.
- e. Dual diameter roller concept: The dual diameter roller concept is shown in Figure 2. This is basically a wagon wheel shaped roller with a large central diameter and two smaller diameters which look very much like an axle through the main wheel. The purpose of this configuration is to reduce cage operating speed. A reduction in cage orbital speed results in a significant reduction of the outer race to roller contact load due to centrifugal effects.

The relative kinematics of a conventional roller bearing and a dual diameter roller bearing are shown in Figure 3. The large outer diameter of the two-diameter roller contacts the inner race surface. The small roller diameters of the two-diameter roller contact the outer race surface. The effects of the relative kinematics are shown graphically in Figure 4. With a small roller (50% of the major roller diameter) it can



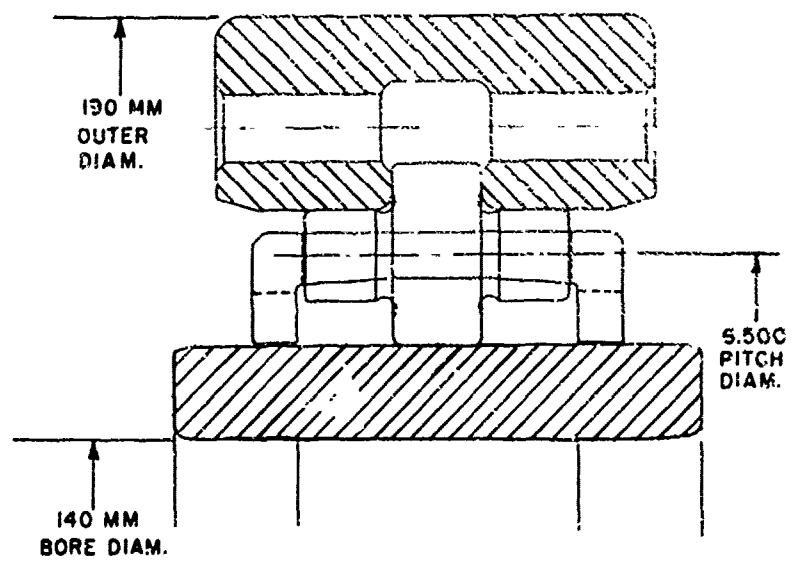


Figure 2. Dual Diameter Roller Bearing Configuration

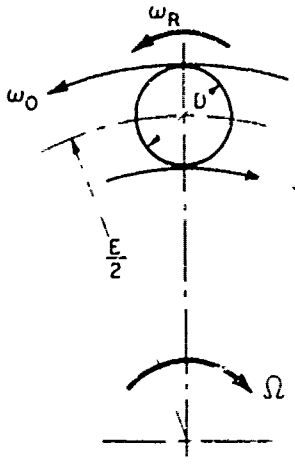
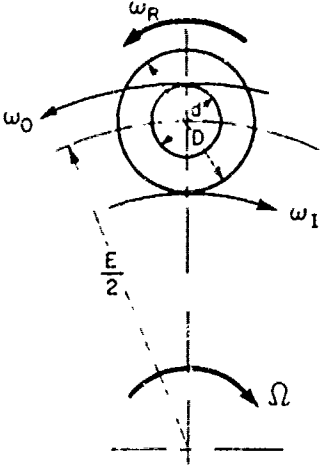
 <p style="text-align: center;">Solid Roller</p>	 <p style="text-align: center;">Two Diam. Roller</p>
$\gamma = D/E$	$\gamma' = d/E \quad \phi = d/D$
$\omega_o = \frac{\gamma \omega_R}{(1 + \gamma)}$	$\omega_o = \frac{\gamma' \omega_R}{(1 + \gamma')}$
$\omega_I = \frac{\gamma \omega_R}{(1 - \gamma)}$	$\omega_I = \frac{\gamma \omega_R}{(1 - \gamma)}$
$\Omega = \omega_o + \omega_I$	$\Omega = \omega_o + \omega_I$
$\epsilon_R = \frac{\Omega (1 - \gamma^2)}{2 (\gamma)}$	$\epsilon_R = \frac{\Omega (1 - \gamma) (1 + \phi \gamma)}{(1 + \phi) (\gamma)}$
$\epsilon_c = - \epsilon_o$	$\epsilon_c = - \epsilon_o$
$\epsilon_c = - \frac{\Omega}{2} (1 - \gamma)$	$\epsilon_c = - \frac{\phi (1 - \gamma)}{(1 + \phi)} \Omega$
Assumes Zero Slip	

Figure 3. Kinematics of Dual Diam. Roller

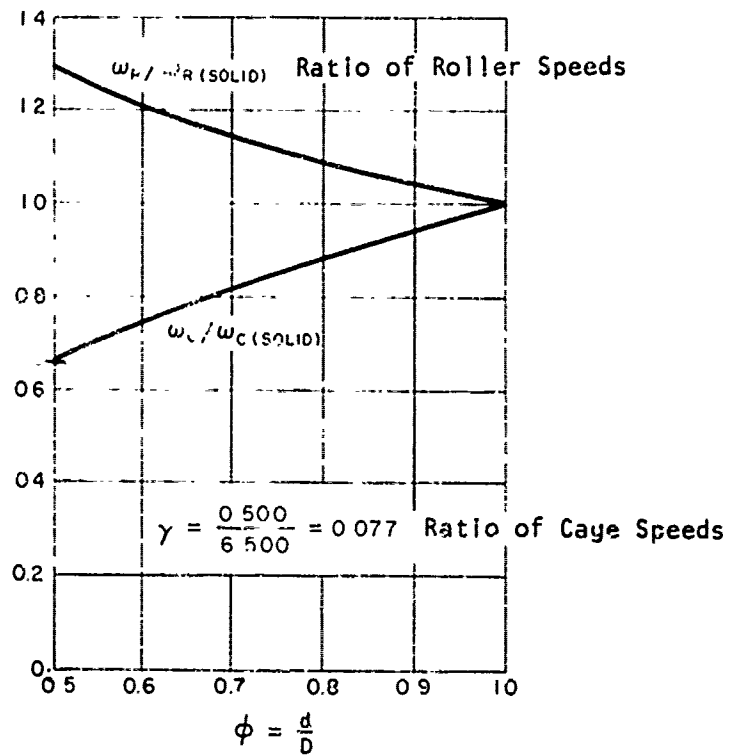


Figure 4. Relative Kinematics of Dual Diameter Roller

be seen that for the same inner race speed, a cage rotative speed  $1/3$  less than that of the conventional bearing can be achieved. At the same time the roller rotative speed about its own axis is about  $1/3$  greater in the dual diameter roller than in the conventional roller design. This increased roller rotative speed enhances the entrainment velocity which is important in the development of a full elastohydrodynamic oil film in the contacts. Higher entrainment velocities of the two-diameter roller will essentially result in thicker EHD oil films in the contact. Thus a  $4.0 \times 10^6$  DN bearing of the two-diameter roller configuration will result in cage rotative speeds and resulting centrifugal effects at the roller to outer race contact comparable to those found in a  $2.67 \times 10^6$  DN bearing of conventional design.

## 2. LOAD-LIFE PARAMETRIC STUDY

Initial calculations indicated that the requirements for greater than 1,000 hours L-10 operating life at  $4.0 \times 10^6$  DN could not be achieved with 2,000 lbs. radial load. The 2,000 lb. load is representative of momentary maneuvering loads and not intended as a long time operating load condition for design of mainshaft bearings. The duty cycle given in Table II was used for the parametric study.

A special short length computer program was used for the parametric study and consisted of a full load deflection analysis of the bearing with elastohydrodynamic films in the race roller contacts. The EHD film thicknesses were computed per the classical isothermal Dowson-Higginson formulas (Reference 2). This is a simplification in that no cage slip was considered. However, for the purposes of load life studies this is a valid assumption especially for preliminary configuration selection. The three radial loads identified in Table II were used to analyze the operating L-10 life and the results were prorated over the percentages of operating times (Reference 3). The figures presented are in terms of the prorated life over the duty cycle.

Table II  
DUTY CYCLE AT  $4.0 \times 10^6$  DN

<u>% Time</u>	<u>Radial Load</u>
10	2000 pounds
20	1000 pounds
70	500 pounds

The parametric studies were run with the following assumptions:

- Constant pitch diameter = 6.50 inches  $\approx E$
- Number of rollers =  $\pi$  times E divided by 1.5 times D
- Effective length of contact = roller diameter (D)
- $4 \times 10^6$  DN (28,740 shaft rpm at 140 mm bore)
- Dual diameter roller .8D outer length, .5D inner length

The L-10 prorated bearing life over the entire duty cycle in hours for the hollow roller concept is shown in Figure 5 where bearing life is plotted as a function of roller diameter. The bottom curve on Figure 5 represents a solid roller of the configurations described in Figure 1a and 1b. A similar plot of the L-10 prorated bearing life over the duty cycle for the dual diameter roller bearing is shown in Figure 6. An obvious knee in the curves is apparent for all of the roller concepts at a roller diameter of 0.5 inches. This can be explained in terms of the exponential reduction in life with increasing load. The larger diameter rollers have a higher outer race contact load because of increased centrifugal force and over 0.5 inch roller diameter this increase in centrifugal effects is greater than the corresponding increase in dynamic capacity of the roller race contact.

The results of the parametric study in terms of the design goal of more than 1,000 hours L-10 life are (a) roller diameter must be 0.5 inches or less for all configurations, (b) solid rollers are not acceptable in any diameter size, (c) hollow rollers should be 0.5 to 0.7 hollow, (d) dual diameter rollers with 0.5 to 0.6 small to large diameter roller ratio

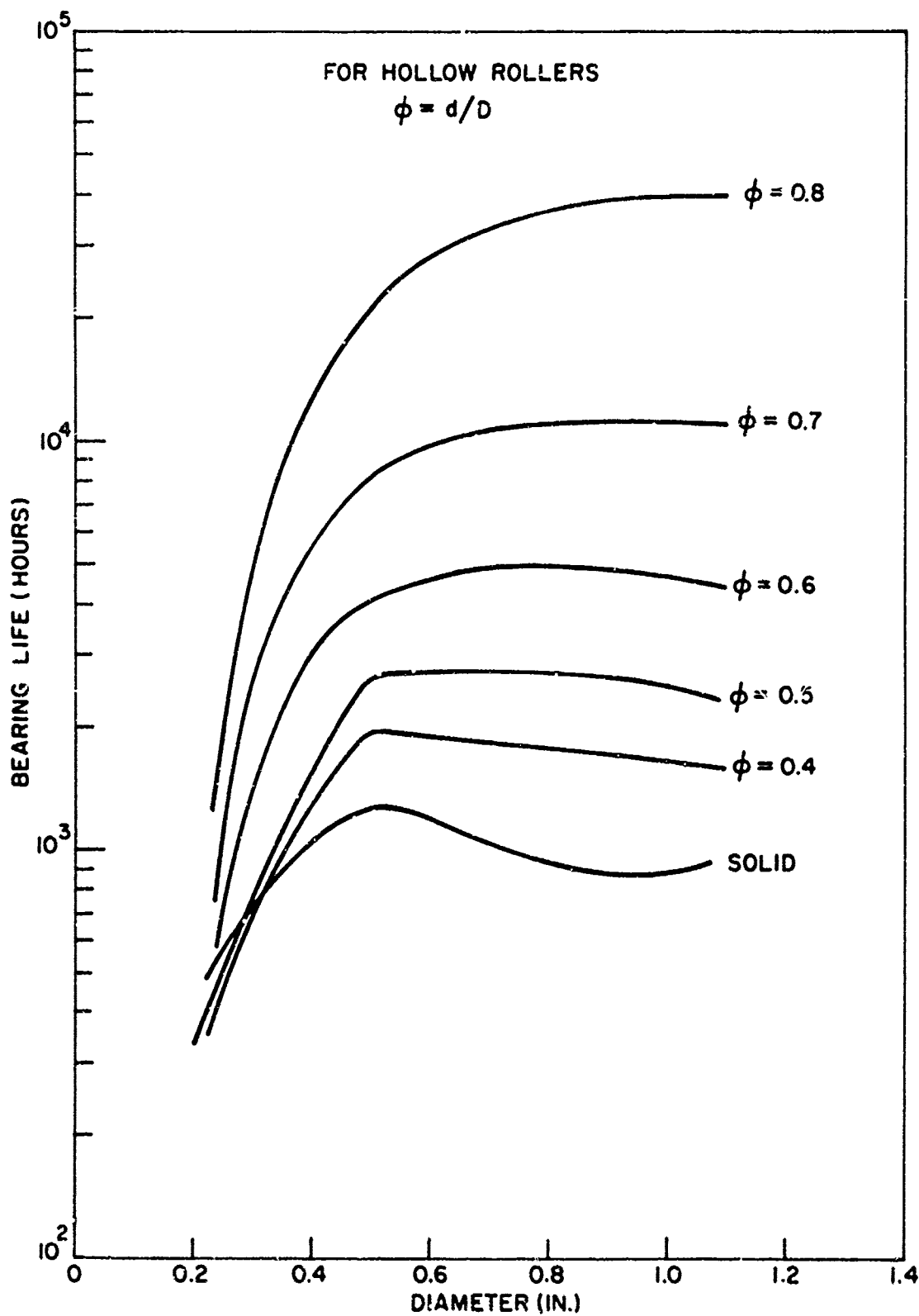


Figure 5. Bearing Life vs. Roller Diam. (Hollow Rollers)

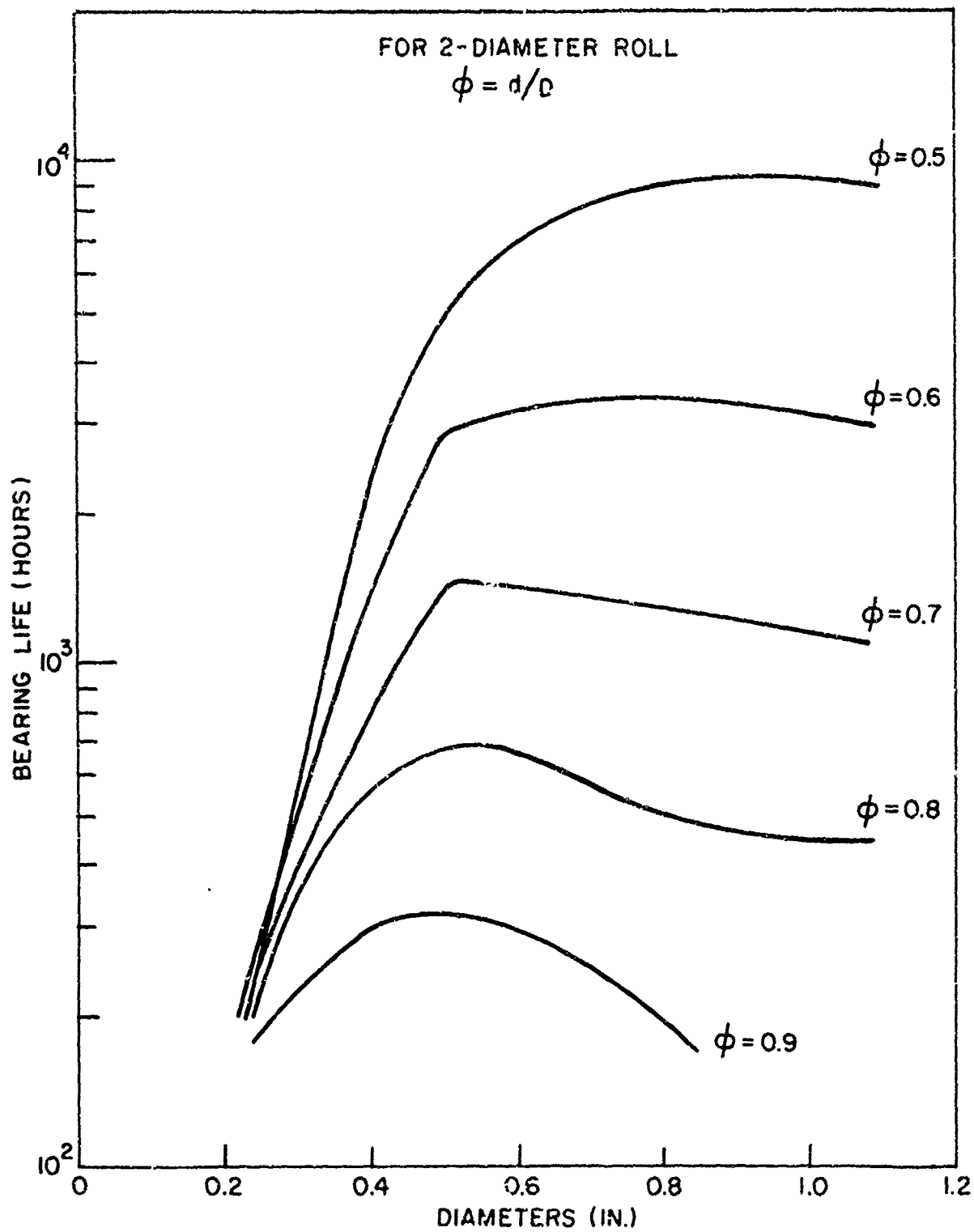


Figure 6. Bearing Life vs. Roller Diam. (Dual Diam. Rollers)

are of interest, (e) the requirement for 0.01 inches maximum radial deformation under 2,000 lbs. load indicates that hollow rollers over 0.7 hollowness are not recommended. The parametric life study also shows that L-10 fatigue life can be a limiting factor at  $4.0 \times 10^6$  DN operation.

### 3. CAGE-SLIP AND HORSEPOWER LOSS STUDY

The most promising configurations resulting from the parametric study were used in a full EHD computer analysis (Reference 1) containing the latest available elastohydrodynamic (EHD) technology (Reference 4). The majority of the computer runs were made with MIL-L-7808 oil at 250°F oil inlet temperature. One check run each for a single diameter and a dual diameter roller configuration were made with Polyphenyl Ether SP4E lubricant at 500°F oil inlet temperature. The actual run data is summarized in Table III, which also contains a summary of results including percentage cage slip and horsepower dissipation. More detailed information is summarized in Table IV. L-10 life, roller load, film thickness, and specific film thickness data as well as sliding speeds at both the outer and inner races are given for the maximum loaded roller.

The primary problem encountered in high speed mainshaft roller bearings is cage slip. This is the phenomena which results in high sliding velocities between the rollers and the inner race contacts. Severe glazing and micro-pitting results in bearing failure. The full EHD computer analysis gives detailed information regarding slip conditions. Figure 7 shows the percentage cage slip as a function of radial load for various operating conditions. An inner race land riding cage with hollow rollers has considerable slip and is used as a reference point in Figure 7. Seven hundred pounds radial load are required for non-slip or synchronous running of the cage. The outer race land riding hollow roller design has considerably higher slip than any of the other configurations and only one check run is plotted on Figure 7. The beneficial effects of having the frictional torque and the cage land contact acting as a driving torque indicates that an inner land riding cage

Table III

## SCHEDULE OF COMPUTER RUNS

Run No.	Symbol	Brg. Type 1. Hollow-Inner 2. Hollow-Outer 3. 2 Dia.-Inner	Load Lbs	Speed UM x 10 <sup>-6</sup>	Lube 7808 @ 250°F 5P4E @ 500°F	% Oil in Brg Cavity	Results		
							% Cage Slip	H.P.	L-10 Life Hours (Fatigue)
1	△	1	666	4.0	7808	.6	11.53	52.8	6,108
2	△	1	666	4.0	7808	.15	SYN	28.4	3,030
3	△	1	333	4.0	7808	.15	21.66	22.5	25,562
4	▽	2	333	4.0	7808	.15	64.97	9.6	953,167
5	△	1	333	3.0	7808	.15	19.85	13.9	131,307
6	△	1	333	2.0	7808	.15	9.02	6.6	487,022
7	△	1	333	1.0	7808	.15	SYN	1.82	2.29x10 <sup>6</sup>
8	▲	1	333	4.0	5P4E	.15	17.14	17.5	17,751
9	□	3	333	4.0	7808	.15	4.58	21.4	9,630
10	■	3	333	4.0	5P4E	.15	SYN	17.2	7,505
11	□	3	100	4.0	7808	.15	25.96	16.0	142,522
12	□	3	333	4.0	7808	.15	SYN	5.2	44,301
									10,961
									8,390
									8,792
									6,510

Table IV

## SUMMARY OF COMPUTER RESULTS

Run No.	Symbol	Speed <sub>6</sub> DNx10 <sup>-6</sup>	Load Lbs	% Cage Slip	MAXIMUM LOADED ROLLER								No. of Loaded Rollers
					OUTER				INNER				
					Roll LD Lbs	EHD Film hx10 <sup>6</sup>	Δ	Slide in./sec	Roll LD Lbs	EHD Film hx10 <sup>6</sup>	Δ	Slide in./sec	
1	Δ	4.0	666	11.53	336	13.08	1.46	0.7	138	13.91	1.55	1079.	9
2	Δ	4.0	666	SYN	378	13.05	1.46	0.5	190	14.20	1.59	2.9	9
3	Δ	4.0	333	21.66	219	13.66	1.53	0	72	15.05	1.68	2028.	9
4	▽	4.0	333	64.97	101	11.35	1.27	0	71	14.29	1.60	6086.	9
5	Δ	3.0	333	19.85	185	13.02	1.46	1.73	99	13.63	1.52	1393.	5
6	Δ	2.0	333	9.02	159	12.12	1.36	2.5	110	12.19	1.36	420	5
7	Δ	1.0	333	SYN	132	9.04	1.01	2.4	117	8.63	0.97	3.2	5
8	▲	4.0	333	17.14	238	2.79	0.31	0	74	2.94	0.33	1606.	9
9	□	4.0	333	4.58	266	8.74	0.98	0.1	139	12.87	1.44	412.	5
10	■	4.0	333	SYN	280	2.09	0.23	0	141	2.23	0.25	0.05	3
11	□	4.0	100	25.96	131	8.85	0.99	0	59	14.57	1.63	2335.	3
12	□	2.0	333	SYN	248	6.68	0.75	0.5	213	11.02	1.23	2.0	3

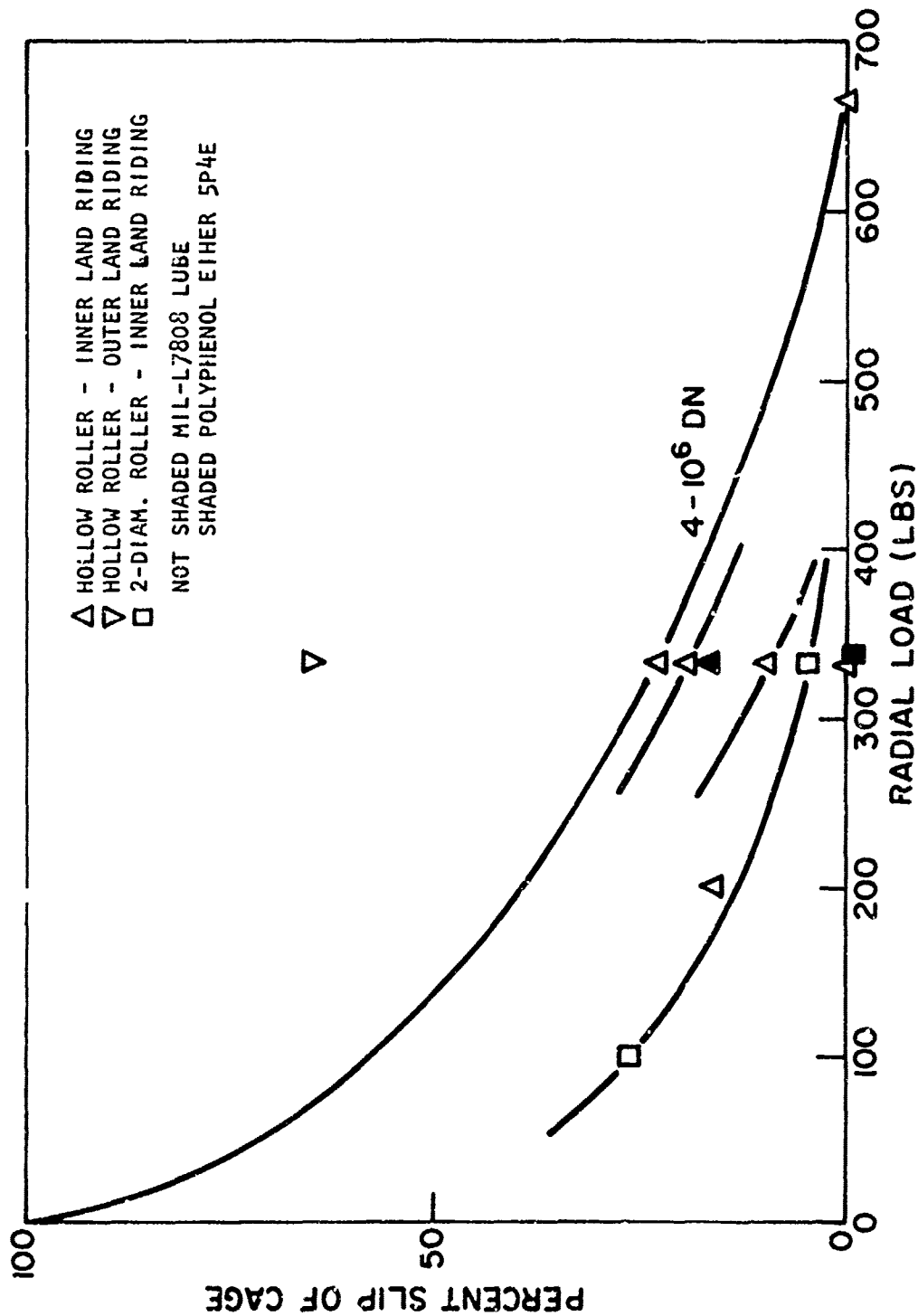


Figure 7. Cage Slip Percent vs. Radial Load

configuration should be considered. For this reason all dual diameter roller computer runs were made with an inner land riding cage configuration. The dual diameter roller bearing has significantly less cage slip as shown on Figure 7. Another way to represent sliding or cage slip is to show the reduction in cage rpm as a function of radial load. This is given in Figure 8. It is immediately apparent that the hollow roller inner-land-riding cage speed or a single diameter roller bearing concept cage speed is considerably higher than the corresponding cage speed for the dual diameter roller concept. As evident in Figure 8, a much lower load is required to prevent sliding or cage slip in the dual diameter roller concept.

An object of the present study is to minimize heat generation in the bearing. An indication of heat generation is the computed horsepower loss of the bearing. As shown on Figure 9, the horsepower losses for both the inner land riding cage configurations (single diameter roller and dual diameter roller) are essentially the same. Horsepower losses are expected to be somewhat lower with the use of Polyphenyl Ether 5P4E lubricant as compared to MIL-L-7808 oil. The oil viscosity of the 5P4E at 500°F is less than that of the 7808 at 250°F. Viscous drag losses predominate in the bearing at  $4.0 \times 10^6$  DN. Therefore, lower oil viscosity (at synchronous cage speed) will result in less power loss.

#### 4. SERIES HYBRID BEARING

The series hybrid bearing concept, Figure 1d, consists of an oil film bearing between the inner race of the roller bearing and the shaft. The concept is one of speed sharing or speed reduction. The rotative speed of the roller bearing inner race is determined by the frictional torque of the oil film journal bearing matching the frictional torque of the roller bearing. The advantage of speed sharing is the fact that reduction speed on the inner race of the roller bearing results in a lower operating DN speed regime.

A three lobe oil film hydrodynamic bearing was considered for this application. Satisfactory bearing stability (absence of half-frequency

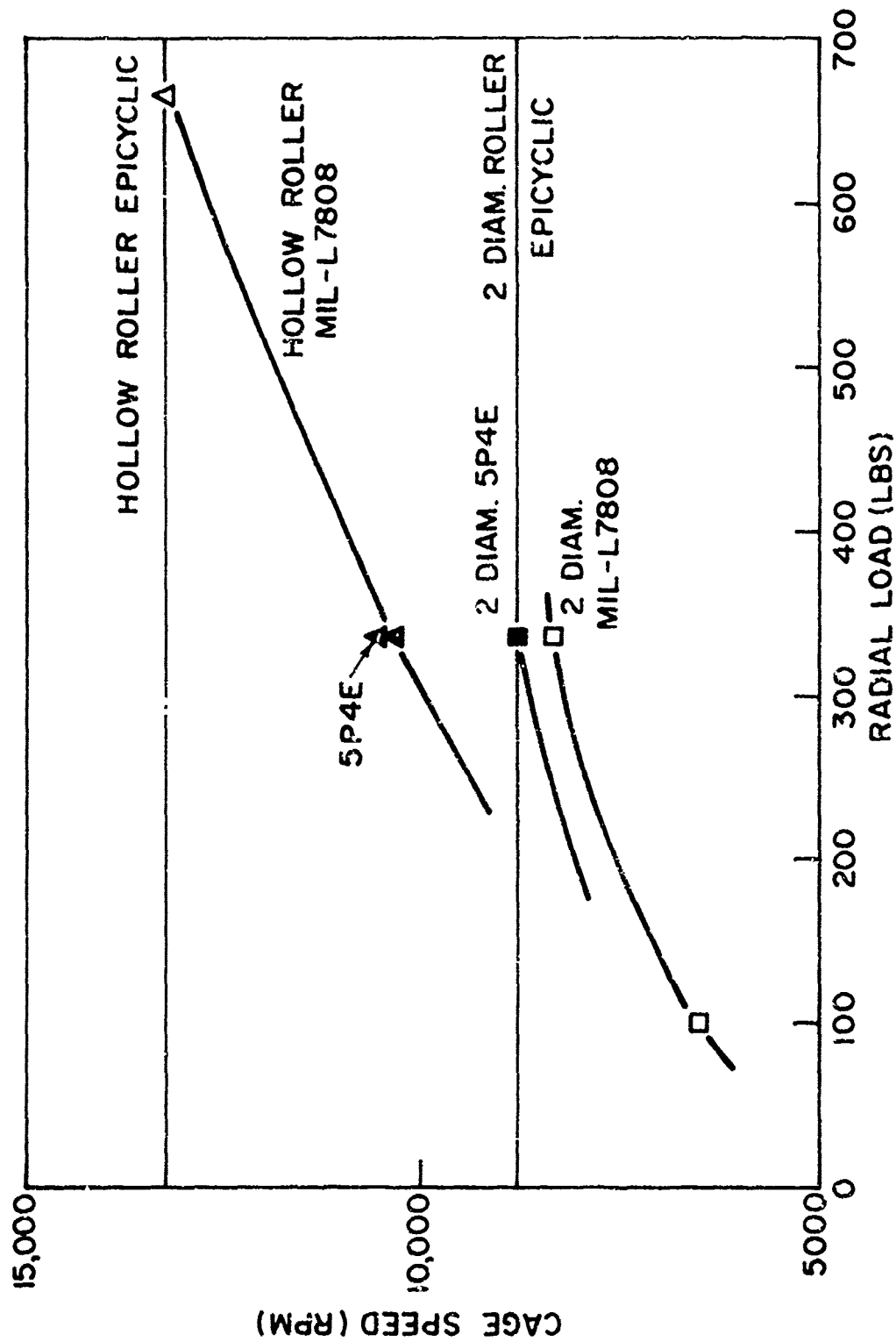


Figure 8. Cage Speed in RPM vs. Radial Load

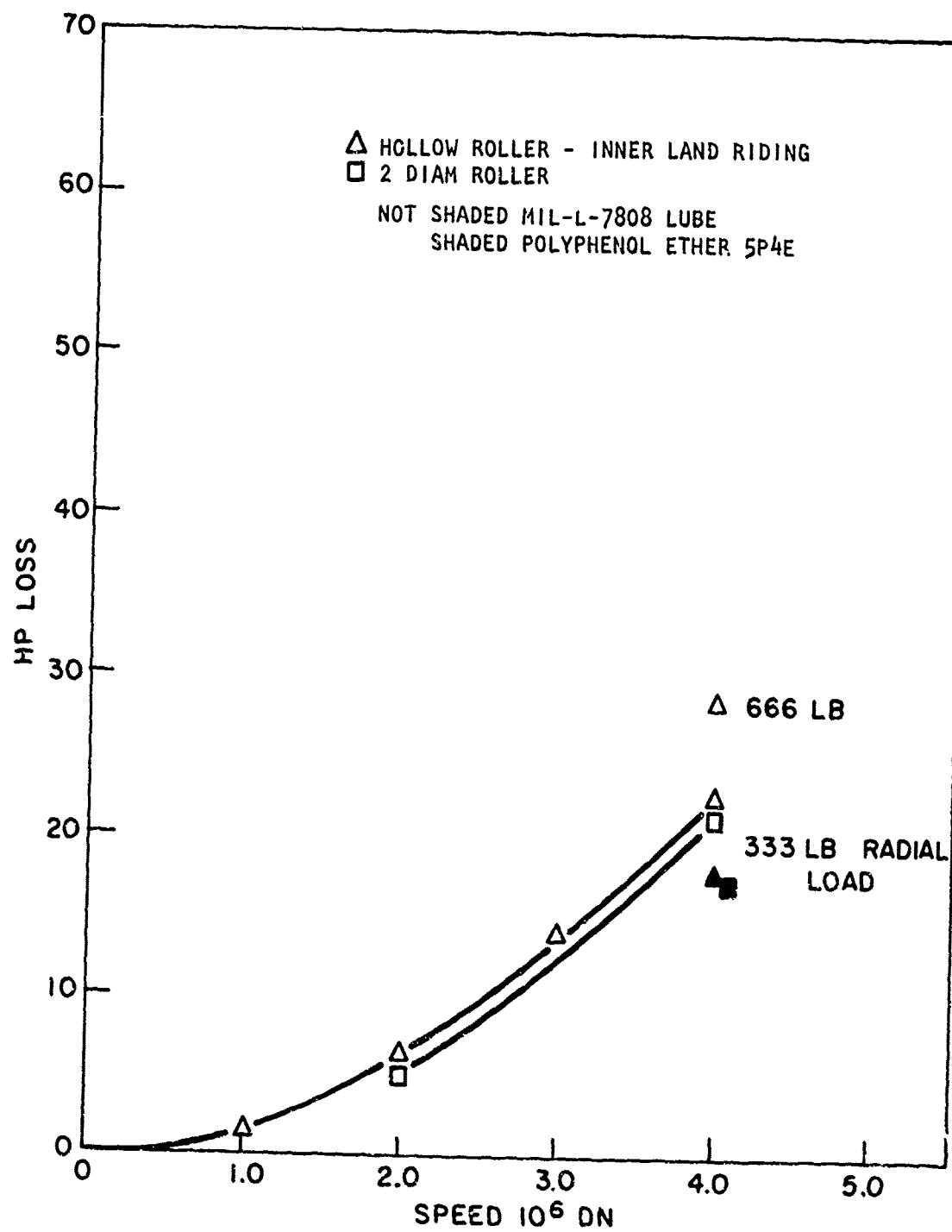


Figure 9. Horsepower Loss vs. Speed

whirl) can be obtained with this type of bearing. Good inherent stability was shown to exist under a shaft weight of 35 lbs. (representing an anticipated test rig shaft). This stability decreases as shaft weight increases, however, satisfactory stability for the bearing under study could be obtained up to 200 lbs. shaft weight. Minimum oil films on the order 0.001 inch can be anticipated under light 200 lb. loadings. The oil films would reduce to 0.0004 inches under the maximum 2,000 lbs. applied external load. The frictional torque of a three-lobe journal bearing was computed. The roller bearing inner race, Figure 1d, when supported on an oil film journal bearing only, would be completely free to move axially with respect to the shaft. Thus locating oil film bearings would be required to maintain the position of the roller bearing inner race. Locating thrust loads would be small. One approach is to use a conical type bearing (Reference 5). A pair of thrust bearings operating against the face of the roller bearing inner race were envisioned as a series of step pad thrust surfaces. The frictional torque of such surfaces amounted to approximately 15 or 20% of the overall journal bearing friction. This amount was added to the oil film bearing system torques.

The operation of the journal bearing would be in the turbulent regime and factors for the computation of turbulent friction are usually applied to laminar friction estimates. This approach was used in arriving at the total journal bearing friction curve. The friction loss vs. speed ratio for MIL-L-78C8 oil at 250° is shown in Figure 10. The solid lines indicate the friction torque expressed in inch pounds of the oil film journal and thrust bearing surfaces is a function of the ratio of the roller bearing inner race speed to shaft speed. The dashed curve represents the frictional torque of the inner land riding cage hollow roller bearing configuration. The point of intersection of these two frictional torque curves defines the operating speed of the roller bearing inner race. It is seen in Figure 10 that the present bearing system would result in a speed ratio of 0.84. Recent work by NASA (Reference 5) with a series hybrid concept using a ball thrust bearing and an oil

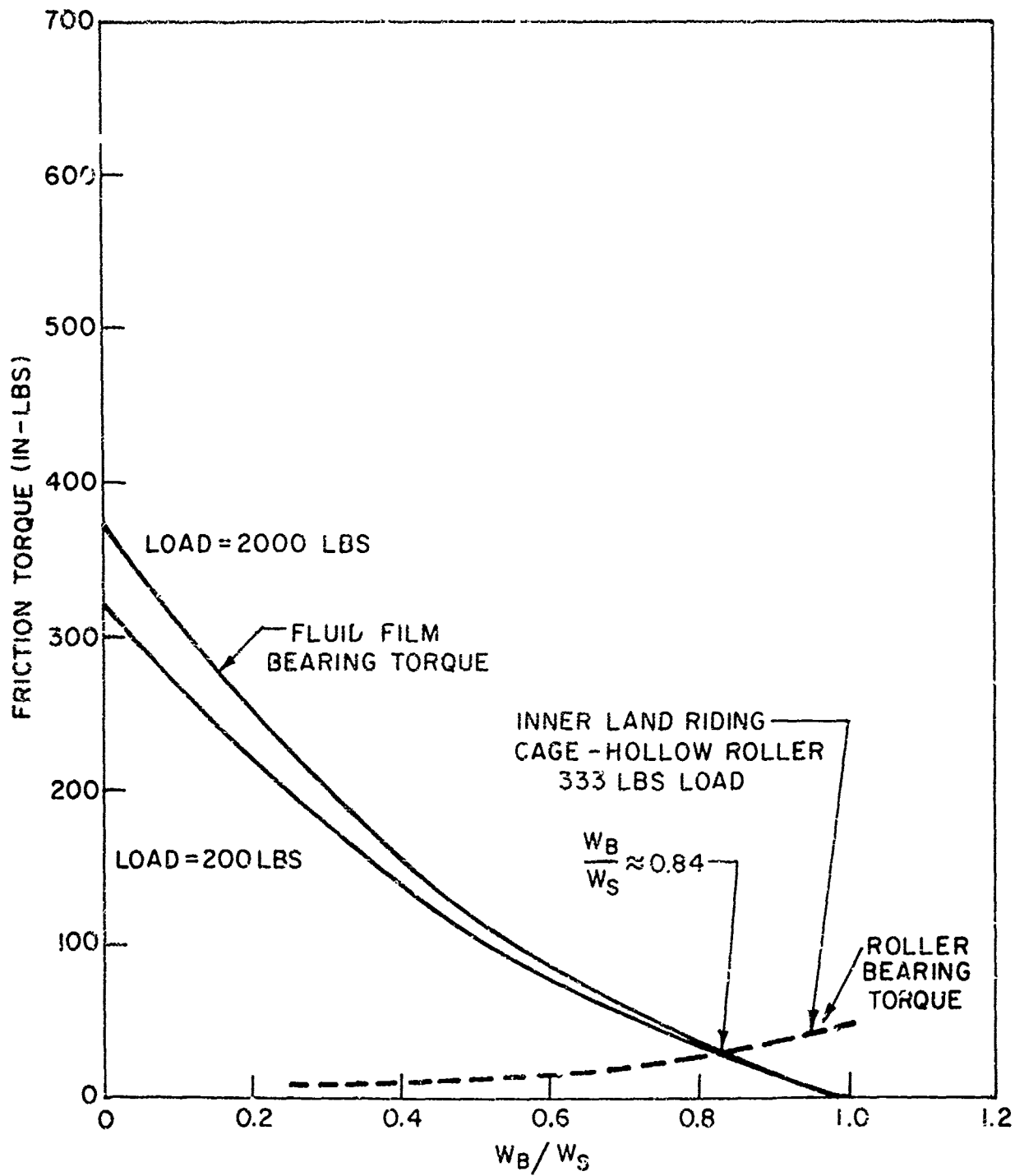


Figure 10. Friction Loss vs. Speed Ratio, MIL-L-7808 Oil

film thrust bearing surface resulted in a speed sharing ratio of approximately 0.66 at best. The analysis is highly dependent upon accurate calculation of frictional torques. The frictional torques even in the turbulent regime of the fluid bearing has been fairly well established and correlated with experimental results and can be considered realistic. High speed roller bearing torque needs to be carefully verified to determine the anticipated speed sharing ratio. It is possible to add frictional torque to the roller bearing concepts by increasing the amount of oil forced through the bearing. Thus, it is possible by raising the frictional torque of the roller bearing to obtain a more favorable speed sharing ratio as could be seen by raising the curve on Figure 10. However, any reductions in roller bearing torque would result in reduction in the anticipated speed sharing ratio.

#### 5. SELECTION OF DUAL DIAMETER ROLLER BEARING

The dual diameter roller bearing concept, Figure 2, with an inner land riding cage was recommended for the thorough design analysis, fabrication and prototype testing. Selection of the dual diameter roller bearing concept was based upon the lower cage speeds obtained which result in significantly less cage slip.

The series hybrid bearing concept is interesting but was not recommended for further study under the present program. Operation of the series hybrid bearing design is highly dependent upon accurate determination of roller bearing friction torque. The horsepower losses of both conventional and dual diameter roller bearing concepts, Figure 9, are shown to be essentially the same. Therefore the selection of a roller bearing configuration for further development at this time does not affect future consideration of development of the series hybrid bearing concept.

### SECTION III

#### LUBRICANT SELECTION

A summary of full scale bearing test results of 8 candidate high temperature (600°F) lubricants is given in Table V, which was taken from Reference 6. All of the lubricants in this study were operated with an inerting blanket of nitrogen gas. Another recent study (References 7 and 8) considered five candidate high temperature lubricants. In this case Table VI, all of the lubricants were again protected by an inert nitrogen blanketing gas with the exception of Polyphenyl Ether 5P4E. The Polyphenyl Ether was operated in an oxygen atmosphere. The only advanced lubricant showing reasonable success without special inert oxidation protection is the 5P4E Polyphenyl Ether. Figure 11 is a reproduction of a report of bearing fatigue life experiments with Polyphenyl Ether (Reference 8). Indications are that Polyphenyl Ether is an acceptable high temperature lubricant up to 600°F but that the failure mode may be one of moderate glazing and micropitting of the races and rolling elements. This is attributed to thinner EHD lubricant films in the operating race and roller contacts. The various bearing configurations were analyzed with 5P4E Polyphenyl Ether at 500°F to determine the operating specific film thicknesses in the roller race contacts.

The properties of MIL-L-7808 and Polyphenyl Ether lubricants are discussed in the elastohydrodynamic lubrication preliminary design manual (Reference 4). Additional data (Reference 9) regarding high pressure viscometer experiments with Polyphenyl Ether 5P4E were also used for estimating properties of this lubricant at 500°F. Lubricant data as a function of operating temperature is given in Table VII for the MIL-L-7808 and 5P4E lubricants. This data as a function of temperature is consistent with the extrapolation routines of Reference 4.

Table V

## SUMMARY OF TEST RESULTS

<u>Performance</u>	<u>Fluid (s)</u>	<u>Measured <math>h/\sigma</math> @ 600°F</u>	<u>Typical Bearing Condition</u>
Excellent	1. Super Refined Mineral Oil Plus 10% High Molecular Weight Resin.	3.6-4.0	Good.
Good	2. Perfluorinated Polyether. 3. Modified Fluorsilicone.	3-4 (Initially) <1.8 (Long-Term) <1.8	Minor Glazing And Micropitting.
Acceptable	4. Synthetic Hydrocarbon Plus 10% High Molecular Weight Resin. 5. Modified Polyphenyl Ether.	<1.8 <1.8	Moderate Glazing And Micropitting
Unacceptable	6. Super Refined Mineral Oil Without High Molecular Weight Resin. 7. Synthetic Hydrocarbon Without High Molecular Weight Resin. 8. Highly Hindered Ester.	2.6-3.6 (Initially) <1.8 (Long-Term) 3.5-4.0 <1.8	Heavy Glazing And Pitting.

Table VI  
PROPERTIES OF TEST LUBRICANTS

Lubricant designation	Base Stock	Additive content	Flash point, °F	Fire point, °F	Kinematic viscosity, cs, at-		Specific heat at 500°F, 8tu/(lb.)(°F)	Density at 500°F lb./ft. <sup>3</sup>	
					100°F	210°F			
NA-XL-10	Super-refined naphthenic mineral oil	(a)	445	495	79	8.4	1.1	0.660	45.7
NA-XL-13	Synthetic paraffinic oil	None	530	580	314	32	<sup>b</sup> 2.9	-	-
NA-XL-16	Polyester-hindered type	(c)	480	540	27.6	5.2	<sup>b</sup> 1.0	-	-
NA-XL-20	Fluorocarbon	None	-	-	335	29	2.1	.317	94
NA-XL-22	5P4E polyphenyl ether	None	550	660	363	13.1	1.2	.496	63.1
NA-XL-23	5P4E polyphenyl ether	(d)	550	660	363	13.1	1.2	.496	63.1
NA-XL-24	Synthetic paraffinic oil	(e)	530	580	314	32	<sup>b</sup> 2.9	-	-

<sup>a</sup>Oxidation inhibitor, extreme pressure additive, and antifoam agent.

<sup>b</sup>Extrapolated.

<sup>c</sup>Oxidation inhibitor and dispersant.

<sup>d</sup>Oxidation inhibitor.

<sup>e</sup>Antiwear additive.

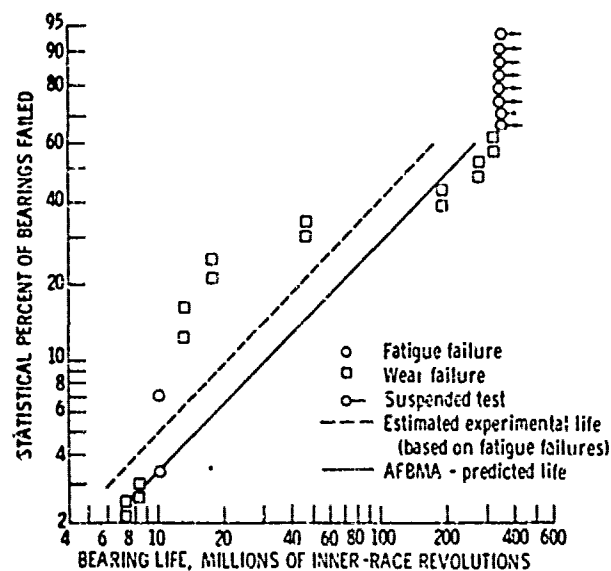


Figure 11. Bearing Life with 5P4E Lubricant

Rolling-element fatigue life of 120-mm bore angular-contact ball bearings run with polyphenyl ether lubricant. Material, AISI M-50 steel; thrust load, 4365 lb; speed, 12,000 rpm; temperature, 600°F air environment; [failure index, 2 out of 26.]

Table VII  
LUBRICANT PROPERTIES USED IN THE ANALYSIS

MIL-L-7808 LUBRICANT PROPERTIES

Temperature (°F)	Viscosity (lb-sec/in <sup>2</sup> )	Alpha (in <sup>2</sup> /lb)	Beta (°F)	Gama (in <sup>2</sup> -°F/lb.)	Therm.Cond. (BTU/°F-HR-FT)	Spec. Heat (BTU/lb.-°F)	Wt. Dens. (lb./in <sup>3</sup> )
.15000+03	.11000-05	.88400-04	.49130+04	.63000-01	.09050+00	.48400+00	.33100-01
.20000+03	.45000-06	.81000-04	.49130+04	.63000-01	.08700-01	.51200+00	.32300-01
.25000+03	.30500-06	.76200-04	.49130+04	.63000-01	.83000-01	.53100+00	.31600-01
.30000+03	.21500-06	.72800-04	.49130+04	.63000-01	.79400-01	.55000+00	.30800-01
.35000+03	.16000-06	.70600-04	.49130+04	.63000-01	.75600-01	.56800+00	.30100-01
.40000+03	.12000-06	.69000-04	.49130+04	.63000-01	.72000-01	.58800+00	.29400-01

Polyphenyl Ether LUBRICANT PROPERTIES (5P4E)

Temperature (°F)	Viscosity (lb/sec/in <sup>2</sup> )	Alpha (in <sup>2</sup> /lb)	Beta (°F)	Gama (in <sup>2</sup> -°F/lb.)	Therm.Cond. (BTU/°F-HR-FT)	Spec. Heat (BTU/lb.-°F)	Wt. Dens. (lb./in <sup>3</sup> )
.30000+03	.80000-06	.66000-04	.65040+04	.18300+00	.77300-01	.46200+00	.40700-01
.35000+03	.44000-06	.54000-04	.65040+04	.18300+00	.77100-01	.47800+00	.40400-01
.40000+03	.26000-06	.43000-04	.65040+04	.18300+00	.76900-01	.49200+00	.40100-01
.45000+03	.16000-06	.33000-04	.65040+04	.18300+00	.76700-01	.51100+00	.39800-01
.50000+03	.10000-06	.26000-04	.65040+04	.18300+00	.76600-01	.52700+00	.39500-01
.55000+03	.65000-07	.19000-04	.65040+04	.18300+00	.76400-01	.54400+00	.39200-01

## SECTION IV

### DUAL DIAMETER BEARING ANALYSIS AND DESIGN

#### 1. DESIGN CONSIDERATIONS

The dual diameter roller bearing concept was selected as a result of the preliminary configuration study. Selection was based upon the lower cage speeds obtained which will result in significantly less cage slip. The orbital cage speed of the dual diameter roller bearing with a diameter ratio of 0.5 will result in a  $1/3$  reduction of cage speed as seen by Figure 4. A major roll diameter of 0.5 inches was selected as an optimum based on Figure 6. The resulting estimated bearing life (under the duty cycle of Table II) would be 5,000 hours L-10 life shown on Figure 6. This is well in excess of the design goal of 1,000 hours.

The primary problem encountered in high speed mainshaft roller bearings is cage slip. This is a phenomena which results in high sliding velocities between rollers and inner race contacts. Severe glazing and micropitting results in bearing failure. The minimum radial load to prevent skid or cage slip in the dual diameter roller bearing is 333 lbs. as shown on Figures 7 and 8. This minimum radial load was used in the design and performance evaluation calculations. Heavier radial loads will result in reduced bearing fatigue life, but do not endanger the bearing from a skid or cage slip standpoint and are of relatively minor interest. It is essential to assure that cage slip will not occur under operating conditions. A complete systems analysis (Reference 1) incorporating the latest available elastohydrodynamic lubrication technology (Reference 4) and including fluid drag forces and thermal effects were selected as the best approach to achieve a practical design.

## 2. INNER RACE STRESSES

A study of the effect of inner race thickness and total interference fit between the inner race and shaft (with the hollow test shaft) to determine race circumferential, hoop or tangential tension stresses was conducted using standard ring formulas. Race radial thickness over 0.25 inches has little effect upon reducing circumferential tangential stresses. Race thicknesses less than 0.250 inches radial thickness can result in unacceptably high stresses. Therefore the inner race thickness should meet or exceed 0.25 inches.

High shaft speeds (up to 28,600 rpm) will create significant circumferential, hoop or tangential stresses in the inner race. Figure 12 shows a magnitude of this maximum tangential stress as a function of shaft speed expressed both in rpm and DN values for the 140 mm bore bearing. Approximately 50,000 psi tangential stress can be anticipated at  $4.0 \times 10^6$  DN with the 0.25 inch thick race of the prototype bearing design.

Approximate physical properties of M-50 fully hardened steel are given in Table VIII. The material is brittle at room temperature and care must be exercised to prevent over-stressing. The material does become more ductile as temperature increases. The effect of stresses due to speed, Figure 12, and stresses due to interference fit are essentially additive. Approximately 0.012 inches diametral interference fit would be required at room temperature to assure a working interference fit of 0.001 at  $4.0 \times 10^6$  DN operation. This heavy interference fit would result in almost 60,000 psi tangential ring stresses initially. It was decided to compromise with a lesser interference fit at room temperature (0.0063 inches) and allow the inner race to become loose with respect to the shaft at approximately  $3.0 \times 10^6$  DN. Key slots in the inner race allow the race to be axially clamped and prevent relative rotation of the race and shaft. The loose fit between inner race and shaft at speeds over  $3.0 \times 10^6$  DN will keep the inner race tangential stresses to less than 60,000 psi.

High tensile ring stresses may have a detrimental effect on inner race rolling contact fatigue. Thermal gradients may also cause the interference

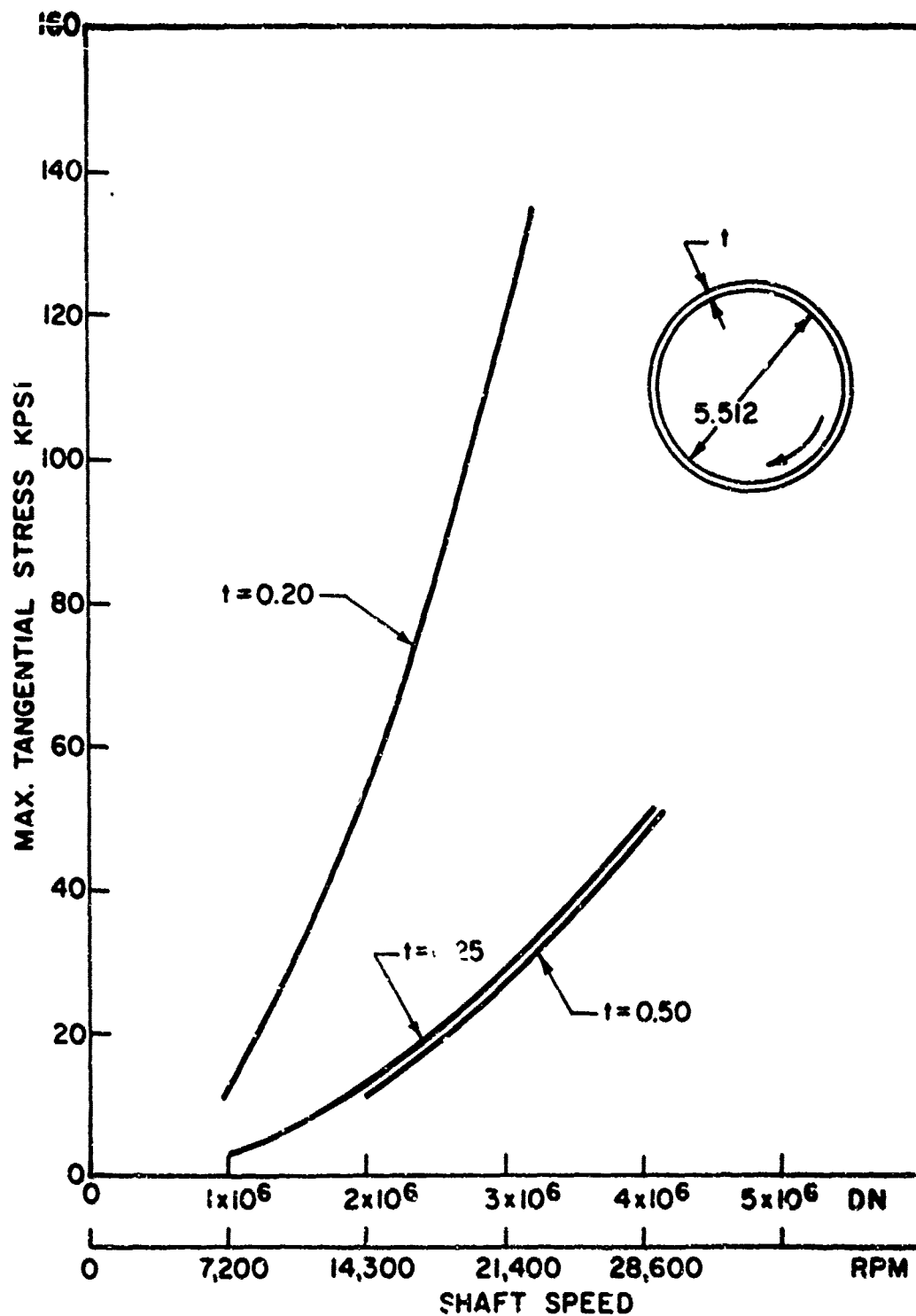


Figure 12. Inner Race Maximum Tangential Stress vs. Shaft Speed

TABLE VIII  
 PROPERTIES OF M-50 HARDENED TO RC-60  
 Per VASCO Technical Bulletin

<u>Property</u>	<u>Room Temp.</u>	<u>800°F</u>
Tensile ULT. (psi)	411,500	345,000
Tensile Yield (psi)	388,000	262,500
Elongation (1.5" gauge) (%)	2	6
Red. of Area (%)	2	17

fit to increase (depending upon the amount of under inner race cooling). Therefore every effort was made to limit inner race tangential stresses at maximum and 500°F operation. A partially hollow or compliant inner race design Figure 13 was selected to provide access for the under and through inner race lubrication scheme. The beam bending compliancy may also provide relief from thermal lockup or thermal preloading at high temperature and high speed operation.

An existing FIRL finite element computer program was used to evaluate the tangential ring stresses in the actual inner race design at  $4.0 \times 10^6$  and  $3.5 \times 10^6$  DN. Figure 13 illustrates the inner race model and the location of various tangential stresses. The stress values of Figure 13 are in good agreement with the approximate solutions used to obtain the values in Figure 12. It is readily apparent that stresses on the order of 57,000 psi will occur in the inner race at  $4.0 \times 10^6$  DN. Stress level will drop to approximately 44,000 psi maximum at  $3.5 \times 10^6$  DN (25,000 rpm). A third case was analyzed where circumferential line loads were applied in the vicinity of the roller inner race contacts to simulate stress conditions under 500 lb. external radial load. It can be seen from Table IX that the stress values range between a high of 43,000 psi and a low of 29,000 psi. The only available data to date for M-50 steel at 500°F in reverse bending fatigue (Reference 10) indicates a life which is asymptotic at 60,000 psi bending stresses beyond  $10^8$  cycles. The fluctuation of inner race bending stresses are all unidirectional and remain tensile as shown in Table IX and do not exceed a maximum value of 43,000 psi. The inner race compliant section calculates to have adequate reverse bending fatigue properties.

### 3. LUBRICATION

The method of lubrication for the dual diameter roller bearing is illustrated in Figure 14. Jet oil is introduced to an undercut in the test shaft as shown. Oil then passes through the shaft to the undercut portion of the inner race which acts as an oil reservoir. Centrifugal force resulting from shaft rotation then provides pressure to force a flow of oil through orifice holes in the inner race. This oil is then

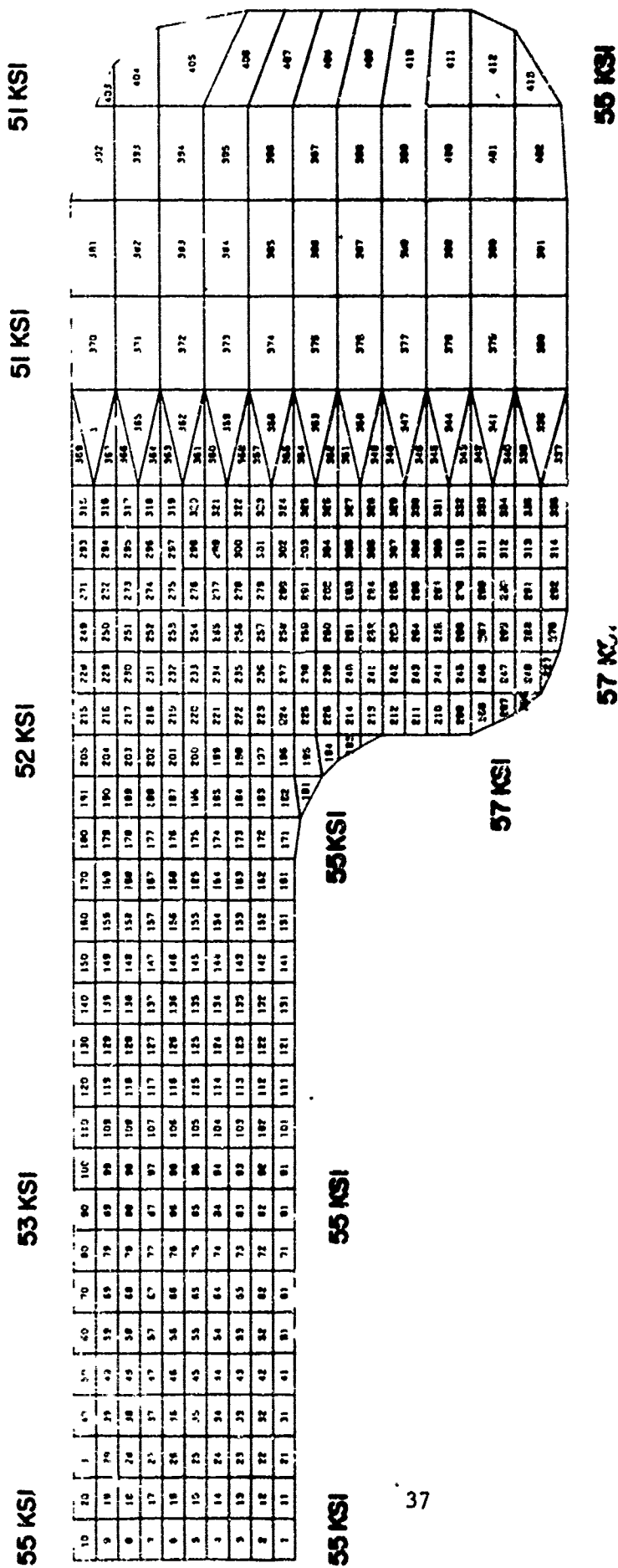


Figure 13. Finite Element Analysis of Inner Race Tangential Stresses at 4.0 x 10<sup>6</sup> DN

TABLE IX

## INNER RACE TANGENTIAL STRESS (KSI)

Loading/Element No.	1	10	81	90	171	208	215	270	370	492	392
$4.0 \times 10^6$ DN	55	55	55	53	55	57	52	57	51	55	51
$3.5 \times 10^6$ DN	42	41	42	41	41	43	40	44	39	43	39
$3.5 \times 10^6$ DN 500 lbs. Radial Load	37	29	36	33	37	40	36	41	38	43	39

AMBIENT AIR

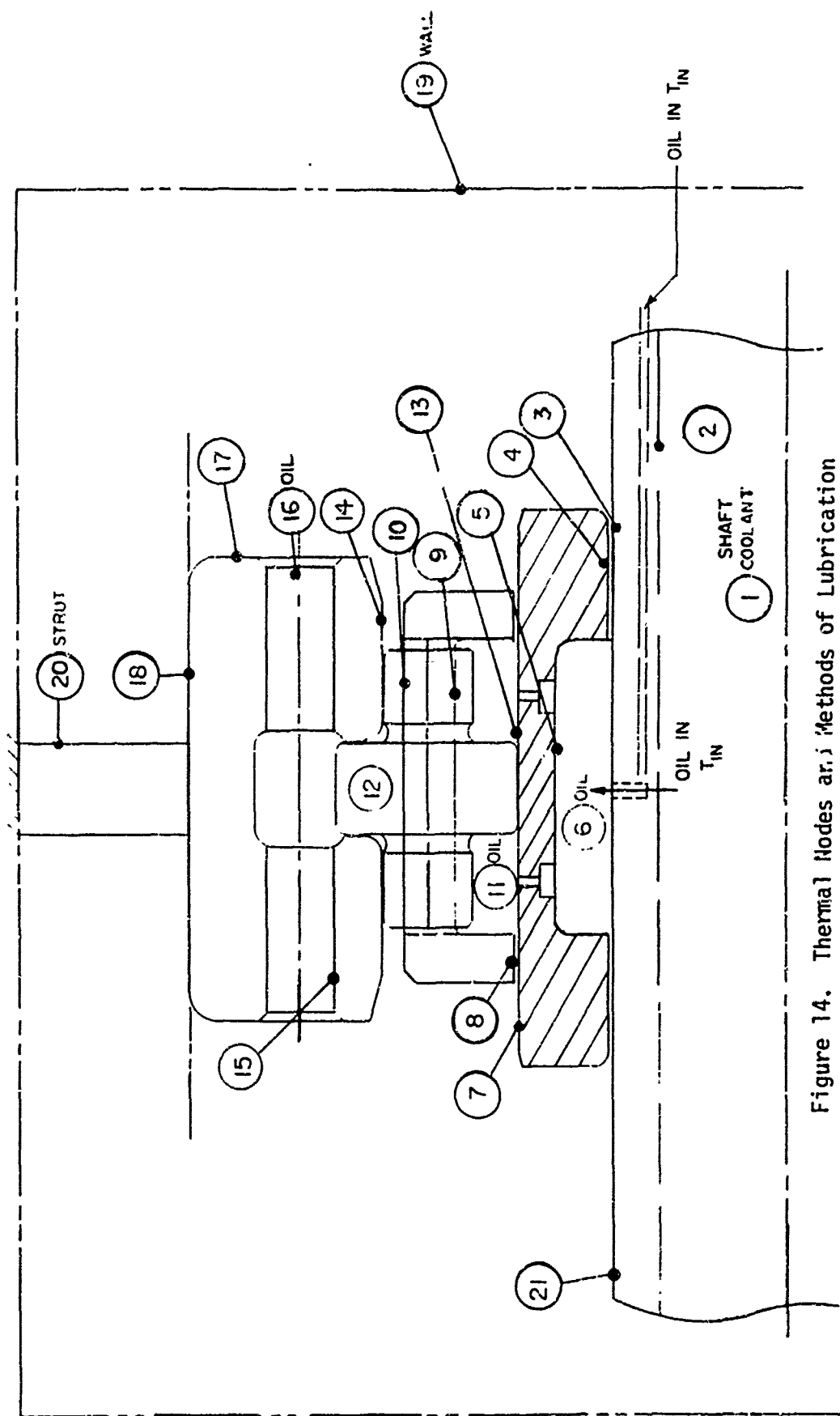


Figure 14. Thermal Nodes and Methods of Lubrication

introduced to the underside of the cage and is further circulated throughout the bearing by the pumping action of the rollers. Auxiliary jet oil lubrication into the sides or faces of the bearing can also be provided as necessary to obtain satisfactory cooling.

Three computer analysis runs were executed using three different flow rates (6.1, 12.0 and 18.0 lbs./min.) of 5P4E at 500°F oil inlet temperature. The minimum load to prevent skid of 333 lbs. and the top design shaft speed of 28,560 rpm ( $4.0 \times 10^6$  DN) were used. A complete thermal analysis was included in the solutions. A summary of the effects of oil flow upon bearing performance is given in Table X and shown graphically in Figure 15. Examination of Figure 15 shows no clear maxima or minima characteristics. It is evident that increased oil flow rate results in reduced outlet temperature and increased bearing horsepower loss. The outlet oil temperature shows some indication of leveling out below 6 lbs. per minute, but at unacceptably high values in excess of 700°F. Increasing the oil flow from 6 to 12 lbs. per minute drops the outlet oil temperature by 51.8°F. Increasing the oil flow from 12-18 lbs. per minute drops the outlet oil temperature by only 22.3°F.

An oil flow rate of 12 lbs./min. was selected as the design point. This flow can be obtained with 6 orifices of 0.028 inches diameter. The calculated oil outlet temperature of  $4.0 \times 10^6$  DN is 598.5°F which is consistent with the program goal of 600°F operation. Table XI gives the resulting oil flow rates for 5P4E at 500°F oil inlet and MIL-L-7808 at 250°F oil inlet as a function of shaft speed.

#### 4. PERFORMANCE ANALYSIS

Eight computer solutions were executed at various shaft speeds with 5P4E and MIL-L-7808 oil lubricant under a constant bearing radial load of 333 pounds. A summary of these computer runs and performance results are contained in Table XII. Initial fit-up conditions are 0.0063 inches shrink fit between bearing inner race and the shaft and 0.011 inches initial (machined or ground) diametral clearance. All of the solutions summarized in Table XII included a full thermal analysis consisting of 21 thermal modes described in Figure 14. Description of the node locations and the temperature

TABLE X

## EFFECT OF OIL FLOW RATE ON BEARING PERFORMANCE

	<u>Run 2P</u>	<u>3P</u>	<u>4P</u>
Flow (lbs/min)	6.1	12.0	18.0
HP (loss)	21.7	23.53	25.4
Temp. Out of Brg. (°F)	650.3	598.5	576.2
Sump. Temp. (°F)	608.1	561.8	544.4

Shaft Speed 28,560 RPM ( $4.0 \times 10^6$  DN)  
 Lubricant: 5P4E @500°F oil inlet  
 Radial Load: 333 lbs

TABLE XI

## OIL FLOW RATE VS. SPEED (DN)

<u>Lubricant</u>	<u>Inlet Temp. °F</u>	<u>Oil Flow Rate lbs/min</u>			
		<u><math>4.0 \times 10^6</math> DN</u>	<u><math>3.0 \times 10^6</math> DN</u>	<u><math>2.0 \times 10^6</math> DN</u>	<u><math>1.0 \times 10^6</math> DN</u>
Polyphenyl Ether 5P4E	500	12.0	9.03	6.05	3.0
MIL-L-7808	250	8.98	6.82	4.60	2.33

Six 0.028" Diam. Orificies in Inner Race

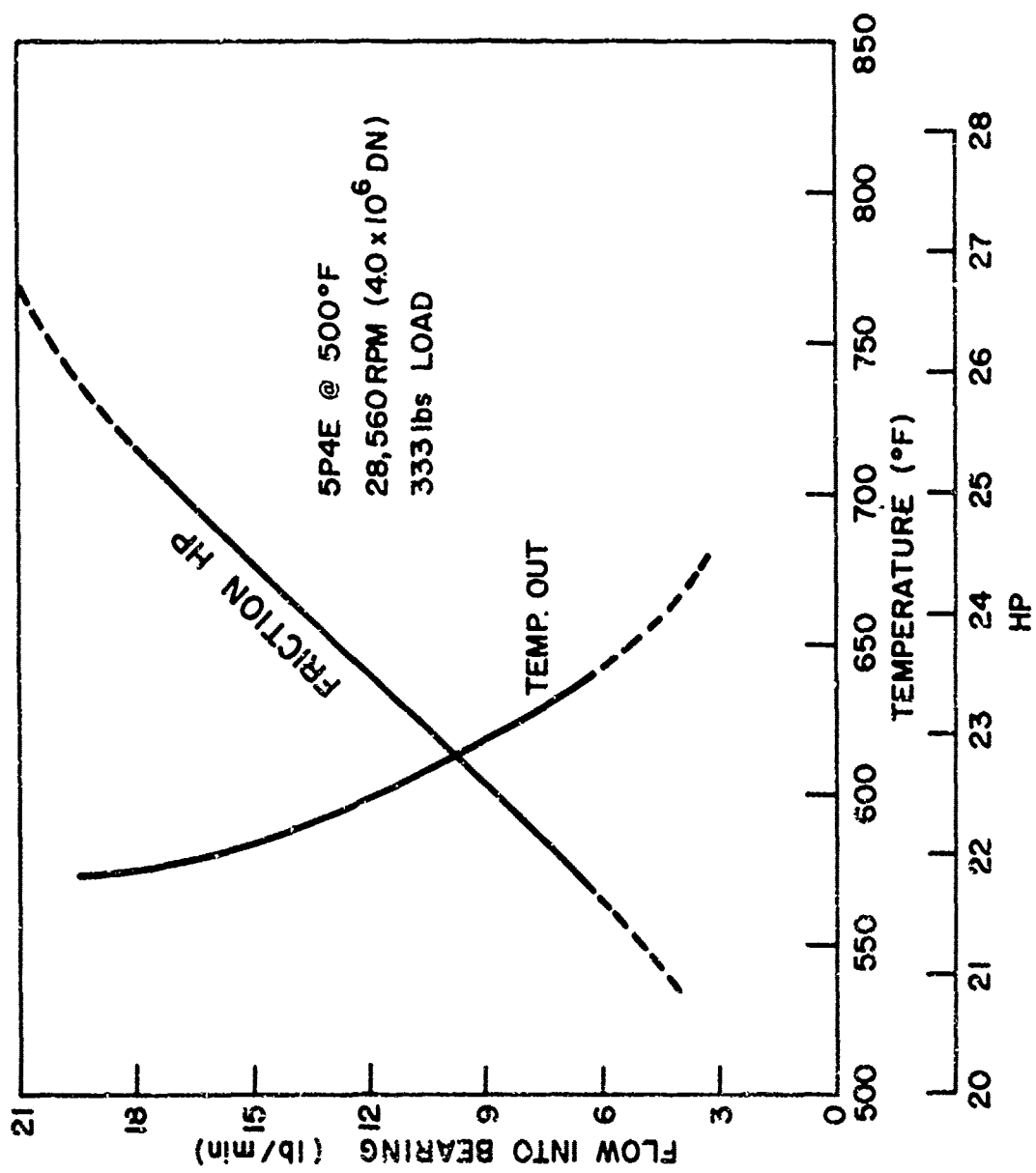


Figure 15. Effect of Oil Flow Rate Upon Outlet Temperature and Bearing Power Loss

TABLE XII

## SUMMARY OF PERFORMANCE ANALYSIS COMPUTER RUNS

Run No.	5P	6P	7P	8P	9P	10P	11P	12P
Speed DN	$4 \times 10^6$	$3 \times 10^6$	$2 \times 10^6$	$1 \times 10^6$	$4 \times 10^6$	$3 \times 10^6$	$2 \times 10^6$	$1 \times 10^6$
Lube Type	5P4E	5P4E	5P4E	5P4E	7808	7808	7808	7808
Lube Flow Rate (lb/min.)	12.0	9.03	6.05	3.0	8.984	6.819	4.6	2.327
L <sub>10</sub> Life (Hrs.)	7,236	22,496	63,329	$1.7 \times 10^6$	8,036	23,962	71,756	$2.1 \times 10^6$
Total Hp.	22.6	10.8	4.0	0.9	26.6	14.4	5.9	1.2
Operating Clear (Mils)	3.3(1)	6.6	7.0	7.3	1.6(1)	6.2	6.3	6.3
Cage Operating Clear (Mils) (Diametral)	32.	32.	32.0	32.0	32.0	34.0	33.0	32.0
No. Loaded Rollers	3	3	3	3	5	3	3	3
Radial Deflect (Mils)	2.0	3.7	3.9	3.9	1.1	3.4	3.5	3.5

(1) Inner Race loose on Shaft

profiles for the 8 performance runs are summarized in Table XIII.

The temperatures when using the Polyphenyl Ether 5P4E lubricant are acceptable at all speeds. The average oil temperature within the bearing (node 11) at  $4.0 \times 10^6$  DN operation of 631.9°F is acceptable for short duration test runs. Operating temperatures with MIL-L-7808 oil are not acceptable and auxiliary side jet lubrication was required during the initial checkout test runs with this lubricant.

The predicted frictional horsepower losses are shown in Figure 16 as a function of the speed parameter DN. Horsepower losses are also summarized in Table XII. A total loss of 22.6 horsepower was predicted at  $4.0 \times 10^6$  DN using Polyphenyl Ether 5P4E at 500°F oil inlet temperatures.

Radial displacements are summarized in Table XII and include one half of the operating internal clearance in the bearing. The specifications require that the total radial displacement not exceed 0.010 inches under 2000 lbs. radial load. An additional elastic deflection between rollers and raceways of 0.0006 inches should be added to the values in Table XII to adjust for the difference between the 333 lb. analysis load and the 2000 lb. specification load. All total displacement values are well below (less than half) maximum allowable values. The largest radial displacements occur at the lowest shaft speeds. The effects of shaft speed and thermal effects in the bearing tend to decrease diametral clearance. A summary of the fluid film forces and roller contact forces acting on the cage are given in Table XIV. It is evident from the table that the driving torque resulting from the loaded rollers contacting the cage pockets is not sufficient to prevent serious cage slip at  $4.0 \times 10^6$  DN operation. The fluid film drag on the inner surface and inner race to cage land is necessary to drive the cage at speed and prevent cage slip. An outer riding cage with resultant fluid drag torques at the outer race land contacts would result in significant cage slip at  $4.0 \times 10^6$  DN. Roller to cage web contact forces of 10.3 pounds are predicted at the maximum DN operation.

TABLE XIII

## SUMMARY OF TEMPERATURE PROFILES FOR DUAL DIAMETER ROLLER BEARING

No.	Location	DN		Lube		Run		5P		6P		7P		8P		9P		10P		11P		12P	
		4x10 <sup>6</sup>		5P4E		5P4E		5P4E		5P4E		5P4E		5P4E		5P4E		5P4E		5P4E		5P4E	
1.	Inner Shaft Coolant	660.8	601.4	545.5	476.5	514.2	470.5	379.5	280.9														
2.	Inner Shaft Surface	556.6	540.7	514.4	488.4	346.6	347.1	307.5	263.7														
3.	Outer Shaft Surface at Bearing	535.6	535.2	512.3	488.9	314.4	337.9	303.4	263.1														
4.	Inner Race at Shaft	613.3	558.4	521.8	491.6	453.8	374.0	320.6	267.1														
5.	Under-cut Surface of Inner Race	615.8	564.0	524.1	492.2	456.3	382.4	324.5	268.0														
6.	Under Race Coolant	529.5	517.4	503.1	485.5	297.8	289.0	274.6	253.9														
7.	Inner Race Beyond Roller Contact	628.1	571.3	526.8	492.8	469.3	391.5	328.6	268.8														
8.	Cage at the Land	665.6	600.8	542.4	498.9	549.7	462.2	369.1	282.0														
9.	Cage Inner Surface	674.2	604.0	543.5	499.4	554.6	465.3	370.4	282.4														
10.	Cage Outer Surface	672.6	603.0	543.1	499.4	552.0	464.1	369.9	282.4														
11.	Internal Lubricant to Bearing	631.9	576.6	529.3	494.5	465.9	404.8	338.9	272.7														
12.	Rollers	673.4	601.8	543.3	498.5	557.9	464.6	370.8	282.3														
13.	Inner Race at Rollers	627.1	570.1	526.1	492.6	465.5	388.8	327.2	268.5														
14.	Inner Surface of Outer Race	623.5	570.7	525.7	492.3	446.4	389.7	329.3	269.1														
15.	Inner Cooled Surface Outer Race	621.6	569.7	525.3	492.1	444.2	388.3	328.6	268.9														
16.	Outer Race Lubricant	620.0	568.9	525.0	491.9	442.3	387.1	328.0	268.8														
17.	Outer Cooled Surface Outer Race	618.5	568.0	524.6	491.8	440.4	386.0	327.5	268.6														
18.	Bearing Outer Diameter	603.8	560.2	521.3	490.3	422.8	374.8	322.0	267.3														
19.	Chamber Wall (Inner Side)	548.5	515.0	484.7	459.2	359.4	325.6	287.5	246.8														
20.	Loading Bolt (Strut) Root	491.3	458.6	429.2	405.7	354.1	317.1	276.0	233.0														
21.	Shaft (External to Bearing)	574.7	545.4	515.6	490.1	371.5	345.9	306.1	263.4														
	Sump Oil Temperature	581.8	547.4	516.2	490.0	385.0	348.5	307.3	263.3														
	EHD Contact Temperature	584.9	548.6	513.8	500.7	377.7	347.0	303.8	267.4														
	Δt Rise (Input - No. 11)	131.9	76.6	29.3	- 5.5	215.9	154.8	88.9	22.7														

5P4E Input Temperature 500°F  
 7808 Input Temperature 250°F

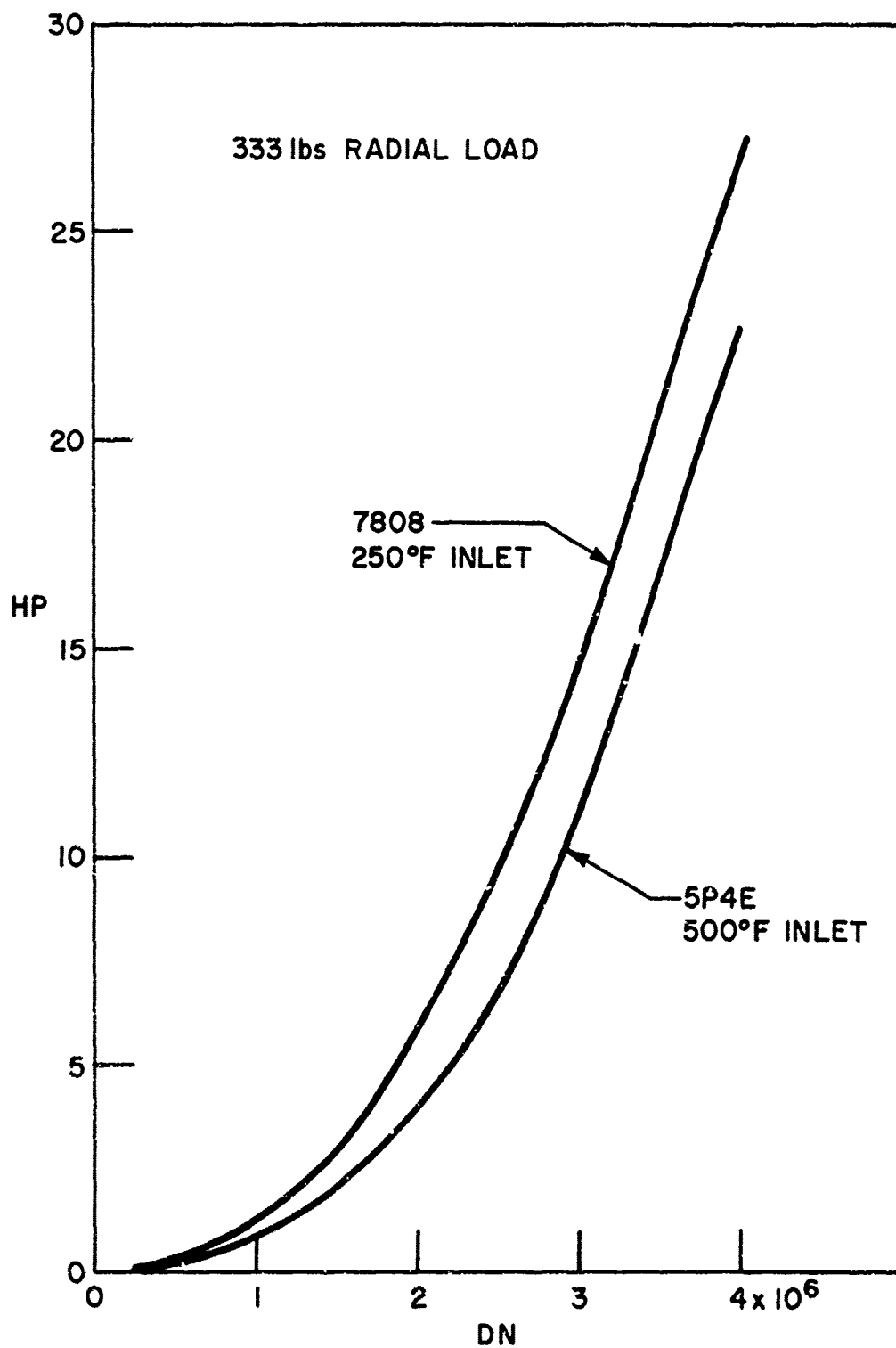


Figure 16. Dual Diameter Roller Bearing Frictional Horsepower Losses

TABLE XIV  
SUMMARY OF CAGE ANALYSIS

Speed(DN) Lube Run No.	4x10 <sup>6</sup>		3x10 <sup>6</sup>		2x10 <sup>6</sup>		1x10 <sup>6</sup>		4x10 <sup>6</sup>		3x10 <sup>6</sup>		2x10 <sup>6</sup>		1x10 <sup>6</sup>	
	5P4E	5P	5P4E	6P	5P4E	7P	5P4E	8P	7808	9P	7808	10P	7808	11P	7808	12P
Cage Clearance (Operating) (Mils)	32.	32.	32.	32.	32.	32.	32.	32.	32.	32.	34.	34.	33.	33.	32.	32.
% Cage Slip from Synchronous Cage Torque (in-lb)	.0006	.0006	.0005	.0005	.0004	.0004	.001	.001	0.31	0.31	.05	.05	.09	.09	.12	.12
From Driving Rollers	48.7	29.7	16.3	6.3	49.9	32.2	18.2	6.8								
At the Land Contact	14.5	10.5	6.3	2.4	19.8	13.7	8.4	3.3								
On Inner Cage Surface	38.6	23.8	11.6	3.3	35.4	21.6	10.8	3.1								
On Outer Cage Surface	4.5	2.8	1.36	.14	4.1	2.5	.59	.4								
On Cage Sides	.51	.33	.10	.04	.32	.23	.14	.06								
Cage Driving Force (lbs) or Max Loaded Roller	10.3	9.6	4.1	4.1	7.4(2)	9.7	7.1	3.9								
Cage Drag Force (lbs) on Unloaded Roller	1.7	1.1	.65	.36	1.97	1.45	.93	.39								

- (1) + Indicates Driving Torque  
- Indicates Drag Torque  
(2) Has 5 rollers in contact  
All others have three.

## 5. EHD PARAMETERS

The outer race to roller contact EHD conditions for unloaded rollers are summarized in Table XV. The outer race to roller conditions for the maximum loaded roller in each case are summarized in Table XVI. The inner race contact EHD conditions for the maximum loaded roller are summarized in Table XVII.

Thin elastohydrodynamic (EHD) oil films (less than  $3.0 \times 10^{-6}$  inches) are predicted with Polyphenyl Ether 5P4E lubricant at 500°F oil inlet temperature for the bearing. The calculated oil inlet temperature at the entrance to the EHD contacts are given in the appropriate tables. The thin EHD films result in low (approximately 0.25) specific film values. Specific film thickness is the ratio of the actual oil film thickness to the root mean square of the contacting surface finishes. Operation at 600°F or higher temperatures with 5P4E lubricant can be expected to result in surface oriented damage or distress prior to any evidence of classical sub-surface oriented fatigue damage.

Somewhat thicker EHD films are predicted with MIL-L-7808 oil applied to the bearing at 250°F. The specific films are approximately 1.0 which is still in the surface related distress region of operation.

The sliding contribution to the total traction values between roller and race contacts is predominant for both contacts of the maximum loaded rollers (Tables XVI and XVII). The rolling contribution to the total traction is significant at the outer race contact of the unloaded rollers, Table XV. All of the rolling contacts are in the low slip (sliding velocities less than 1.0 inches per second) region, with the exception of  $1.0 \times 10^6$  DN operation with 5P4E lubricant.

## 6. DESIGN DRAWINGS

The five drawings (Figures 17-21) completely describe the final design of the dual diameter roller bearing.

TABLE XV

## TRACTION VALUES - OUTER RACE CONTACT - UNLOADED ROLLERS

Oil	DN	% Cage Slip	Rolling Entrain- ment: Velocity (in/sec)	Sliding Velocity (in/sec)	Load P lbs	Coefficient of Trac- tion	Sliding Tract.	Rolling Tract.	Total Tract.	Oil Film Thick.	EHD Contact Temp.	Traction Ratio Roll/ Slide	Specific Film
5P4E	4x10 <sup>6</sup>	.00065	3112	0.0112	139	.7x10 <sup>-5</sup>	.00097	-1.512	1.513	1.41x10 <sup>-6</sup>	585°F	1.0	.249
5P4E	3x10 <sup>6</sup>	.0005	2332	0.187	78	0.03	2.34	-1.42	.920	1.7x10 <sup>-6</sup>	549°F	1.54	.306
5P4E	2x10 <sup>6</sup>	.00038	1555	0.622	35	0.037	1.295	-0.80	.495	1.9x10 <sup>-6</sup>	520°F	1.62	.337
5P4E	1x10 <sup>6</sup>	.0005	762	15.56	8.7	0.034	.296	-0.04	.256	1.7x10 <sup>-6</sup>	501°F	.156	.299
MIL-L 7808	4x10 <sup>6</sup>	.035	3109	.995	139	0.013	1.807	-0.083	1.724	6.2x10 <sup>-6</sup>	378°F	.048	1.09
7808	3x10 <sup>6</sup>	.055	2329	2.70	78	0.017	1.326	-0.10	1.226	6.4x10 <sup>-6</sup>	347°F	.082	1.13
7808	2x10 <sup>6</sup>	.09	1545	9.12	35	0.024	0.84	-0.12	.72	6.7x10 <sup>-6</sup>	304°F	.167	1.19
7808	1x10 <sup>6</sup>	.116	762	15.5	8.7	0.036	0.31	-0.074	.236	6.2x10 <sup>-6</sup>	267°F	.313	1.09

TABLE XVI  
TRACTION VALUES - OUTER RACE CONTACT - MAXIMUM LOADED ROLLERS

Oil	DN	% Cage Slip	Rolling Entrain- ment Velocity (in/sec)	Sliding Velocity (in/sec)	P of lbs.	Traction Coeff.	Sliding Tract.	Rolling Tract.	Total Tract.	Oil Film Thick.	EHD Contact Temp.	Ratio Roll/ Toj	Spec. Film
5P4E	4x10 <sup>6</sup>	.00065	3112	-0.007	294	0.02	-5.88	-.219	-6.099	1.28x10 <sup>-6</sup>	585°F	.036	.226
5P4E	3x10 <sup>6</sup>	.0005	2334	-0.0097	266	0.02	-5.32	-.50	-5.82	1.47x10 <sup>-6</sup>	549°F	.086	.260
5P4E	2x10 <sup>6</sup>	.00038	1556	-0.0053	226	0.016	-3.54	-.08	-3.62	1.49x10 <sup>-6</sup>	520°F	.022	.264
5P4E	1x10 <sup>6</sup>	.0005	778	-.0032	201	0.012	-2.41	-.14	-2.55	1.13x10 <sup>-6</sup>	501°F	.055	.200
MIL-L 7808	4x10 <sup>6</sup>	.035	3110	-.261	269	0.015	-4.04	-.013	-4.17	5.7x10 <sup>-6</sup>	378°F	.031	1.0
7808	3x10 <sup>6</sup>	.055	2333	-.90	260	0.022	-5.72	-.07	-5.79	5.5x10 <sup>-6</sup>	347°F	.012	.97
7808	2x10 <sup>6</sup>	.09	1556	-1.21	218	0.019	-4.14	-.016	-4.30	5.3x10 <sup>-6</sup>	304°F	.037	.94
7808	1x10 <sup>6</sup>	.116	778	-.78	191	0.012	-2.29	-.009	-2.38	4.2x10 <sup>-6</sup>	267°F	.038	1.09

TABLE XVII

## TRACTION VALUES - INNER RACE CONTACT - MAXIMUM LOADED ROLLERS

Oil	$\frac{Dm}{10^6}$	% Cage Slip	Rolling Entrain- ment Velocity (in/sec)	Sliding Velocity (in/sec)	$P_{ij}$ lbs	Trac- tion Coeff.	Sliding Tract.	Rolling Tract.	Total Tract.	Oil Film Thick.	EHD Contact Temp.	Ratio Roll/ oj	Spec. Film
5P4E	$4 \times 10^6$	.00065	6224	.05	155	0.028	4.340	-0.145	4.195	$2 \times 10^{-6}$	585°F	0.033	.355
5P4E	$3 \times 10^6$	.0005	4668	.013	188	0.021	3.948	-0.194	3.754	$2.5 \times 10^{-6}$	549°F	0.052	.449
5P4E	$2 \times 10^6$	.00038	3112	.0065	191	0.013	2.480	-0.110	2.37	$3.0 \times 10^{-6}$	520°F	0.046	.532
5P4E	$1 \times 10^6$	.0005	1556	.0047	193	0.0086	1.659	-0.059	1.60	$2.2 \times 10^{-6}$	501°F	0.036	.396
MIL-L 7808	$4 \times 10^6$	.035	6220	2.60	131	0.0258	3.379	-0.160	3.219	$9.6 \times 10^{-6}$	378°F	0.049	1.70
7808	$3 \times 10^6$	.055	4666	1.91	182	0.022	4.004	-0.087	3.917	$9.3 \times 10^{-6}$	347°F	0.022	1.64
7808	$2 \times 10^6$	.09	3112	1.65	183	0.016	2.928	-0.116	2.812	$9.4 \times 10^{-6}$	304°F	0.041	1.67
7808	$1 \times 10^6$	.116	1556	1.06	182	0.0087	1.58	-0.09	1.49	$7.8 \times 10^{-6}$	267°F	0.06	1.38

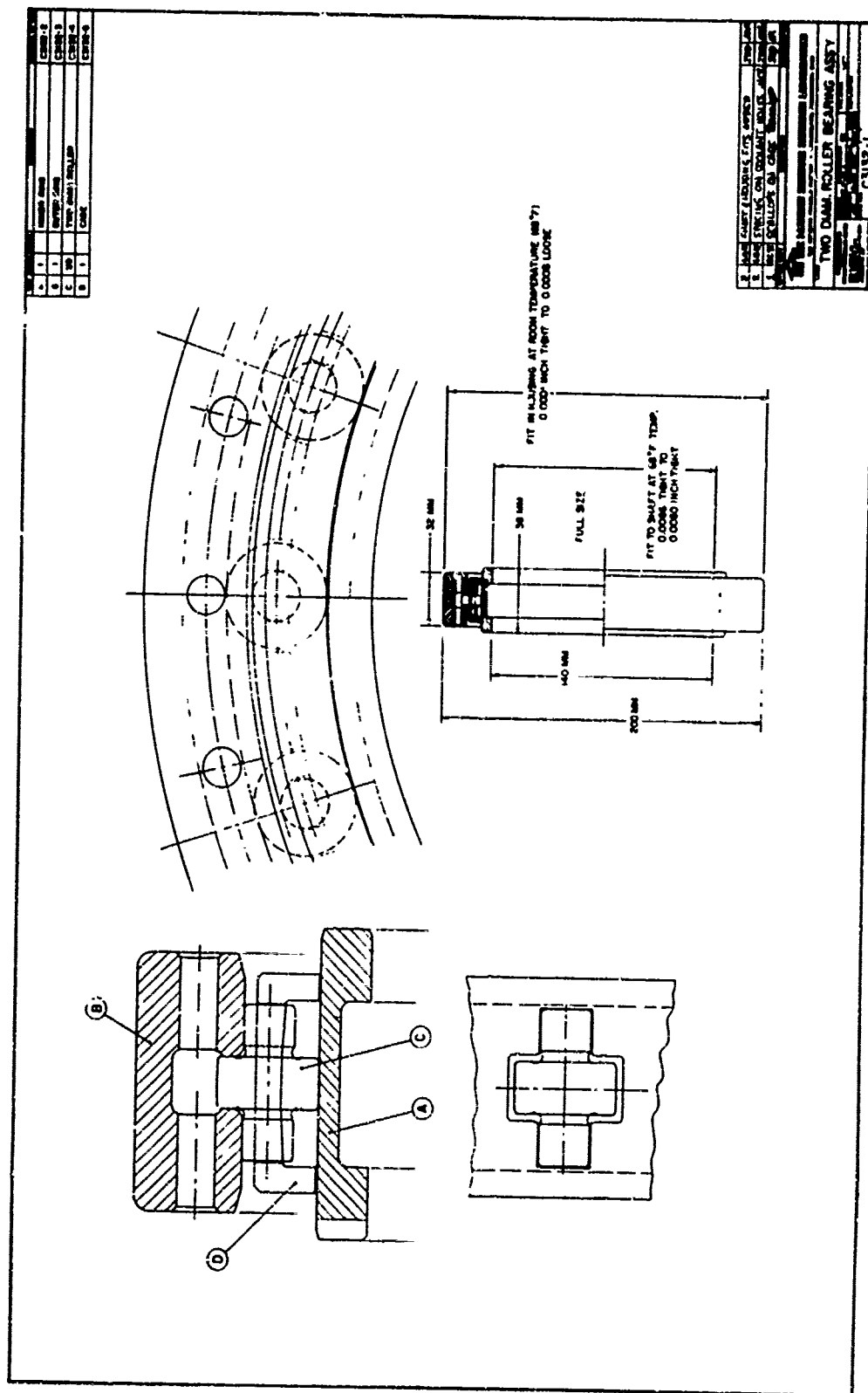
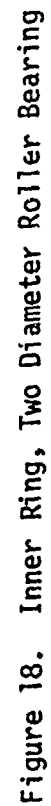


Figure 17. Two Diameter Roller Bearing Assembly





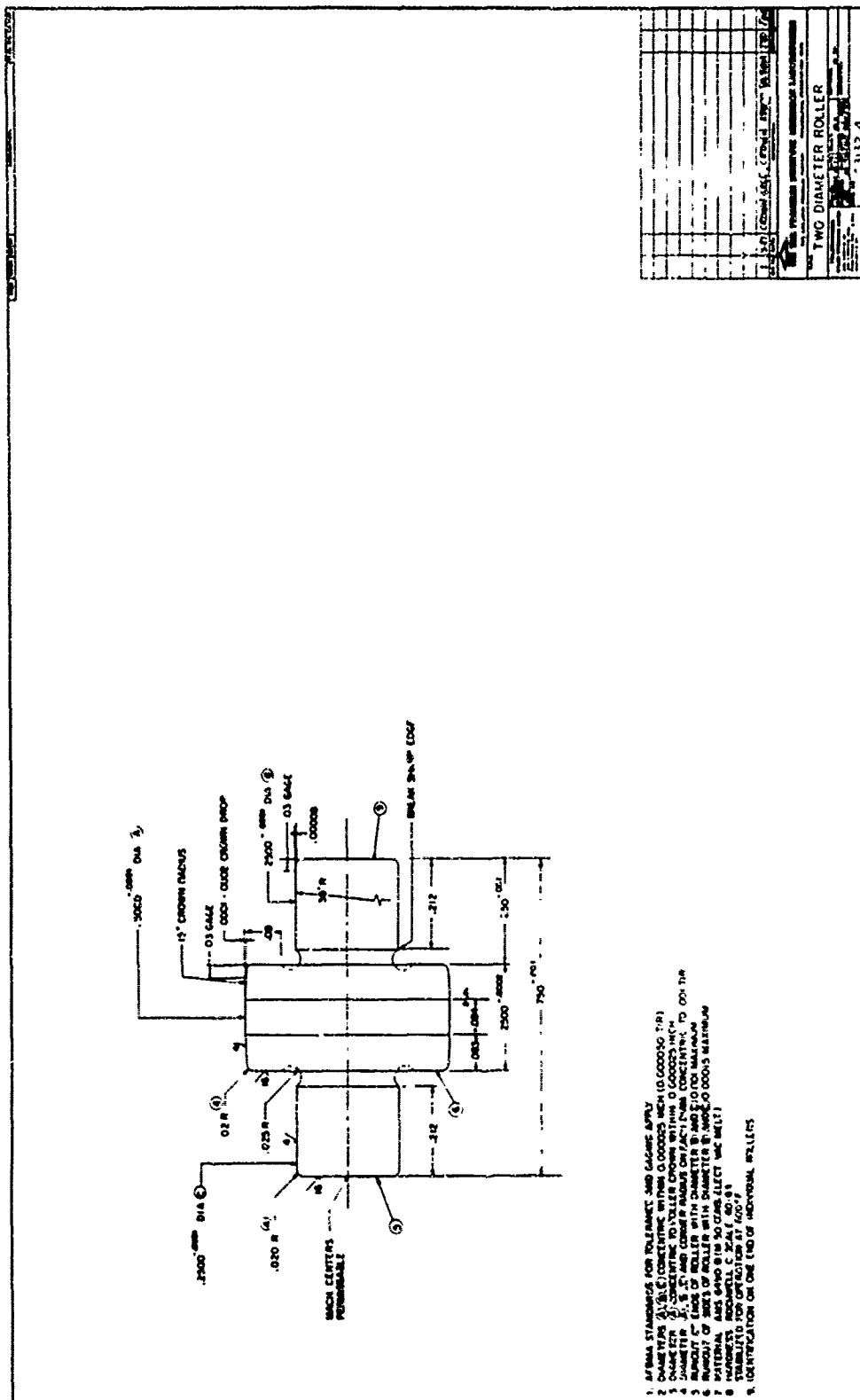
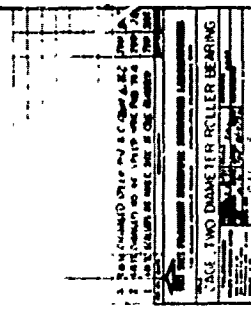


Figure 20. Two Diameter Roller



	1	2	3	4	5	6	7	8	9	10	11	12	13	14	15	16	17	18	19	20	21	22	23	24	25	26	27	28	29	30	31	32	33	34	35	36	37	38	39	40	41	42	43	44	45	46	47	48	49	50	51	52	53	54	55	56	57	58	59	60	61	62	63	64	65	66	67	68	69	70	71	72	73	74	75	76	77	78	79	80	81	82	83	84	85	86	87	88	89	90	91	92	93	94	95	96	97	98	99	100
1	1	2	3	4	5	6	7	8	9	10	11	12	13	14	15	16	17	18	19	20	21	22	23	24	25	26	27	28	29	30	31	32	33	34	35	36	37	38	39	40	41	42	43	44	45	46	47	48	49	50	51	52	53	54	55	56	57	58	59	60	61	62	63	64	65	66	67	68	69	70	71	72	73	74	75	76	77	78	79	80	81	82	83	84	85	86	87	88	89	90	91	92	93	94	95	96	97	98	99	100
2	1	2	3	4	5	6	7	8	9	10	11	12	13	14	15	16	17	18	19	20	21	22	23	24	25	26	27	28	29	30	31	32	33	34	35	36	37	38	39	40	41	42	43	44	45	46	47	48	49	50	51	52	53	54	55	56	57	58	59	60	61	62	63	64	65	66	67	68	69	70	71	72	73	74	75	76	77	78	79	80	81	82	83	84	85	86	87	88	89	90	91	92	93	94	95	96	97	98	99	100
3	1	2	3	4	5	6	7	8	9	10	11	12	13	14	15	16	17	18	19	20	21	22	23	24	25	26	27	28	29	30	31	32	33	34	35	36	37	38	39	40	41	42	43	44	45	46	47	48	49	50	51	52	53	54	55	56	57	58	59	60	61	62	63	64	65	66	67	68	69	70	71	72	73	74	75	76	77	78	79	80	81	82	83	84	85	86	87	88	89	90	91	92	93	94	95	96	97	98	99	100
4	1	2	3	4	5	6	7	8	9	10	11	12	13	14	15	16	17	18	19	20	21	22	23	24	25	26	27	28	29	30	31	32	33	34	35	36	37	38	39	40	41	42	43	44	45	46	47	48	49	50	51	52	53	54	55	56	57	58	59	60	61	62	63	64	65	66	67	68	69	70	71	72	73	74	75	76	77	78	79	80	81	82	83	84	85	86	87	88	89	90	91	92	93	94	95	96	97	98	99	100
5	1	2	3	4	5	6	7	8	9	10	11	12	13	14	15	16	17	18	19	20	21	22	23	24	25	26	27	28	29	30	31	32	33	34	35	36	37	38	39	40	41	42	43	44	45	46	47	48	49	50	51	52	53	54	55	56	57	58	59	60	61	62	63	64	65	66	67	68	69	70	71	72	73	74	75	76	77	78	79	80																				

## SECTION V

### DUAL DIAMETER BEARING FABRICATION

Six prototype test bearings Figure 22 were fabricated to the design drawings (Figures 17-21) by the Bower Bearing Div., Federal-Mogul Corporation, Detroit, Mich. A summary of the six prototype bearing dimensional sizes and variations are given in Table XVIII.

The inner race roller path circularity and contour for test bearing No. 3 are shown in Figures 23 and 24 and are representative of all of the bearings. The circularity and raceway contour of the outer race roller path are shown in Figures 25 and 26 for test bearing No. 3.

The roller design for the dual diameter roller, Figure 20, is not an easy shape to produce. However, the test bearing rollers were centerless ground and crowns were maintained within drawing limits on all three roller portions, as shown by the typical roller traces, Figure 27.

All material specifications, silver plating, balance, etc., are given in the design drawings, Figures 17-21. All prototype bearings met or exceeded the design drawing requirements.

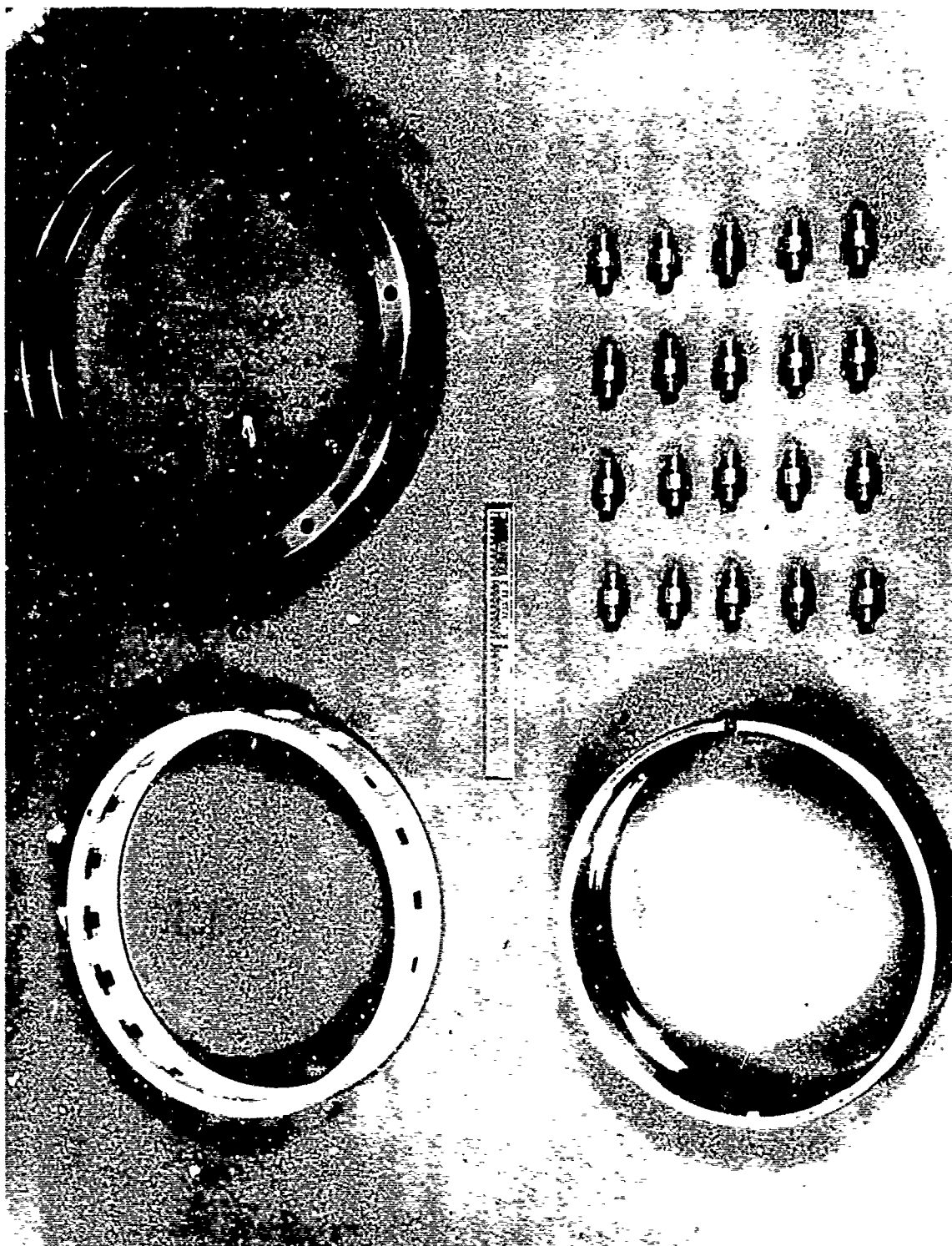


Figure 22. Dual Diameter Roller Brg. Ass'y.

Table XVIII

Serial Number	A1	B2	C3	D4	E5	F6
<u>Inner Races - C3132-2</u>						
O.D. Size	6.00384	6.00385	6.00395	6.00396	6.00385	6.00390
Taper	0.000020	0.00040	0.000070	0.000070	0.000020	0.000038
Out-of-Round	0.000050	0.000050	0.000050	0.000050	0.000050	0.000050
Bore Land	5.51160	5.51160	5.51165	5.51170	5.51165	5.51165
Bore Land	5.57160	5.51165	5.57165	5.51170	5.51165	5.51165
Out-of-Round	0.000050	0.00015	0.00015	0.00015	0.00015	0.00015
Concentric	0.00010	0.00025	0.00015	0.00013	0.00012	0.00010
Width	1.4955	1.4951	1.4955	1.4955	1.4954	1.4954
O.D. Surface Finish	2AA	2-1/2/3AA	2/2-1/2AA	1-1/2/2AA	1-1/2/2AA	2AA
<u>Outer Races - C3132-2</u>						
O.D. Size	7.8739	7.8736	7.8738	7.8736	7.8739	7.8738
Taper	6.001	0.0001	0.0001	0.0001	0.0001	0.0001
Out-of-Round	0.0001	0.001	0.0001	0.0001	0.0001	0.0001
I.D. Track	6.76416	6.76414	6.76416	6.76420	6.76416	6.76412
Out-of-Round	0.00015	0.00015	0.00015	0.00015	0.00015	0.0001
Taper	0.000050	0.000050	0.000050	0.000050	0.000050	0.000050
Concentric	0.00010	0.000050	0.00015	0.00015	0.00010	0.0010
Flange Opening	0.2508	0.2508	0.2512	0.2508	0.2508	0.2511
Parallel Face to Wall	0.00015	.0001	0.00015	0.00015	0.00015	0.00015
Parallel Wall to Wall	0.0001	0.0001	0.0001	0.0001	0.00015	0.0001
I.D. Surface Finish	SAA	4AA	SAA	SAA	3-1/2/4AA	4/5AA
Flange Surface Ion	2AA	2-1/2/3AA	2/2-1/2AA	1-1/2/2AA	1-1/2/2AA	2AA
<u>Cage - C3132-5</u>						
O.D. Size (A)	6.6436/6.6442	6.6428/6.6434	6.6423/6.6438	6.6426/6.6430	6.6427/6.6433	6.6422/6.6428
O.D. Size (B)	6.6434/6.6444	6.6427/6.6432	6.6424/6.6436	6.6427/6.6432	6.6424/6.6433	6.6423/6.6424
O.D. Out-of-Round	.0006/.001	.0006/.0005	.0013/.0012	.0004/.0005	.0006/.0005	.0003/.0001
I.D. Size (A)	6.0404/6.0415	6.0408/6.0412	6.0408/6.0414	6.0410/6.0417	6.0408/6.0412	6.0412/6.0422
I.D. Size (B)	6.0408/6.0412	6.0408/6.0412	6.0404/6.0412	6.0409/6.0413	6.0405/6.0412	6.0412/6.042
Concentric ID/OD	.001 TIR	.001 TIR	.001 TIR	.0012 TIR	.0012 TIR	.0008 TIR
Squareness	.001 TIR	.001 TIR	.0011 TIR	.001 TIR	.00105 TIR	.0008 TIR
Width	1.057	1.0572	1.0565	1.055	1.055	1.055
Cage Balance GM/cm @ 500 rpm	0.2-0.3	0.3-0.2	0.4-0.3	0.2-0.2	0.5-0.3	0.5-0.1
Pkt. Flg. from Side	-.0004	-.0004	-.0004	-	-	-
<u>Rollers - C3132-4</u>						
Large O.D.	.5000/.49995					
Out-of-Round	.000050 max.					
Width	.2500/.2501					
Width Sq. w 5 OD	.00010 max.					
Wt/l to .2500	.00010 max.					
Small OD	.249975/.249925					
Out-of-Round	.000050 max.					
Length	.2500/.24901					
Face Lg. w .25 OD	.0012 max.					
Overall Length	.7500/.7490					
3 Dia's Concentric	0.000050 TIR					
Finish Dia's	3 RMS					
Finish End	5 RMS					
ASSEMBLED DIAM CLEARANCE	0.0103	0.0103	0.0102	0.0102	0.0103	0.0102

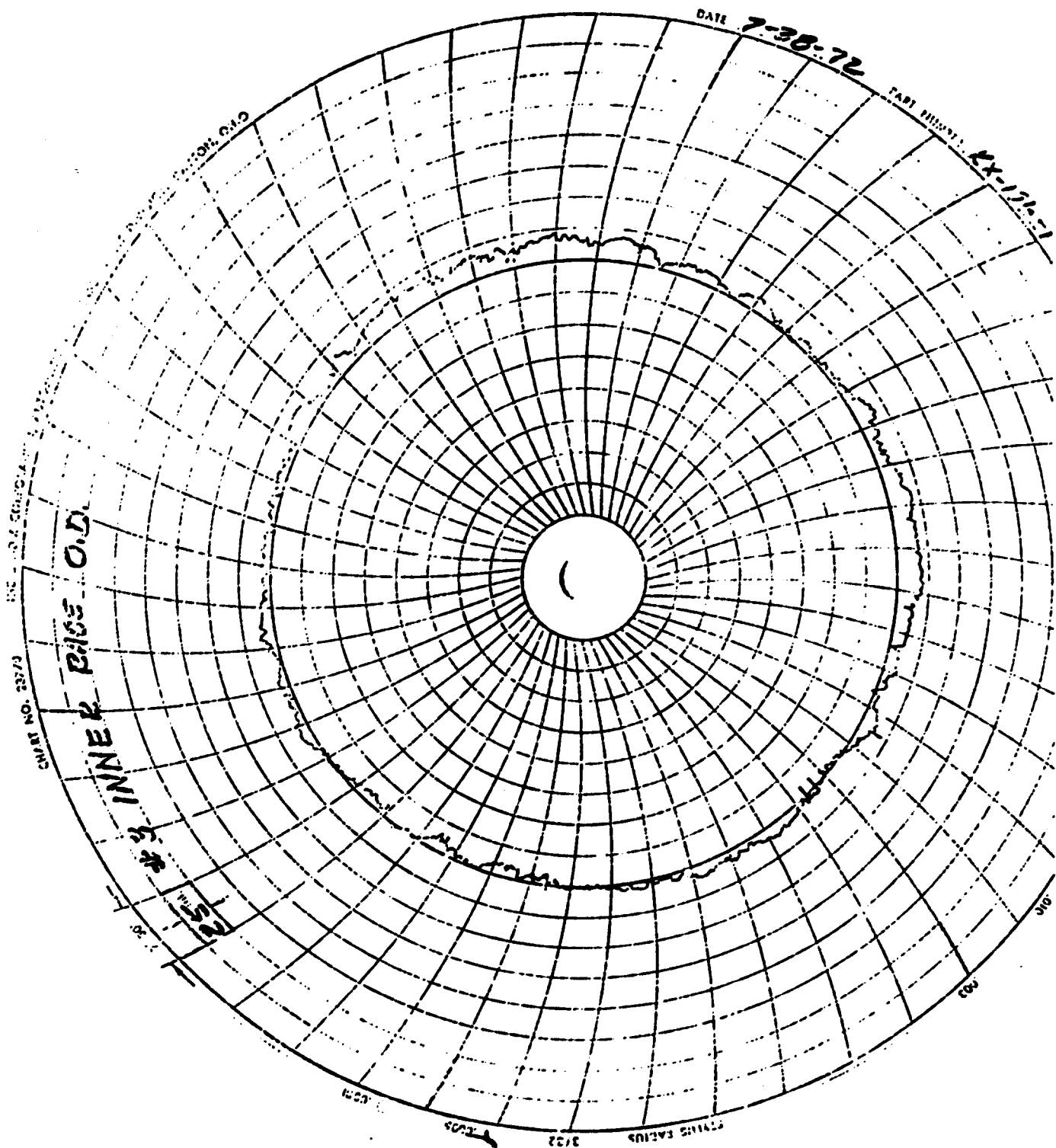
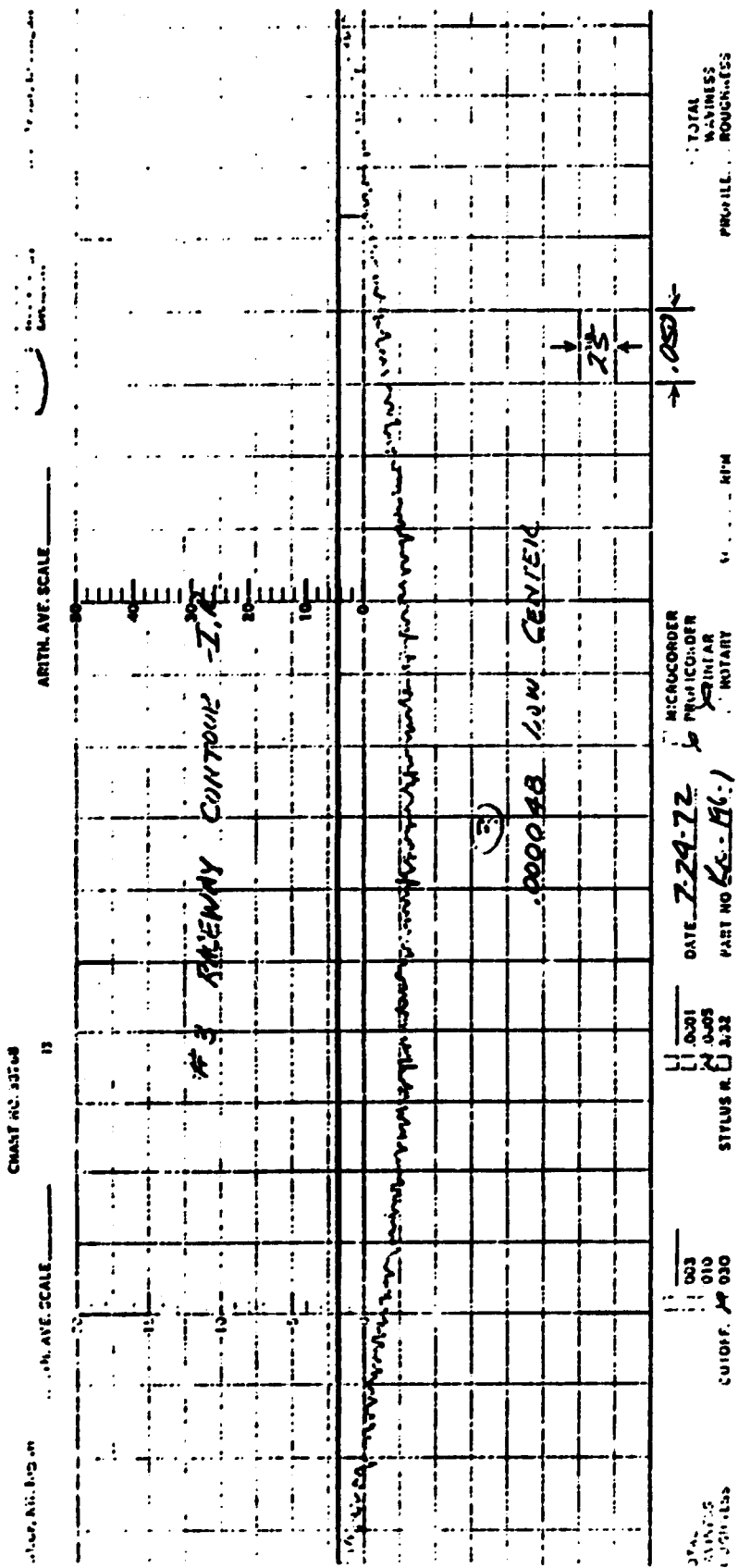


Figure 23. Bearing No. C3 Inner Race Circularity



**Figure 24. Bearing llo. C3 Inner Raceway Contour**







## SECTION VI

### DUAL DIAMETER BEARING TESTS

#### 1. TEST RIG

The dual diameter bearing testing was performed at Midwest Aero Industries, Div. Pure Carbon Co., St. Mary's, Pa., on an existing 250 hp drive test stand with an eddy current clutch and speed increaser gear box. The test rig is shown in Figures 28 and 29. A cross-sectional drawing of the rig is given in Figure 30. The numbered locations correspond to the thermocouple temperature readings of the actual test data. All of the original test log sheets are contained in the Appendix.

The test rig consists of a short hollow shaft supported by two 75 mm bore slave roller bearings. The dual diameter roller bearing, 140 mm bore, is supported midway between the two slave bearings. Radial load is applied by pulling upward on the test bearing housing through a large ring as shown on Figure 30. Oil to the dual diameter bearing is introduced through three orifices, location No. 1, and jetted to a scoop on the test shaft. The oil then travels to the recess under the dual diameter bearing, up through the bearing, out into the rig cavity, and exits the drain through points 2 and 4. The test shaft is driven by a splined quill shaft between the rig and the speed increaser gear box. The area for the quill shaft drive is shown with the cover removed in Figure 28. The entire test head shown in Figure 30 and a transition cone covering the quill drive shaft are cantilevered from the speed increaser gear box, as can be seen in Figures 28 and 29.

Two prototype dual diameter roller bearings were tested under the current contract. The first bearing was operated with MIL-L-7808 oil at approximately 250°F inlet temperature to gain a feel for the power losses and general operation of the bearing with a known lubricant. The first test bearing was then operated with Polyphenyl Ether 5P4E lubricant at approximately

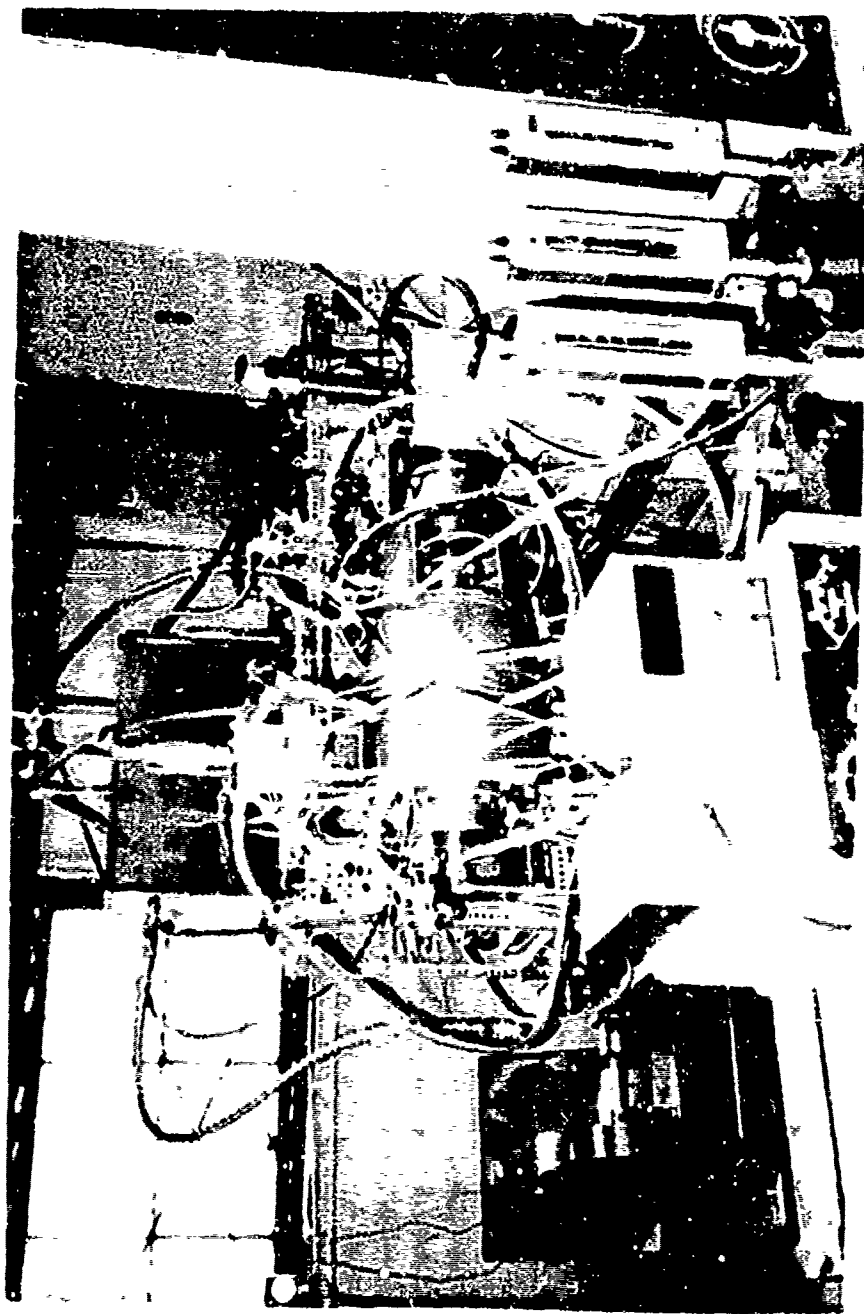


Figure 28. Dual Diameter Roller Bearing Test Stand

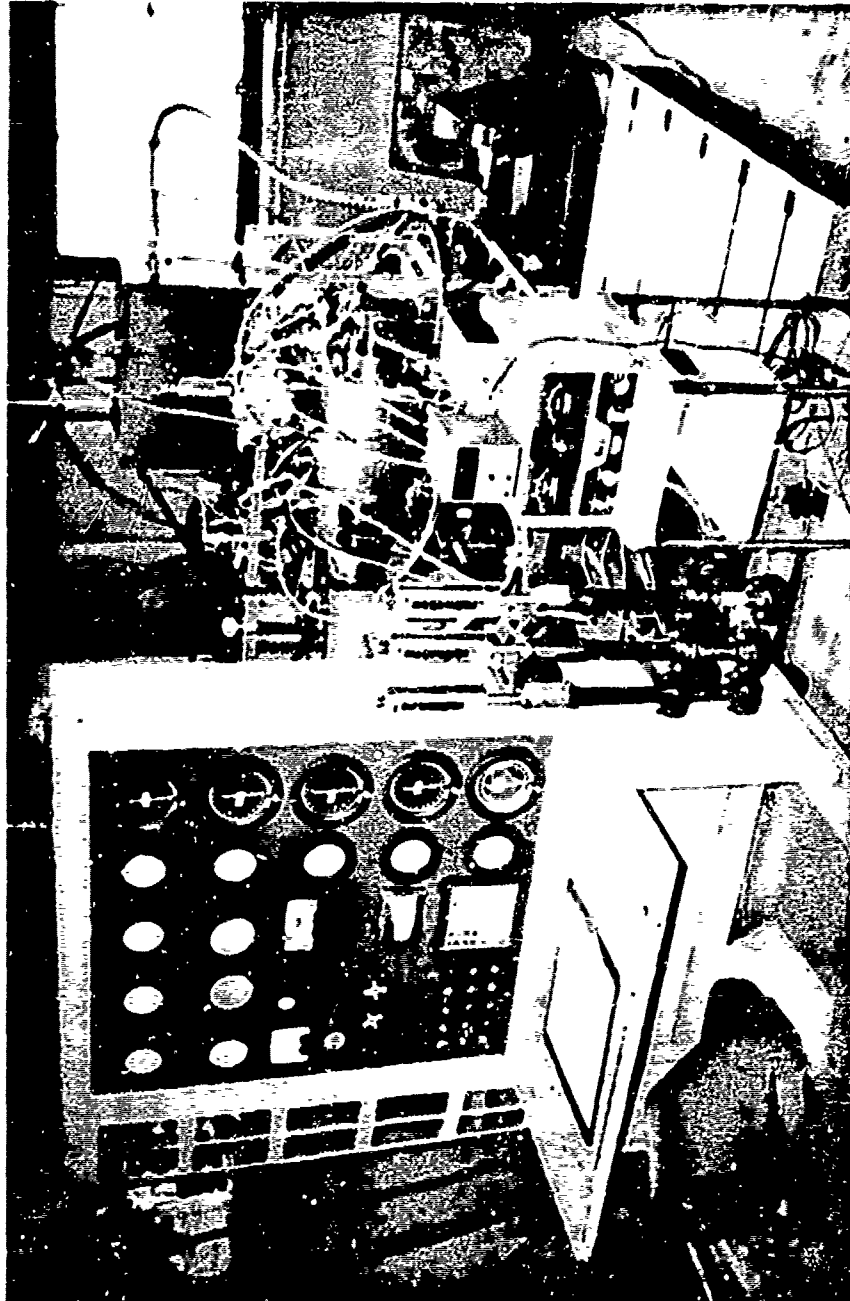


Figure 29. Dual Diameter Roller Bearing Instrumentation

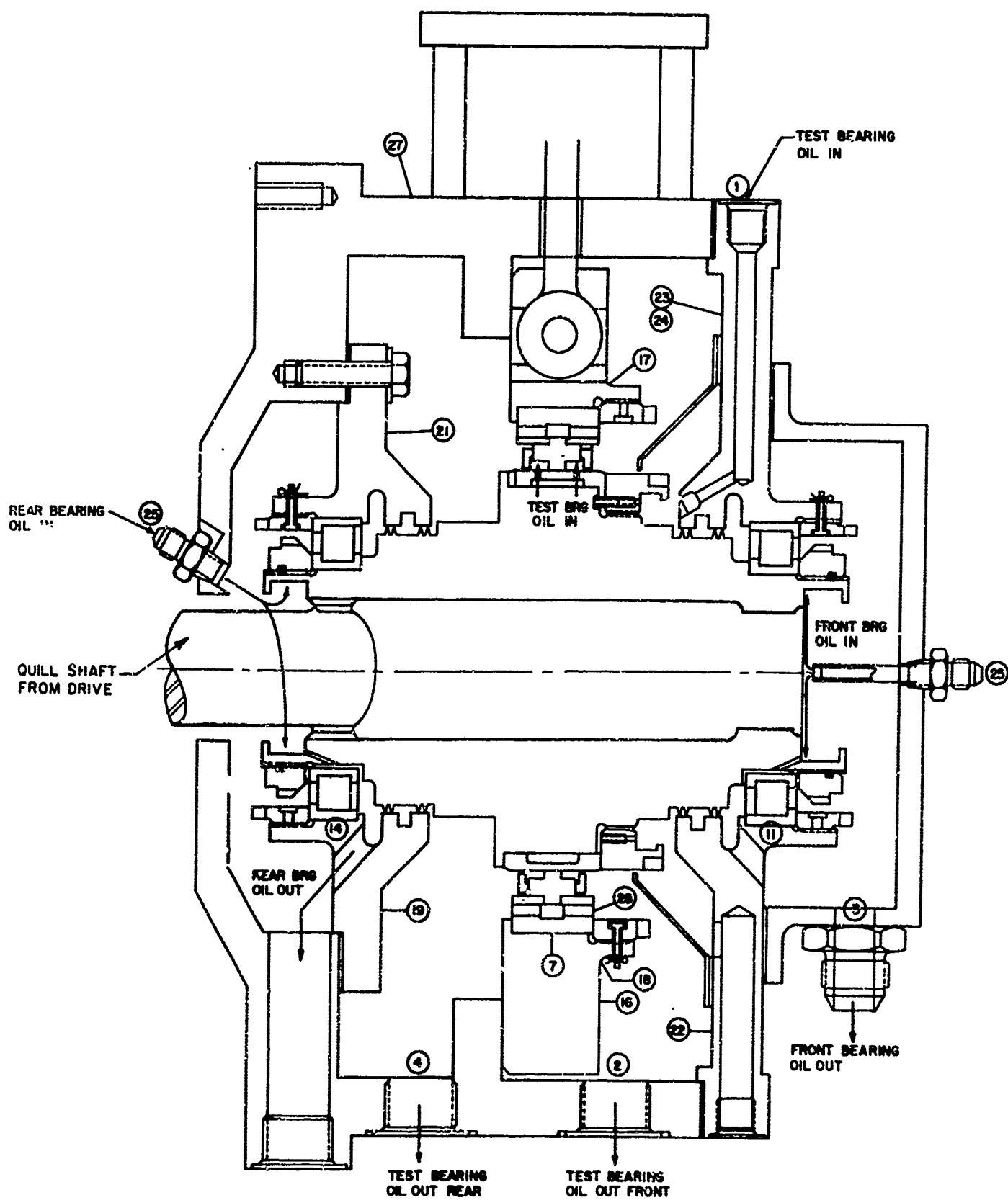


Figure 30. Cross Section of Dual Diameter Bearing Test

500°F oil inlet temperatures up to and including  $3.25 \times 10^6$  DN operation. The second test bearing was operated with Polyphenyl Ether 5P4E lubricant at approximately 500°F oil inlet temperature and successfully completed 30 minutes of continuous operation at  $3.5 \times 10^6$  DN (25,000 rpm) with stabilized temperatures. The second test bearing was then subjected to a series of rapid acceleration/deceleration tests and removed for visual inspection.

## 2. MIL-L-7808, TEST BEARING A1

A data summary sheet for the operation of the first test bearing s/n No. A1 is shown in Table XIX. The bearing outer race and front and rear drain oil temperature increases as a function of bearing speed for the testing shown in Figure 31.

Twenty-five minutes of successful operation at  $3.50 \times 10^6$  DN was obtained (see runs 49 and 50). The bearing was removed from the test cell and visually inspected. The inner race, rollers and outer race showed some discoloration due to operating at 300°F average outer race temperatures. The rolling surfaces looked to be in excellent condition with only the normal amount of burnishing to be expected after completion of 13 hours and 40 minutes accumulated running time.

The cage was found to be badly worn on the inner land riding diameters over approximately a 35 degree arc on both lands. The worn areas had penetrated the silver plating and significantly deformed the steel. The worn areas were directly under one of the cage pins used for cage speed instrumentation. It appeared that the cage had excessive mass unbalance in operation which led to the localized wear on the inner land surfaces. The s/n No. A1 cage was not reused. The inner race, outer race and roller complement however were in excellent condition and were reused for the second set of tests.

## 3. 5P4E, TEST BEARING A1

s/n No. A1 bearing with the s/n No. B2 cage was assembled in the test rig for the high temperature Polyphenyl Ether test. A data summary sheet

DATA SUMMARY SHEET FIRST TEST BEARING - MIL-L-7808 OIL

70

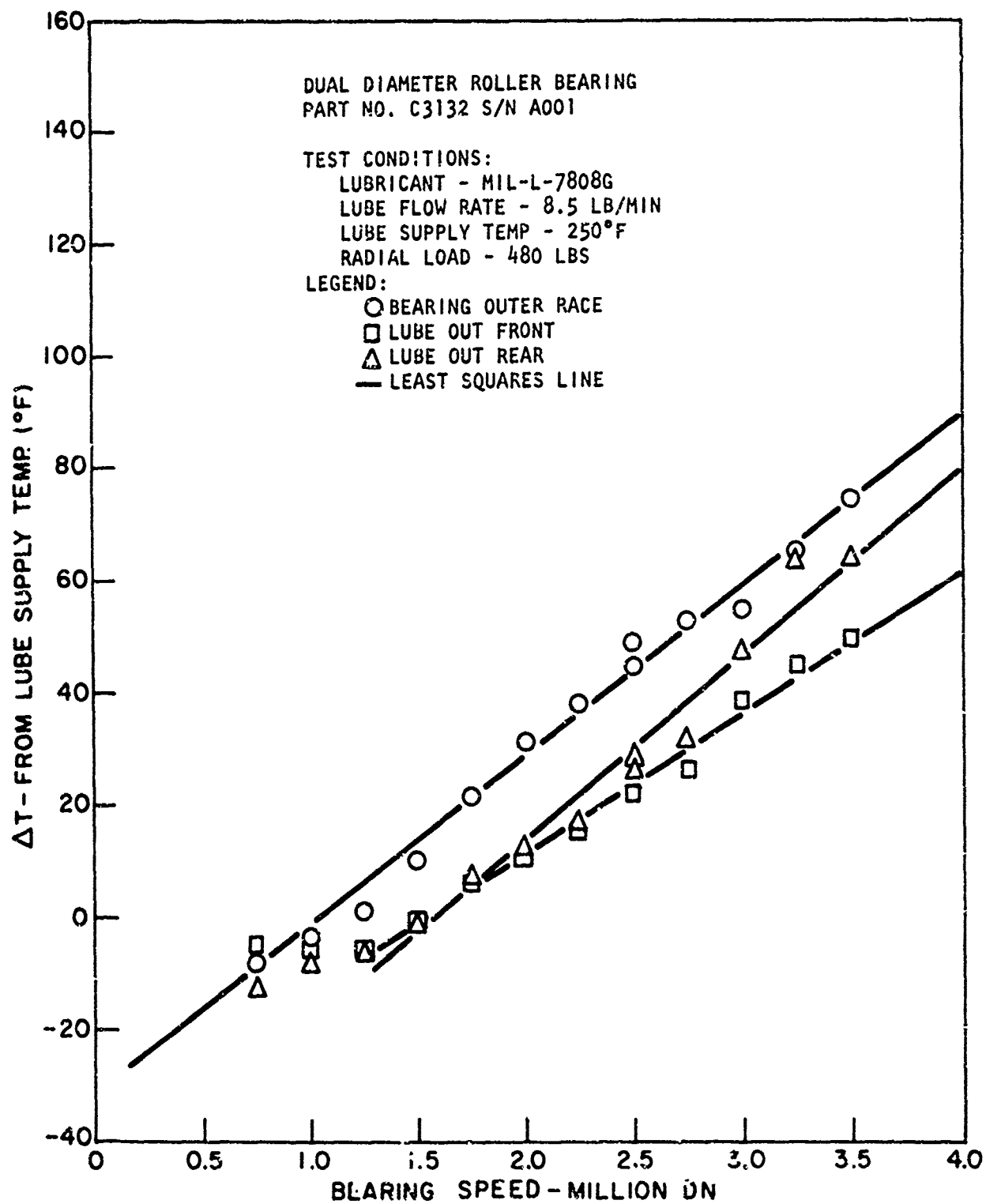


Figure 31. Test Bearing No. 1,  $\Delta T$   
vs. Speed, MIL-L-7808 G

is given in Table XX. The temperature differentials in the bearing for the outer race and drain temperatures are shown on Figure 32. The bearing was initially operated up to and including  $3.0 \times 10^6$  DN operation. At this point the Polyphenyl Ether lubricant was being pumped back through the quill shaft Figure 30, to the gear box and mixing with MIL-L-7808 oil in the gear box system. The rig was shut down and lube system changed so that the gear box as well as the test head would operate on 5P4E lubricant and would avoid the loss of excessive amounts of the test oil. Testing was then resumed and resulted in the second set of curves as shown on Figure 32.

Successful operation of the test bearing was accomplished up to and including  $3.25 \times 10^6$  DN operation. After approximately 10 minutes operation at  $3.50 \times 10^6$  DN operation (run No. 86), the bearing failed abruptly as evidenced by a seizure and a dead stop of the test shaft. The failed test bearing was then removed for visual examination. The inner race had separated and formed into two circumferential halves approximately in the center of the race. The rings had also snapped open at a location corresponding to one of the key slots as shown in Figure 33. A considerable amount of debris was trapped between the inner race cavity and the shaft. Figure 34 is a photograph of the rollers, cage and outer race assembly still in the outer race loading ring. The rollers all had a flat surface on the major diameter which presumably was caused when the rollers locked up and braked the inner race to a complete halt. Several of the rollers are shown on Figure 35. All of the rollers had at least one of the small diameters separated from the body of the roller as shown in Figure 35 and in several cases both minor diameters had been separated. Subsequent metallurgical examination of the fractured surfaces supports the fact that the small diameters were twisted or torqued out of the major diameter. They were not reversed bending fatigue failures. Complete seizure of the inner race creating sufficient friction to grind flat from the rollers (as shown in Figure 35) would create tremendous torques on the minor roller diameters. The outer race is shown in Figure 36 and the cage is shown in Figure 37. The cage suffered serious distortion as would be anticipated.

DATA SUMMARY SHEET FIRST TEST BEARING - POLYPHENYL ETHER 5P4E

PURE CARBON CO-DATA SUMMARY SHEET

73

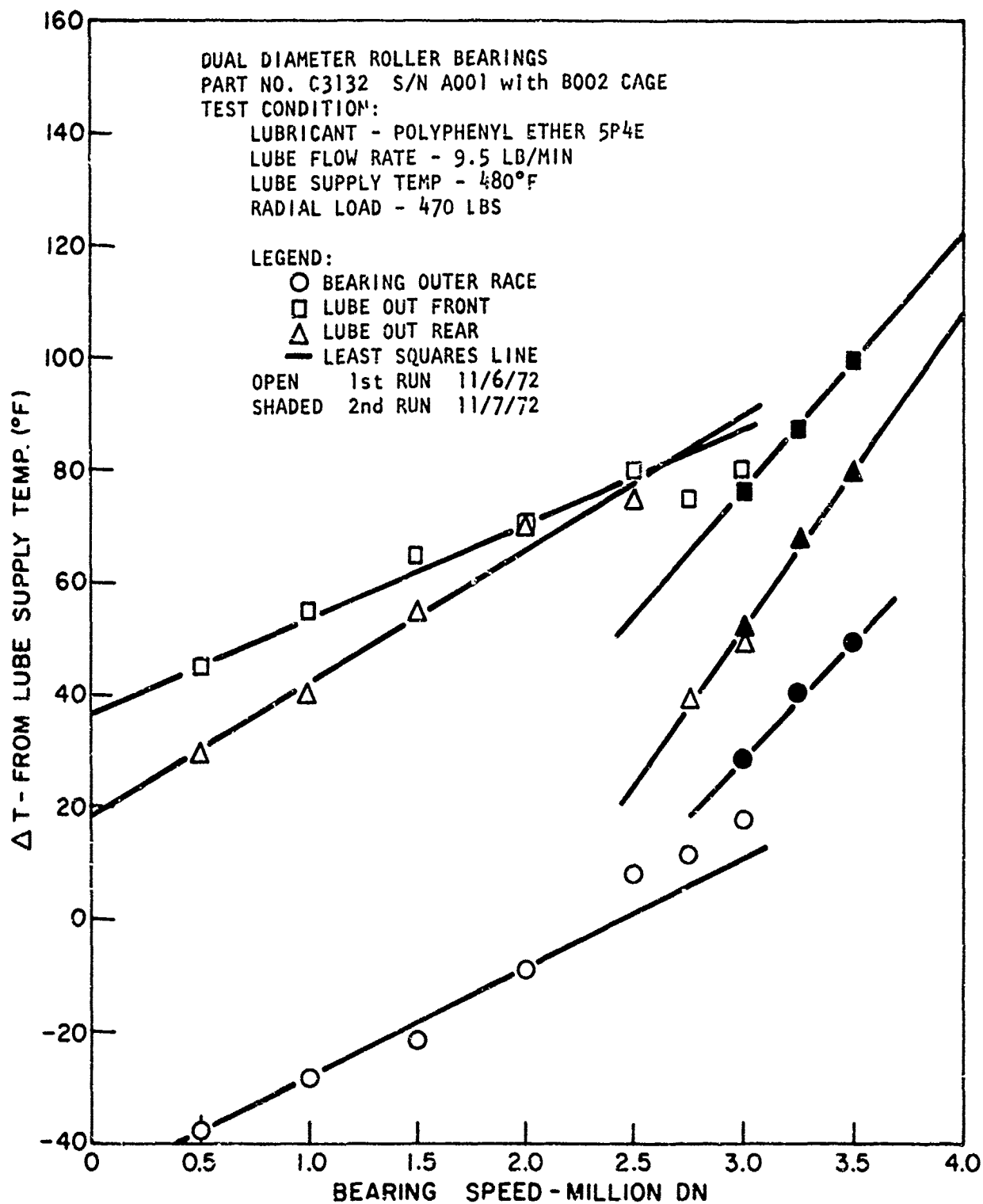


Figure 32. Test Bearing No. 1,  $\Delta T$  vs. Speed, Polyphenyl Ether, 5P4E



Figure 33. Test Bearing No. 1,  
Inner Race Failure



Figure 34. Test Bearing No. 1 Outer Race  
Cage Roller Assembly Failure

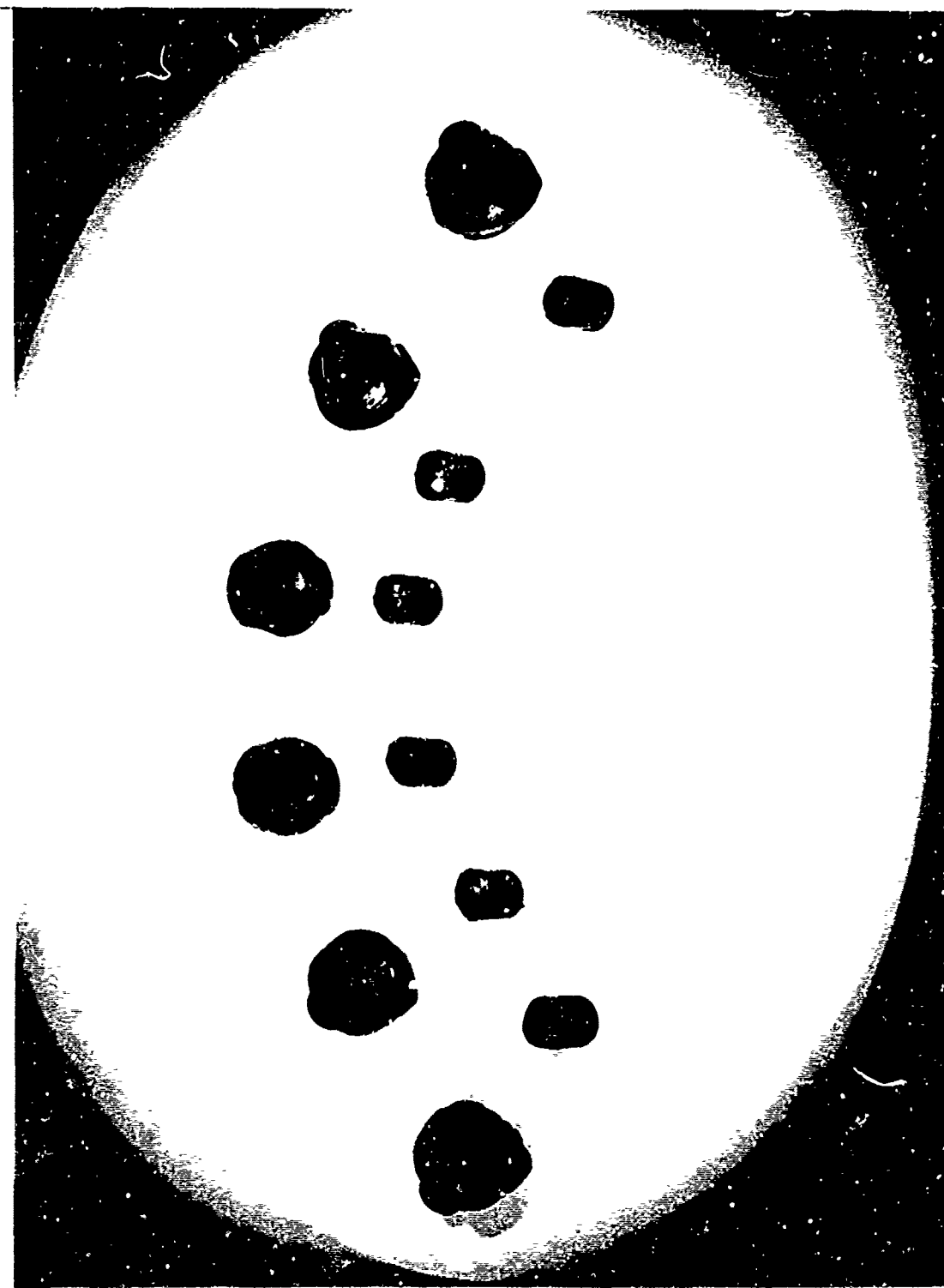


Figure 35. Failed Rollers



Figure 36. Test Bearing No. 1 Outer Ring Failure



Figure 37. Test Bearing No. 1 Cage Failure

The test bearing A1 accumulated a total of 24 hours operation at various speeds of which 10 hours and 20 minutes were with the Polyphenyl Ether lubricant at high temperature. The failure of the inner race, Figure 33, can be explained by two possible failure modes, the first being thermal lockup of the bearing where the growth of the inner race both thermally and due to centrifugal forces exceeds the growth rate of the outer race resulting in internal diametral preload. Roller bearings are exceptionally stiff and small amounts of diametral preload (on the order of 0.0002 inches or more) can result in very high roller loadings. Greatly increased roller loadings at the inner race contact (see Figure 17) would then undoubtedly fail in reverse bending fatigue. The second possible failure mode is that sufficient clearance did remain in the bearing and that failure of the inner race was due entirely to reverse bending fatigue. The finite element analysis of the inner ring as shown on Figure 13 and summarized in Table IX did not indicate that excessive stress variation would be anticipated at  $3.5 \times 10^6$  DN operation. Therefore, thermal lockup was suspected. The fact that the bearing did operate for approximately 10 minutes at the higher speed level, however, is not indicative of thermal lockup. Thermal lockup occurs very rapidly after an increase of speed.

The concern over thermal lockup was resolved by additional thermal analysis of the test bearing operating conditions. The initial thermal gradients in the bearing for design purposes did not include any effects of external energy being introduced into the system because of dissipation in the slave bearing. Table XXI shows the results of the thermal analysis with external energy introduced at node 21 on the shaft surface external to the test bearing. Also the effect of insulation around the outer diameter or outer surface of the test head was introduced into this analysis. The results of the improved thermal analysis for the actual load, speed and lubricant supply conditions of the test agree closely with the observed temperatures of Table XX. The outer race temperature per analysis (node 18), was 527.86°F as compared to average observed outer race temperatures of 520°F. The total  $\Delta T$  to the oil by analysis in Table XXI was (node 11)

TABLE XXI

Thermal Analysis of First Test Bearing Conditions with 5P4E

THE CONVERGED TEMPERATURE DISTRIBUTION: (DEG F.) IS AS FOLLOWS:

1	INNER SHAFT COULANT	=	695.516692
2	INNER SHAFT SURFACE	=	545.986656
3	OUTER SHAFT SURFACE AT BEARING	=	522.194206
4	INNER RACE AT SHAFT	=	540.528114
5	UNDER-CUT SURFACE OF INNER RACE	=	544.477996
6	UNDER RACE COULANT	=	500.870003
7	INNER RACE BEYOND ROLLER CONTACT	=	550.633530
8	CAGE AT THE LAND	=	576.809593
9	CAGE INNER SURFACE	=	542.211388
10	CAGE OUTER SURFACE	=	581.600281
11	INTERNAL LUBRICANT TO BEARING	=	555.119461
12	ROLLERS	=	586.775314
13	INNER RACE AT ROLLERS	=	550.068855
14	INNER SURFACE OF OUTER RACE	=	647.625595
15	INNER COOLED SURFACE OUTER RACE	=	546.366028
16	OUTER RACE LUBRICANT	=	545.315437
17	OUTER COOLED SURFACE OUTER RACE	=	544.274139
18	BEARING OUTER DIAMETER	=	527.860451
19	CHAMBER WALL (INNER SIDE)	=	513.459312
20	LOADING BOLT (STRUT) ROOT	=	474.929092
21	SHAFT (EXTERNAL TO BEARING)	=	575.953255
	BULK TEMPERATURE RISE OF LUBRICANT	=	41.275596
	AVERAGE BULK OIL TEMPERATURE	=	528.370239

555° less oil inlet temperature of 470° resulting in an 85°  $\Delta T$  to the oil. This compares very favorably to the 90° average of the oil out front and oil out rear of Table XX. The calculated internal diametral clearance in the bearing under the thermal gradients shown in Table XXI is 0.0051 inches. This number includes all thermal and centrifugal growths. A number of variations in the assumptions of the thermal analysis such as percentage air oil mixture, etc. were tried and found to have little effect on the thermal gradients in the bearing. Therefore the conclusion was reached that the bearing did not fail due to thermal lockup but rather failed due to reverse bending fatigue of the undercut inner race. The finite element analysis summarized in Table IX would indicate that the stress variations with roller loading should not have exceeded the long term life value in reverse bending fatigue. However, the test bearing at the point of failure had experienced  $39.7 \times 10^6$  cycles of stress or roller load variations between rollers and inner races with both MIL-L-7808 and the 5P4E lubricant. The values were essentially equal with each type of oil. The decision was made to proceed with testing of the second bearing on the assumption that thermal lockup was not the failure mode and to limit the bearing load to no more than 500 pounds so as not to significantly increase the danger of failure due to reverse bending fatigue.

#### 4. 5P4E, TEST BEARING C3

The second test bearing, Serial No. C3, was assembled in the rig for high temperature testing with 5P4E lubricant. A summary data sheet of the test is given in Table XXII and the  $\Delta T$ 's as a function of speed are plotted in Figure 38. This bearing achieved 30 minutes of temperature stabilized operation at  $3.5 \times 10^6$  DN (25,000 rpm) under a 471 lb. radial load. The only variation in test conditions over the first test bearing was the addition of an auxiliary jet towards the rear of the bearing at the inner race and cage land contact. This auxiliary jet supplied approximately 2 lbs. per minute oil flow of the total reported in the test log.

The test bearing was then subjected to four rapid acceleration and deceleration tests between  $1.5 \times 10^6$  DN and  $3.5 \times 10^6$  DN in 15 seconds each.

DATA SUMMARY SHEET, SECOND TEST BEARING POLYPHENYL ETHER 5P4E

PURE CARBON CO-DATA SUMMARY SHEET

TEST OF - Dual Diaphragm Ruler B-9 443				CUSTOMER - F&C				DATE - 12-23-72	
W Polyphenyl Ether 50GF @ 500°F				PROJ. NO. - 11501				TEST DATE - 12-21-72	
Reading No	DN	Load lbs	Oil Flow lb/min	Oil Temp OF	OR Temp Avg OF	Oil Over Oil OF		Oil Cryst. Approx	AT
						AT	Oil Out FAT		
109	0.5	476	12.5	355	308	-17	366	300	-55
106	1.0	453	12.5	400	372	-28	420	405	+5
112	1.5	453	13.0	420	397	-23	460	450	+30
114	2.0	453	13.1	455	449	-11	490	480	+25
116	2.5	453	13.0	455	466	+11	500	490	+35
119	0.5	459	13.4	330	291	-39	345	280	-50
125	3.0	488	9.3	460	500	+40	515	490	+30
126	3.0	477	15.6	495	463	+18	470	455	+10
127	3.25	471	17.9	475	501	+28	530	515	+40
128	3.43	471	16.8	495	525	+30	550	540	+45
129	3.45	471	14.3	510	534	+24	565	555	+45
130	3.53	471	21.4	515	542	+27	570	565	+50
131	3.43	471	21.4	530	545	+25	575	570	+50
132	1.60	471	21.4	500	493	-7	540	535	+35
133	.63	471	23.3	430	439	+9	450	470	+10

may 30/ 1950

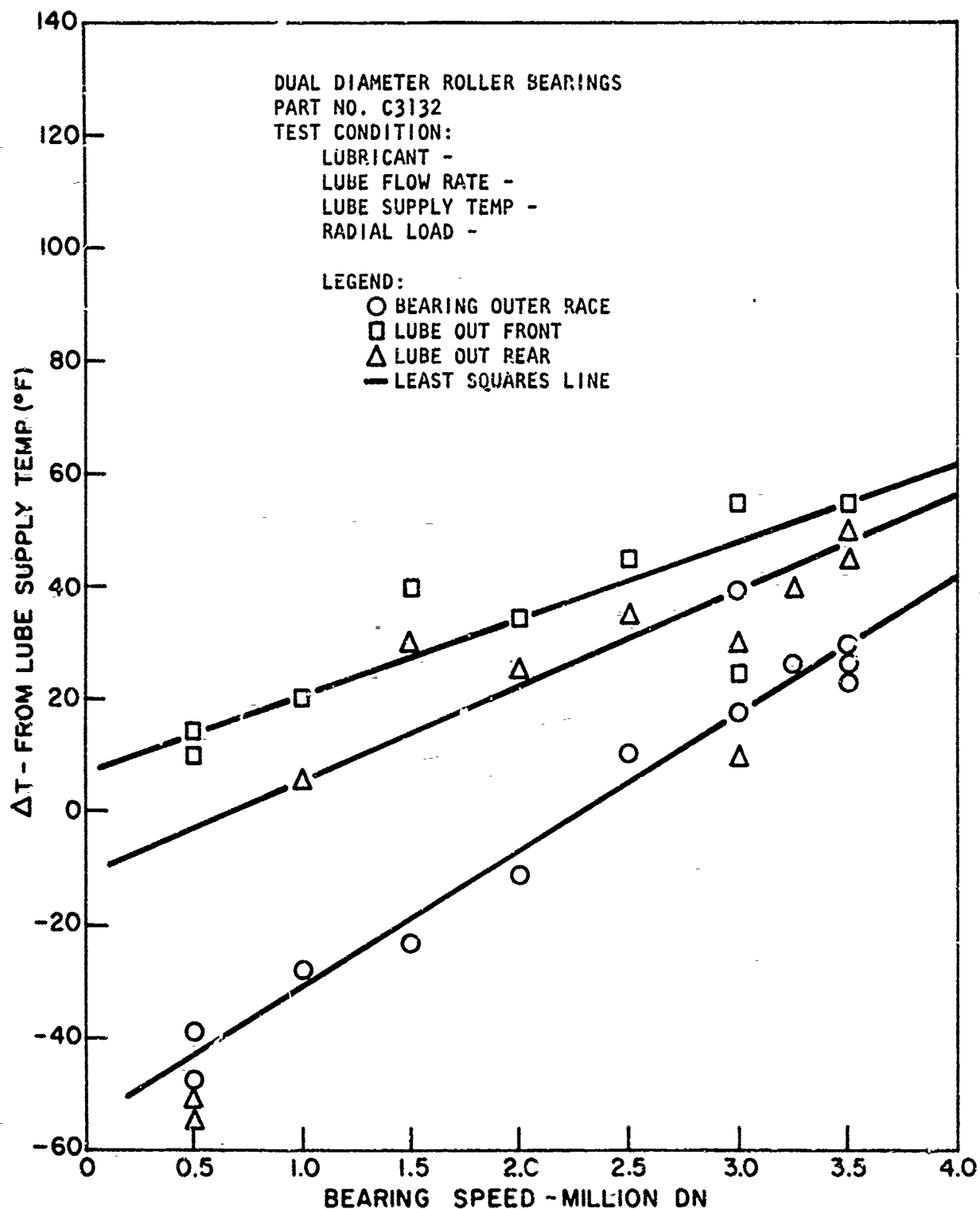


Figure 38. Test Bearing No. 2  $\Delta T$  vs. Speed, Polyphenyl Ether, 5P4E

The second test bearing is shown in Figure 39. All of the race and roller operating surfaces were in excellent condition. The cage was in good condition and showed even burnished wear areas in the cage roller to pocket contacting surfaces. With the exception of the riding land, the cage was in excellent condition. The silver plate was not worn through at any position and very little discoloration was noticed. The cage inner land riding surfaces however were discolored over a 90° arc indicating insufficient lubricant to the cage lands. The inner race shows a uniformly burnished area in the center of the race where the rollers contacted. Distress is noted in the cage land riding areas on the inner race. The outer race was in excellent condition. There was some indication in the discoloration due to temperature that the rear of the bearing was cooler than the front face of the bearing. This can be attributed to the auxiliary oil jet directed at the rear face of the bearing.

The Polyphenyl Ether 5P4E lubricant used in the test was supplied by the Aero Propulsion Laboratory, Wright-Patterson Air Force Base. Some of the fluid was new fluid and some of the fluid furnished was reconstituted fluid. It was noted that when new 5P4E fluid was added to the oil sump, that foaming of the oil occurred for a period of 10 to 20 minutes and then subsided. This foaming did not occur when reconstituted 5P4E fluid was added to the sump. The foaming action did not seem to have any effect upon bearing operation.

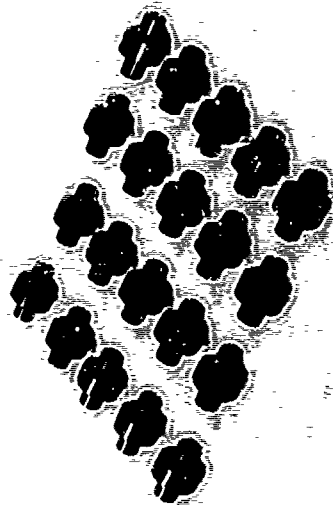
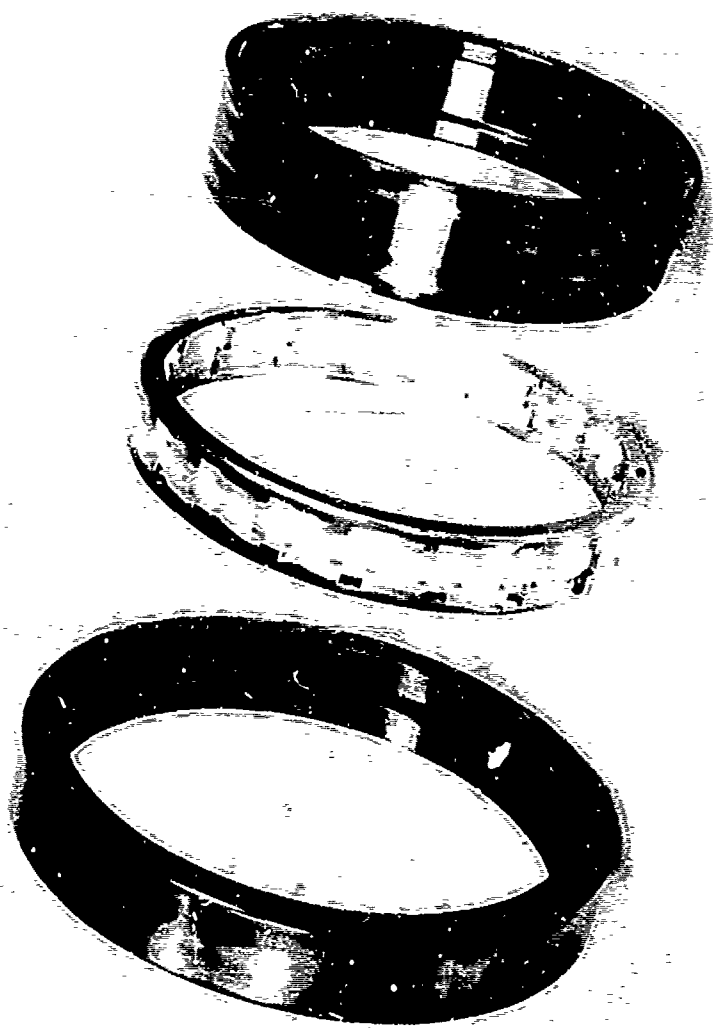


FIG 39

Figure 39. Second Dual Diameter Test Bearing

## SECTION VII

### CONCLUSIONS

The second dual diameter roller bearing successfully operated for 30 minutes of stabilized temperature operation at a shaft speed of 25,000 rpm. This is  $3.5 \times 10^6$  DN operation of a 140 mm bore bearing. External radial load was 471 lbs. and the lubricant was 5P4F Polyphenyl Ether at approximately 500°F oil inlet temperature.

The failure of the first test bearing was attributed to reverse bending fatigue of the M-50 steel inner race at high speed and 600°F operating temperatures. The calculated stress levels were below known allowable stress levels for long term operation. This suggests that additional carefully controlled reverse bending fatigue data is required for M-50 bearing steels for elevated temperature operation. Any future tests of the dual diameter should use a solid inner race, eliminating the undercut.

The lubrication method of introducing the oil to a cavity in the inner race and through orifices directly into the bearing interring was generally successful, however distress and wear was observed at the cage inner land riding surface.

The successful operation of the second test bearing establishes the validity of the design approach. A complete systems analysis using existing state-of-the-art elastohydrodynamic technology, fluid mechanics, theory and thermal analysis techniques, can be used to design a completely new bearing concept and enable initial prototype testing to be successful at speeds and temperatures beyond the realm of current experience.

# APPENDIX I

## TEST LOGS

TEST LOG SHEET-		TECHNICIAN		MIDWEST AERO INDUSTRIES CORP.		PROJ NO. 81001		SHEET A	
		WITNESS				CUSTOMER F.I.R.L.		PAGE	
		WITNESS				P.O. NO. 19046		DATE 10-12-72	
		WITNESS				TEST CELL 35014			
TEST	TIME	REV	REV	REV	REV	REV	REV	REV	REV
1	1100	0	0	0	0	0	0	0	0
2	1150	0	0	0	0	0	0	0	0
3	1200	0	0	0	0	0	0	0	0
4	1210	0	0	0	0	0	0	0	0
5	1215	0	0	0	0	0	0	0	0
6	1220	0	0	0	0	0	0	0	0
7	1225	0	0	0	0	0	0	0	0
8	1230	0	0	0	0	0	0	0	0
9	1235	0	0	0	0	0	0	0	0
10	1240	0	0	0	0	0	0	0	0
11	1245	0	0	0	0	0	0	0	0
12	1250	0	0	0	0	0	0	0	0
13	1255	0	0	0	0	0	0	0	0
14	1300	0	0	0	0	0	0	0	0
15	1305	0	0	0	0	0	0	0	0
16	1310	0	0	0	0	0	0	0	0
17	1315	0	0	0	0	0	0	0	0
18	1320	0	0	0	0	0	0	0	0
19	1325	0	0	0	0	0	0	0	0
20	1330	0	0	0	0	0	0	0	0
21	1335	0	0	0	0	0	0	0	0
22	1340	0	0	0	0	0	0	0	0
23	1345	0	0	0	0	0	0	0	0
24	1350	0	0	0	0	0	0	0	0
25	1355	0	0	0	0	0	0	0	0
26	1400	0	0	0	0	0	0	0	0
27	1405	0	0	0	0	0	0	0	0
28	1410	0	0	0	0	0	0	0	0
29	1415	0	0	0	0	0	0	0	0
30	1420	0	0	0	0	0	0	0	0
31	1425	0	0	0	0	0	0	0	0
32	1430	0	0	0	0	0	0	0	0
33	1435	0	0	0	0	0	0	0	0
34	1440	0	0	0	0	0	0	0	0
35	1445	0	0	0	0	0	0	0	0
36	1450	0	0	0	0	0	0	0	0
37	1455	0	0	0	0	0	0	0	0
38	1500	0	0	0	0	0	0	0	0
39	1505	0	0	0	0	0	0	0	0
40	1510	0	0	0	0	0	0	0	0
41	1515	0	0	0	0	0	0	0	0
42	1520	0	0	0	0	0	0	0	0
43	1525	0	0	0	0	0	0	0	0
44	1530	0	0	0	0	0	0	0	0
45	1535	0	0	0	0	0	0	0	0
46	1540	0	0	0	0	0	0	0	0
47	1545	0	0	0	0	0	0	0	0
48	1550	0	0	0	0	0	0	0	0
49	1555	0	0	0	0	0	0	0	0
50	1600	0	0	0	0	0	0	0	0
51	1605	0	0	0	0	0	0	0	0
52	1610	0	0	0	0	0	0	0	0
53	1615	0	0	0	0	0	0	0	0
54	1620	0	0	0	0	0	0	0	0
55	1625	0	0	0	0	0	0	0	0
56	1630	0	0	0	0	0	0	0	0
57	1635	0	0	0	0	0	0	0	0
58	1640	0	0	0	0	0	0	0	0
59	1645	0	0	0	0	0	0	0	0
60	1650	0	0	0	0	0	0	0	0
61	1655	0	0	0	0	0	0	0	0
62	1700	0	0	0	0	0	0	0	0
63	1705	0	0	0	0	0	0	0	0
64	1710	0	0	0	0	0	0	0	0
65	1715	0	0	0	0	0	0	0	0
66	1720	0	0	0	0	0	0	0	0
67	1725	0	0	0	0	0	0	0	0
68	1730	0	0	0	0	0	0	0	0
69	1735	0	0	0	0	0	0	0	0
70	1740	0	0	0	0	0	0	0	0
71	1745	0	0	0	0	0	0	0	0
72	1750	0	0	0	0	0	0	0	0
73	1755	0	0	0	0	0	0	0	0
74	1800	0	0	0	0	0	0	0	0
75	1805	0	0	0	0	0	0	0	0
76	1810	0	0	0	0	0	0	0	0
77	1815	0	0	0	0	0	0	0	0
78	1820	0	0	0	0	0	0	0	0
79	1825	0	0	0	0	0	0	0	0
80	1830	0	0	0	0	0	0	0	0
81	1835	0	0	0	0	0	0	0	0
82	1840	0	0	0	0	0	0	0	0
83	1845	0	0	0	0	0	0	0	0
84	1850	0	0	0	0	0	0	0	0
85	1855	0	0	0	0	0	0	0	0
86	1900	0	0	0	0	0	0	0	0
87	1905	0	0	0	0	0	0	0	0
88	1910	0	0	0	0	0	0	0	0
89	1915	0	0	0	0	0	0	0	0
90	1920	0	0	0	0	0	0	0	0
91	1925	0	0	0	0	0	0	0	0
92	1930	0	0	0	0	0	0	0	0
93	1935	0	0	0	0	0	0	0	0
94	1940	0	0	0	0	0	0	0	0
95	1945	0	0	0	0	0	0	0	0
96	1950	0	0	0	0	0	0	0	0
97	1955	0	0	0	0	0	0	0	0
98	2000	0	0	0	0	0	0	0	0
99	2005	0	0	0	0	0	0	0	0
100	2010	0	0	0	0	0	0	0	0



[illegible]

0-121

TEST LOG SHEET				TECHNICIAN				MIDWEST ARMO INDUSTRIES CORP.				PROJ. NO. 11001				SHEET A OF C.			
				WITNESS								CUSTOMER FILE				PAGE 1 OF 2			
				WITNESS				TEST OF - 2nd Series - Lot - 25 - 30112700				P.Q. NO. 19091				DATE 10-26-92			
TECH. INIT.	CLOCK TIME	Class. Rtg	Load Pres.	Oil Flow T-B	Oil Flow T-B	Oil Flow T-B	Oil Flow T-B	Oil Flow T-B	Oil Flow T-B	Oil Flow T-B	Oil Flow T-B	Oil Flow T-B	Oil Flow T-B	Oil Flow T-B	Oil Flow T-B	Oil Flow T-B	Oil Flow T-B	Oil Flow T-B	
NO.	MIN.	RPM	PSI	1/2 in	3/4 in	1 in	1 1/2 in	2 in	3 in	4 in	5 in	6 in	7 in	8 in	9 in	10 in	11 in	12 in	
42	1575	515	340	445	494	588	8.4	3.0	3.2	3.0	3.2	3.0	3.2	3.0	3.2	3.0	3.2	3.0	
43	1607	507	340	445	494	588	8.4	3.0	3.2	3.0	3.2	3.0	3.2	3.0	3.2	3.0	3.2		
44	1625	507	340	445	494	588	8.4	3.0	3.2	3.0	3.2	3.0	3.2	3.0	3.2	3.0	3.2		
45	1630	507	340	445	494	588	8.4	3.0	3.2	3.0	3.2	3.0	3.2	3.0	3.2	3.0	3.2		
46	1635	507	340	445	494	588	8.4	3.0	3.2	3.0	3.2	3.0	3.2	3.0	3.2	3.0	3.2		
47	1640	507	340	445	494	588	8.4	3.0	3.2	3.0	3.2	3.0	3.2	3.0	3.2	3.0	3.2		
48	1645	507	340	445	494	588	8.4	3.0	3.2	3.0	3.2	3.0	3.2	3.0	3.2	3.0	3.2		
49	1650	507	340	445	494	588	8.4	3.0	3.2	3.0	3.2	3.0	3.2	3.0	3.2	3.0	3.2		
50	1655	507	340	445	494	588	8.4	3.0	3.2	3.0	3.2	3.0	3.2	3.0	3.2	3.0	3.2		
51	1660	507	340	445	494	588	8.4	3.0	3.2	3.0	3.2	3.0	3.2	3.0	3.2	3.0	3.2		
52	1665	507	340	445	494	588	8.4	3.0	3.2	3.0	3.2	3.0	3.2	3.0	3.2	3.0	3.2		
53	1670	507	340	445	494	588	8.4	3.0	3.2	3.0	3.2	3.0	3.2	3.0	3.2	3.0	3.2		
54	1675	507	340	445	494	588	8.4	3.0	3.2	3.0	3.2	3.0	3.2	3.0	3.2	3.0	3.2		
55	1680	507	340	445	494	588	8.4	3.0	3.2	3.0	3.2	3.0	3.2	3.0	3.2	3.0	3.2		
56	1685	507	340	445	494	588	8.4	3.0	3.2	3.0	3.2	3.0	3.2	3.0	3.2	3.0	3.2		
57	1690	507	340	445	494	588	8.4	3.0	3.2	3.0	3.2	3.0	3.2	3.0	3.2	3.0	3.2		
58	1695	507	340	445	494	588	8.4	3.0	3.2	3.0	3.2	3.0	3.2	3.0	3.2	3.0	3.2		
59	1700	507	340	445	494	588	8.4	3.0	3.2	3.0	3.2	3.0	3.2	3.0	3.2	3.0	3.2		
60	1705	507	340	445	494	588	8.4	3.0	3.2	3.0	3.2	3.0	3.2	3.0	3.2	3.0	3.2		
61	1710	507	340	445	494	588	8.4	3.0	3.2	3.0	3.2	3.0	3.2	3.0	3.2	3.0	3.2		
62	1715	507	340	445	494	588	8.4	3.0											

Reproduced from  
best available copy.















[illegible]











TEST LOG SHEET-										PURE CARBON CO. ST. MARY, PA.										SHEET A OF C	
TECHNICAL WITNESS										CUSTOMER										PAGE	
WITNESS										P.O. NO.										DATE 12-23-72	
WITNESS										TEST CELL											
CLOCK TIME	TEST NO.	TEST NO.	TEST NO.	TEST NO.	TEST NO.	TEST NO.	TEST NO.	TEST NO.	TEST NO.	TEST NO.	TEST NO.	TEST NO.	TEST NO.	TEST NO.	TEST NO.	TEST NO.	TEST NO.				
10:00	1	2	3	4	5	6	7	8	9	10	11	12	13	14	15	16	17				
10:05	100	101	102	103	104	105	106	107	108	109	110	111	112	113	114	115	116				
10:10	117	118	119	120	121	122	123	124	125	126	127	128	129	130	131	132	133				
10:15	134	135	136	137	138	139	140	141	142	143	144	145	146	147	148	149	150				
10:20	151	152	153	154	155	156	157	158	159	160	161	162	163	164	165	166	167				
10:25	168	169	170	171	172	173	174	175	176	177	178	179	180	181	182	183	184				
10:30	185	186	187	188	189	190	191	192	193	194	195	196	197	198	199	200	201				
10:35	202	203	204	205	206	207	208	209	210	211	212	213	214	215	216	217	218				
10:40	219	220	221	222	223	224	225	226	227	228	229	230	231	232	233	234	235				
10:45	236	237	238	239	240	241	242	243	244	245	246	247	248	249	250	251	252				
10:50	253	254	255	256	257	258	259	260	261	262	263	264	265	266	267	268	269				
10:55	270	271	272	273	274	275	276	277	278	279	280	281	282	283	284	285	286				
11:00	287	288	289	290	291	292	293	294	295	296	297	298	299	300	301	302	303				
11:05	304	305	306	307	308	309	310	311	312	313	314	315	316	317	318	319	320				
11:10	321	322	323	324	325	326	327	328	329	330	331	332	333	334	335	336	337				
11:15	338	339	340	341	342	343	344	345	346	347	348	349	350	351	352	353	354				
11:20	355	356	357	358	359	360	361	362	363	364	365	366	367	368	369	370	371				
11:25	372	373	374	375	376	377	378	379	380	381	382	383	384	385	386	387	388				
11:30	389	390	391	392	393	394	395	396	397	398	399	400	401	402	403	404	405				
11:35	406	407	408	409	410	411	412	413	414	415	416	417	418	419	420	421	422				
11:40	423	424	425	426	427	428	429	430	431	432	433	434	435	436	437	438	439				
11:45	440	441	442	443	444	445	446	447	448	449	450	451	452	453	454	455	456				
11:50	457	458	459	460	461	462	463	464	465	466	467	468	469	470	471	472	473				
11:55	474	475	476	477	478	479	480	481	482	483	484	485	486	487	488	489	490				
12:00	491	492	493	494	495	496	497	498	499	500	501	502	503	504	505	506	507				
12:05	508	509	510	511	512	513	514	515	516	517	518	519	520	521	522	523	524				
12:10	525	526	527	528	529	530	531	532	533	534	535	536	537	538	539	540	541				
12:15	542	543	544	545	546	547	548	549	550	551	552	553	554	555	556	557	558				
12:20	559	560	561	562	563	564	565	566	567	568	569	570	571	572	573	574	575				
12:25	576	577	578	579	580	581	582	583	584	585	586	587	588	589	590	591	592				
12:30	593	594	595	596	597	598	599	600	601	602	603	604	605	606	607	608	609				
12:35	610	611	612	613	614	615	616	617	618	619	620	621	622	623	624	625	626				
12:40	627	628	629	630	631	632	633	634	635	636	637	638	639	640	641	642	643				
12:45	644	645	646	647	648	649	650	651	652	653	654	655	656	657	658	659	660				
12:50	661	662	663	664	665	666	667	668	669	670	671	672	673	674	675	676	677				
12:55	678	679	680	681	682	683	684	685	686	687	688	689	690	691	692	693	694				
13:00	695	696	697	698	699	700	701	702	703	704	705	706	707	708	709	710	711				
13:05	712	713	714	715	716	717	718	719	720	721	722	723	724	725	726	727	728				
13:10	729	730	731	732	733	734	735	736	737	738	739	740	741	742	743	744	745				
13:15	746	747	748	749	750	751	752	753	754	755	756	757	758	759	760	761	762				
13:20	763	764	765	766	767	768	769	770	771	772	773	774	775	776	777	778	779				
13:25	780	781	782	783	784	785	786	787	788	789	790	791	792	793	794	795	796				
13:30	797	798	799	800	801	802	803	804	805	806	807	808	809	810	811	812	813				
13:35	814	815	816	817	818	819	820	821	822	823	824	825	826	827	828	829	830				
13:40	831	832	833	834	835	836	837	838	839	840	841	842	843	844	845	846	847				
13:45	848	849	850	851	852	853	854	855	856	857	858	859	860	861	862	863	864				
13:50	865	866	867	868	869	870	871	872	873	874	875	876	877	878	879	880	881				
13:55	882	883	884	885	886	887	888	889	890	891	892	893	894	895	896	897	898				
14:00	899	900	901	902	903	904	905	906	907	908	909	910	911	912	913	914	915				
14:05	916	917	918	919	920	921	922	923	924	925	926	927	928	929	930	931	932				
14:10	933	934	935	936	937	938	939	940	941	942	943	944	945	946	947	948	949				
14:15	950	951	952	953	954	955	956	957	958	959	960	961	962	963	964	965	966				
14:20	967	968	969	970	971	972	973	974	975	976	977	978	979	980	981	982	983				
14:25	984	985	986	987	988	989	990	991	992	993	994	995	996	997	998	999	1000				

NOTES: READINGS FOR 125 FROM 45 THERM # 10 COULD HAVE BEEN 50°F LOWER.



TEST LOG SHEET										MIDWEST AERO INDUSTRIES CORP.										PROJ. NO. 81001		SHEET 5 OF 5	
TECHNICIAN										CUSTOMER F.I.R.L.										PAGE 2		DATE 10-25-72	
WITNESS										TEST OF = Fuel No. 100-82-101 is 71.1% 255.66										P.O. NO. 19046		TEST CELL 255.66	
WITNESS										TEST OF = Fuel No. 100-82-101 is 71.1% 255.66										P.O. NO. 19046		TEST CELL 255.66	
TEST TIME	TIME	WIND	WIND	WIND	WIND	WIND	WIND	WIND	WIND	WIND	WIND	WIND	WIND	WIND	WIND	WIND	WIND	WIND	WIND				
TEST TIME	TIME	WIND	WIND	WIND	WIND	WIND	WIND	WIND	WIND	WIND	WIND	WIND	WIND	WIND	WIND	WIND	WIND	WIND	WIND				
0.25	3.3	1430																					
1.0	3.3	1430																					
2.0	3.3	1430																					
3.0	3.3	1430																					
4.0	3.3	1430																					
5.0	3.3	1430																					
6.0	3.3	1430																					
7.0	3.3	1430																					
8.0	3.3	1430																					
9.0	3.3	1430																					
10.0	3.3	1430																					
11.0	3.3	1430																					
12.0	3.3	1430																					
13.0	3.3	1430																					
14.0	3.3	1430																					
15.0	3.3	1430																					
16.0	3.3	1430																					
17.0	3.3	1430																					
18.0	3.3	1430																					
19.0	3.3	1430																					
20.0	3.3	1430																					
21.0	3.3	1430																					
22.0	3.3	1430																					
23.0	3.3	1430																					
24.0	3.3	1430																					
25.0	3.3	1430																					
26.0	3.3	1430																					
27.0	3.3	1430																					
28.0	3.3	1430																					
29.0	3.3	1430																					
30.0	3.3	1430																					
31.0	3.3	1430																					
32.0	3.3	1430																					
33.0	3.3	1430																					
34.0	3.3	1430																					
35.0	3.3	1430																					
36.0	3.3	1430																					
37.0	3.3	1430																					
38.0	3.3	1430																					
39.0	3.3	1430																					
40.0	3.3	1430																					
41.0	3.3	1430																					
42.0	3.3	1430																					
43.0	3.3	1430																					
44.0	3.3	1430																					
45.0	3.3	1430																					
46.0	3.3	1430																					
47.0	3.3	1430																					
48.0	3.3	1430																					
49.0	3.3	1430																					
50.0	3.3	1430																					
51.0	3.3	1430																					
52.0	3.3	1430																					
53.0	3.3	1430																					
54.0	3.3	1430																					
55.0	3.3	1430																					

TEST LOG SHEET-				TECHNICIAN				MIDWEST AERO INDUSTRIES CORP.				PROJ. NO.				SHEET C OF C			
WITNESS				WITNESS				CUSTOMER				P.O. NO.				P.O. NO.			
WITNESS				WITNESS				TEST OF PURPOSE =				TEST CELL				DATE 11-6-72			
TECH INIT	CLOCK TIME	Vibration	Vibration	Vibration	Vibration	Vibration	Vibration	Core	Core	Core	Core	Core	Core	Core	Core	Core	Core	Core	
56	10:25	0.15	0.15	0.15	0.15	0.15	0.15	0.15	0.15	0.15	0.15	0.15	0.15	0.15	0.15	0.15	0.15	0.15	
57	10:30	0.15	0.15	0.15	0.15	0.15	0.15	0.15	0.15	0.15	0.15	0.15	0.15	0.15	0.15	0.15	0.15	0.15	
58	11:00	0.15	0.15	0.15	0.15	0.15	0.15	0.15	0.15	0.15	0.15	0.15	0.15	0.15	0.15	0.15	0.15	0.15	
59	11:30	0.15	0.15	0.15	0.15	0.15	0.15	0.15	0.15	0.15	0.15	0.15	0.15	0.15	0.15	0.15	0.15	0.15	
60	11:40	0.15	0.15	0.15	0.15	0.15	0.15	0.15	0.15	0.15	0.15	0.15	0.15	0.15	0.15	0.15	0.15	0.15	
61	11:55	0.15	0.15	0.15	0.15	0.15	0.15	0.15	0.15	0.15	0.15	0.15	0.15	0.15	0.15	0.15	0.15	0.15	
62	12:15	0.15	0.15	0.15	0.15	0.15	0.15	0.15	0.15	0.15	0.15	0.15	0.15	0.15	0.15	0.15	0.15	0.15	
63	12:30	0.15	0.15	0.15	0.15	0.15	0.15	0.15	0.15	0.15	0.15	0.15	0.15	0.15	0.15	0.15	0.15	0.15	
64	12:45	0.15	0.15	0.15	0.15	0.15	0.15	0.15	0.15	0.15	0.15	0.15	0.15	0.15	0.15	0.15	0.15	0.15	
65	13:00	0.15	0.15	0.15	0.15	0.15	0.15	0.15	0.15	0.15	0.15	0.15	0.15	0.15	0.15	0.15	0.15	0.15	
66	13:15	0.15	0.15	0.15	0.15	0.15	0.15	0.15	0.15	0.15	0.15	0.15	0.15	0.15	0.15	0.15	0.15	0.15	
67	13:30	0.15	0.15	0.15	0.15	0.15	0.15	0.15	0.15	0.15	0.15	0.15	0.15	0.15	0.15	0.15	0.15	0.15	
68	13:45	0.15	0.15	0.15	0.15	0.15	0.15	0.15	0.15	0.15	0.15	0.15	0.15	0.15	0.15	0.15	0.15	0.15	
69	14:00	0.15	0.15	0.15	0.15	0.15	0.15	0.15	0.15	0.15	0.15	0.15	0.15	0.15	0.15	0.15	0.15	0.15	
70	14:15	0.15	0.15	0.15	0.15	0.15	0.15	0.15	0.15	0.15	0.15	0.15	0.15	0.15	0.15	0.15	0.15	0.15	
71	14:30	0.15	0.15	0.15	0.15	0.15	0.15	0.15	0.15	0.15	0.15	0.15	0.15	0.15	0.15	0.15	0.15	0.15	
72	14:45	0.15	0.15	0.15	0.15	0.15	0.15	0.15	0.15	0.15	0.15	0.15	0.15	0.15	0.15	0.15	0.15	0.15	
73	15:00	0.15	0.15	0.15	0.15	0.15	0.15	0.15	0.15	0.15	0.15	0.15	0.15	0.15	0.15	0.15	0.15	0.15	
74	15:15	0.15	0.15	0.15	0.15	0.15	0.15	0.15	0.15	0.15	0.15	0.15	0.15	0.15	0.15	0.15	0.15	0.15	
75	15:30	0.15	0.15	0.15	0.15	0.15	0.15	0.15	0.15	0.15	0.15	0.15	0.15	0.15	0.15	0.15	0.15	0.15	
76	15:45	0.15	0.15	0.15	0.15	0.15	0.15	0.15	0.15	0.15	0.15	0.15	0.15	0.15	0.15	0.15	0.15	0.15	
77	16:00	0.15	0.15	0.15	0.15	0.15	0.15	0.15	0.15	0.15	0.15	0.15	0.15	0.15	0.15	0.15	0.15	0.15	
78	16:15	0.15	0.15	0.15	0.15	0.15	0.15	0.15	0.15	0.15	0.15	0.15	0.15	0.15	0.15	0.15	0.15	0.15	
79	16:30	0.15	0.15	0.15	0.15	0.15	0.15	0.15	0.15	0.15	0.15	0.15	0.15	0.15	0.15	0.15	0.15	0.15	
80	16:45	0.15	0.15	0.15	0.15	0.15	0.15	0.15	0.15	0.15	0.15	0.15	0.15	0.15	0.15	0.15	0.15	0.15	
81	17:00	0.15	0.15	0.15	0.15	0.15	0.15	0.15	0.15	0.15	0.15	0.15	0.15	0.15	0.15	0.15	0.15	0.15	
82	17:15	0.15	0.15	0.15	0.15	0.15	0.15	0.15	0.15	0.15	0.15	0.15	0.15	0.15	0.15	0.15	0.15	0.15	
83	17:30	0.15	0.15	0.15	0.15	0.15	0.15	0.15	0.15	0.15	0.15	0.15	0.15	0.15	0.15	0.15	0.15	0.15	
84	17:45	0.15	0.15	0.15	0.15	0.15	0.15	0.15	0.15	0.15	0.15	0.15	0.15	0.15	0.15	0.15	0.15	0.15	
85	18:00	0.15	0.15	0.15	0.15	0.15	0.15	0.15	0.15	0.15	0.15	0.15	0.15	0.15	0.15	0.15	0.15	0.15	



**TEST LOG  
-13HS-  
SHEET-**

TECHNICAL  
WITNESS  
WITNESS

11531531

**PURE CARBON CO.**  
**ST. MARYS, PA.**

PROJ. NO.	
CUSTOMER	
P. O. NO.	

SHEET 5 OF 5  
PAGE 5 OF 5  
DATE 11-16-72

[illegible]



APPENDIX II

GAS TURBINE ENGINE MAINSHAFT  
ROLLER BEARING - SYSTEM ANALYSIS

By

J. H. Rumbarger, Principal Engineer, Member ASME  
E. G. Filetti, Senior Staff Engineer, Member ASME  
D. Gubernick Student, Drexel University, Coop Employee, FIRL

The Franklin Institute Research Laboratories  
Philadelphia, Pennsylvania

Submitted to  
Lubrication Division of ASME  
For Publication (without presentation) in  
Journal of Lubrication Technology

August 1972.

## ABSTRACT

An interdisciplinary systems analysis is presented for high-speed gas turbine engine mainshaft roller bearings which will enable the designer to meet the demands for ever higher rotative speeds and operating temperatures. The latest elastohydrodynamic experimental traction data is included. Analytical results cite a need for better definition of the rolling friction portion of the total traction. A fluid mechanics model for the detailed analysis of fluid drags is developed based upon a turbulent vortex-dominated flow and includes the effect of lubricant flow through the bearing. Typical cage equilibrium solutions show evidence of possible unstable operation. A complete thermal analysis including dynamic and thermal effects upon bearing dimensions and resulting clearances is also included. Heat transfer coefficients are given in detail. Shaft power loss and cage slip predictions as a function of load, speed, and lubricant supply correlate well with available experimental data.

## LIST OF FIGURES

<u>Fig. No.</u>		<u>Page</u>
1	Surface Velocities and Relative Rotational Speeds of Raceways and Rollers Including Slip at Each Contact as a Result of Cage Slip . . . . .	38
2	Forces and Moments Acting on a Loaded Roller . . . . .	39
3	Forces and Moments Acting on an Unloaded Roller . . . . .	40
4	Solution Techniques Flow Chart . . . . .	41
5	Roller Clearance Distribution in Cage . . . . .	42
6	Mathematical Model of Horizontal and Vertical Relative Velocity Distributions in Roller-Shoulder Contact . . . . .	43
7	Roller Bearing Cage Speed Correlation . . . . .	44
8	Influence of Oil/Air Ratio on Each Solution . . . . .	45
9	Influence of Oil/Air Ratio on Each Solution . . . . .	46

## LIST OF TABLES

<u>Table No.</u>		<u>Page</u>
1	Dimensional Models . . . . .	47
2	Description of Thermal Analysis by Nodes . . . . .	48
3	Typical Thermal Analysis . . . . .	49
4	Typical EHD Film Thickness and Traction Values . . . . .	50

## INTRODUCTION

The use of elastohydrodynamic lubrication theory for rolling bearing analysis was first suggested by Dowson and Higginson<sup>[1]</sup>. The first use of digital computers for the analysis of high speed roller bearing performance was by Harris<sup>[2]</sup>. The Harris paper presented an analytical method to predict skidding in high-speed roller bearings. The influence of the amount of lubricant supply on cage and roller motion in high speed roller bearings was experimentally described and analytically discussed by Boness<sup>[3]</sup>. A refinement was introduced by Poplawski<sup>[4]</sup> with the solution of all of the loaded rollers under the varying load pattern resulting from external radial load. He also introduced a fluid "churning" loss and cage pilot surface friction formulations.

All of the previous analytical work used the Dowson-Higginson<sup>[1]</sup> isothermal elastohydrodynamic (EHD), formulation. A recent comprehensive review of EHD theory and experimental data by McGrew, et al<sup>[5]</sup> resulted in selection and recommendation of the latest and most applicable EHD formulations. This preliminary EHD design manual<sup>[5]</sup> also presents computer subroutines for the calculation of oil film thickness including thermal effects developed by Cheng<sup>[6]</sup> and EHD traction subroutines fitted to available disk machine experimental data.

The present paper presents a system analysis of a high-speed roller bearing under radial loading as commonly used on gas turbine engine mainshafts. Oil film thickness, traction, and hydrodynamic pressure forces acting in an elastohydrodynamic roller-race contact are computed according to the latest available techniques<sup>[5]</sup>. A complete fluid mechanics model is developed in order to more accurately predict the fluid drag losses acting upon roller, race, and cage moving surfaces. Turbulent vortex-dominated flow theory is used to calculate boundary layer stresses. Finally, a complete thermal analysis is described.

Combining the resulting thermal deformations with deformations of the bearing components due to centrifugal growth completely defines changes in critical bearing operating parameters at each step of the iterative solution process. The thickness of an EHD oil film is determined by the temperature and viscosity at the inlet to the contact. This inlet oil temperature is very sensitive to the temperature gradients which exist within the bearing. Oil viscosity changes and dimensional changes throughout the bearing as a function of temperatures are included. The thermal solution as expected is dependent upon lubricant flow rate, method of application (under inner race, thorough bearing, etc.) and external heat paths.

## LOAD AND SPEED EQUILIBRIUM

### Elastohydrodynamic Pressure Forces and Traction

The surface velocities and relative rotational speeds of rollers and raceways are shown in Fig. 1 and follow the nomenclature of Harris<sup>[2]</sup>. Sliding velocities,  $V_{ij}$  and  $V_{oj}$  are defined as positive when the surface velocity of the race is greater than the surface velocity of the roller and is equal to their difference. The rolling or entrainment velocities  $U_{ij}$  and  $U_{oj}$  are always positive and defined as the average of raceway and roller surface velocities. The sliding velocities and entrainment velocities are made dimensionless by introduction of the fluid entrance viscosity,  $\eta_e$ , reduced modulus of elasticity,  $E'$ , and equivalent cylinder radius,  $R$ , for each contact as suggested by Dowson<sup>[1]</sup>.

Forces and moments acting on a loaded roller are shown in Fig. 2 and those acting on an unloaded roller are shown in Fig. 3. The effect of cage orbital speed,  $\omega_c$ , is to create a dynamic body force on the roller acting radially outwards. Figs. 2 and 3 use D'Alembert's principle<sup>[7]</sup> to represent the summation of this roller body forces as an inertia force  $CF^*$  acting through the center mass of the rollers.

$$CF^* = \frac{1}{2} M_r E \omega_c^2 \quad (1)$$

Thus Figs. 2 and 3 are free body diagrams of the roller in static and dynamic steady state equilibrium with all static and dynamic forces shown.

Fluid pressure forces  $Q_{ij}$  and  $Q_{oj}$  tending to translate the roller relative to the raceways are described by Dowson, et al<sup>[1]</sup> and approximated by Harris<sup>[2]</sup> for synthetic lubricants as:

$$\left. \begin{aligned} \bar{Q}_{ij} &= 18.4 (1-\gamma) G^{-0.3} \bar{U}_{ij}^{0.7} \\ \bar{Q}_{oj} &= 18.4 (1+\gamma) G^{-0.3} \bar{U}_{oj}^{0.7} \end{aligned} \right\} \quad (2)$$

Traction forces  $T_{ij}$  and  $T_{oj}$  consist of fluid frictional drag forces as described by elastohydrodynamic lubrication theory. They consist of rolling and sliding friction forces. Using the Harris<sup>[2]</sup> approximation for  $Q_{ij}$  and  $Q_{oj}$  they are expressed as:

$$\left. \begin{aligned} T_{ij} &= -9.2 G^{-0.3} \bar{U}_{ij}^{0.7} \ell_{ij} E' R_i + \frac{|V_{ij}|}{V_{ij}} f(T_e)_i P_{ij} \\ T_{oj} &= -9.2 G^{-0.3} \bar{U}_{oj}^{0.7} \ell_{oj} E' R_o + \frac{|V_{oj}|}{V_{oj}} f(T_e)_o P_{oj} \end{aligned} \right\} \quad (3)$$

The coefficient of traction,  $f$ , for the sliding portion has been obtained by experiment from disk machines. This coefficient has been curve fitted to existing data by McGrew, et al<sup>[5]</sup> as a function of three dimensionless parameters  $G_1$ ,  $G_2$ ,  $G_3$  and is represented symbolically as:

$$f(T_e) = F[G_1, G_2, G_3, 30^\circ\text{C}] - 0.001 (T_e - 86^\circ\text{F}) \quad (4)$$

where  $T_e$  is the temperature, °F, at the entrance to the EHD contact. The three dimensionless parameters (given in the nomenclature) express shear rate effects, thermal heating effects, and pressure viscosity effects, respectively. Graphs and computer subroutines for the traction coefficient,  $f$ , are given in reference, [5] and are not repeated in this paper.

It should be noted that this representation of experimentally obtained traction data is extrapolated for both high and low sliding velocities to make the data useful over a wide range for the analysis of bearing systems. At small values of  $G_1$  all curves of,  $f$ , have a  $45^\circ$  slope. This corresponds to the fact that at small sliding speeds the frictional coefficient varies linearly with sliding speed.

$P_{oj}$  and  $P_{ij}$  are raceway normal forces transmitted to the roller by the external bearing load.  $F_{add}$  is a force resulting from contact between the roller and the guiding shoulders of the raceway.  $M_{rj}$  is a symbolic representation of all of the fluid resisting moments acting on the roller.  $F_{cj}$  is loading due to the cage. A loaded roller, Fig. 2, which drives the cage results in a positive value of  $F_{cj}$  as shown. An unloaded roller is driven by the cage as shown in Fig. 3. A retarding torque is always present as a result of rubbing coulomb friction between the roller and cage pocket.

#### Load Roller Equilibrium

Summation of forces in the horizontal and vertical directions, Fig. 2, for the loaded roller must equal zero for steady state translating equilibrium.

$$Q_{ij} + T_{ij} - Q_{oj} - T_{oj} - F_{cj} + F_{add} = 0 \quad (5)$$

$$P_{ij} + CF^* - \mu F_{cj} - P_{oj} = 0 \quad (6)$$

Summation of moments about the roller axis of rotation, Fig. 2, must equal zero for steady state rotary motion equilibrium: (The term  $F_{add}$  resulting from roller end contact with the guiding shoulder is described later by Eq. (36)).

$$T_{ij} \frac{d}{2} + T_{oj} \frac{d}{2} - \mu F_{cj} \frac{d}{2} - M_{rj} \neq 0 \approx I_{rj} \frac{\partial \omega_{rj}}{\partial t} \quad (7)$$

The equations of equilibrium for the unloaded roller are similar and can easily be derived from Fig. 3. (Also Ref. [2]).

## EHD Oil Film Thickness

The average oil film thickness in the Hertzian zone is computed according to the Dowson, et al.<sup>[1]</sup> isothermal theory for line contact and modified with the Cheng<sup>[6]</sup> thermal correction factor,  $\phi_T$ .<sup>[5]</sup> The film thickness is determined by the lubricant velocity,  $\eta_e$ , at the inlet.

$$h = \frac{1.6 G^{0.6} \bar{U}^{0.7} R \phi_T}{\bar{W}^{0.13}} \quad (8)$$

## Roller Load Distribution

The summation of all inner race loadings,  $P_{ij}$ , equals the applied external radial load,  $F_x$ . For simplicity, the solution will be given in a single degree of freedom, along X. Then:

$$F_x - \sum_{j=1}^2 P_{ij} \cos \phi_j \neq 0 = \epsilon LD \quad (9)$$

$$\text{where } \cos \phi_j = \frac{2 j \pi}{Z} \quad (10)$$

## Cage Equilibrium

Steady state rotation of the cage requires that the summation of all fluid film forces and roller to cage forces acting on the cage be in equilibrium. The sum of the moments of all of the fluid film forces acting on the cage surfaces and taken about the center of bearing rotation will be represented symbolically by  $M_c$  and will be considered to be a drag or retarding moment when expressed in the positive sense. An inner land riding cage will develop a driving torque in the land, which helps to drive the cage. An outer land riding cage develops a drag torque in the lands. An unloaded roller by definition has a negative cage force  $F_c$ , Fig. 3. A loaded roller has either a positive driving cage force,  $F_c$ , or a negative drag force, per Eq. (5) and Fig. 2.

$$\frac{E}{2} \sum_{j=1}^2 (F_{cj}) - M_c \neq 0 = I_c \frac{\partial \omega_c}{\partial t} \quad (11)$$

## Method of Solution

A flow chart of the method of solution is given in Fig. 4. The solution consists of six nested single degree of freedom iterative loops. Two convergence schemes are used. Load distribution solutions are solved using classical Newton-Raphson matrix inversion techniques<sup>[8]</sup> Roller speed and cage speed solutions use a modified time step solution because of the multiple valued traction function.

Equations (7) and (11) are written as inequalities where the right hand side is the product of the polar moment of inertia and the first time derivative of the rotational speed. The desired steady state solution will occur when the right hand side vanishes. The magnitude and sign of the right hand side is used to compute the increment of cage or roller speed. Roller inertias are small, and extremely small time steps would be required for solution. A modified time step in the form of cage or roller speed steps proportional to the right hand side (or moment unbalance) are used for the solution. Initial step size is determined by experience to minimize computer execution time. Changes in speed regimens (DN values) and change of lubricant usually requires an adjustment in step size.

## Determination of Loaded Rollers

The radial displacement,  $\delta\phi_j$ , at any location angle,  $\phi_j$ , is:

$$\delta\phi_j = X\cos\phi_j - \frac{Pd}{2} + x'_{\phi} \quad (12)$$

where  $x'_{\phi}$  is a constant deviation from a true circular profile. A plus value of  $x'_{\phi}$  means a radially outward deviation of the inner race or a radial inward deviation of the outer race at location  $\phi$ , or the algebraic sum of deviations of both races from a true circular profile. An elliptical out-of-round race or any race shape in general<sup>[9]</sup> can be described by specifying values of  $x'$  for every location angle,  $\phi_j$ .

A quantity,  $\delta_{TOTAL}$ , is defined as the total deflection requirement for an unloaded roller assuming that it is initially in dry line contact (no EHD film, no roller load, no bearing clearance) with both inner and outer races.

$$\delta_{TOTAL} = \delta_o - h_o - h_l - \delta_{ROT} + \delta_{CF} \quad (13)$$

where:  $\delta_o = \left( \frac{CF^*}{K_o} \right)^{9/10} \quad (14)$

$$K_o = 11.4 \times 10^6 \ell_o^{8/9} \quad (15)$$

$\delta_o$  is the elastic compression or approach of the roll center-line towards a distant point in the outer race using the Palmgren<sup>[8]</sup> approximation.

$h_o$  is the EHD film thickness at the outer race contact per Eq. (8).

$h_l$  is the EHD film thickness at the inner race contact per Eq. (8) with a load of  $P_{ij}/\ell_{ij} = 1.0$  lbs./inch.

$\delta_{ROT}$  is the increase in diameter of the unloaded roller caused by rotation,  $\omega_{rj}$ , about its own axis. (See Table 1).

$\delta_{CF}$  is the compression of a hollow roller as a ring due to the inertia force  $CF^*$ <sup>[10]</sup>.

$$\delta_{CF} = \frac{CF^* r^3}{EI} \left( \frac{0.4674}{2\pi} \right) \quad (16)$$

$r$  = the mean radius of the hollow roller (in.)

$I$  = area moment of Inertia of the ring section (in.<sup>4</sup>)

Determination of a loaded roller is then made by:

$$\left. \begin{array}{ll} \delta_{\phi_j} \leq \delta_{\text{TOTAL}} & P_{ij} = 0 \text{ UNLOADED} \\ \delta_{\phi_j} > \delta_{\text{TOTAL}} & P_{ij} > 0 \text{ LOADED} \end{array} \right\} \quad (17)$$

Eq. (17) states that if the total radial displacement,  $\delta_{\phi_j}$ , is greater than the radial displacement value,  $\delta_{\text{TOTAL}}$  of an unloaded roller; then the roller is loaded. If  $\delta_{\phi_j} > \delta_{\text{TOTAL}}$  then  $P_{ij}/\ell_{ij}$  must equal or exceed 1.0 lb/inch. This test is made at each roller location as shown by iteration loop 4, Fig. 4, for the radial load solution.

#### Solution of a Loaded Roller

The solution of a loaded roller according to Eq: (5), (6), and (7) is accomplished by means of two nested iterations #5-Inner Race Roll Load,  $P_{ij}$  and #6-Roll Speed,  $\omega_{rj}$ , as shown in Fig. 4.

The inner loop #6 to determine roll speed  $\omega_{rj}$  (by means of Eq. (7)) is solved using the modified time step technique described above. This solution requires a known value of the inner race load,  $P_{ij}$ .

The inner race loading,  $P_{ij}$ , of a loaded roller is determined by using Newton-Raphson iteration (loop 5 of Fig. 4) and assuming an initial value of  $P_{ij}$  and then calculating corrections to it. An initial value can be closely determined from the external radial load and using Stribeck's constant for the maximum roller load.

The cage to roller contact force  $F_{cj}$  is solved directly from Eq. (5) for a given value of  $\omega_{rj}$ . Roller speed is determined by iteratively solving Eq. (7) with a modified time step or incremental values of  $\omega_{rj}$ . The solution of Eq. (7) is very sensitive to small changes to torques about the roll axis.

The  $\mu F_{cj}$  term of Eq. (6) is neglected in the solution. The coulomb coefficient of friction  $\mu$  is usually less than 0.1. The traction coefficient in the EHD contact,  $f(T_e)$ , is always less than 0.1 and usually

less than .01. Thus the  $F_{cj}$  term is always less than 1% and usually less than 0.1% of  $P_{oj}$ .

The relationship of radial displacement,  $x$ , of the inner ring upon a loaded roller is:

$$\delta_{oj} + \delta_{ij} - h_{oj} - h_{ij} + \delta_{CFj} + \delta_{rj} - \delta_{rotj} - X \cos \phi_j + \frac{Pd}{2} - X' \neq 0 = \epsilon_j \quad (18)$$

Where  $\delta_{CFj}$  and  $\delta_{rj}$  refer to a hollow roller and are omitted from Eq. (18) when solving solid rollers.  $\delta_{rj}$  is the ring compression of a hollow roller per Timoshenko<sup>[11]</sup> as:

$$\delta_{rj} = \frac{C_{rj}}{l_{ij}} \cdot P_{ij} \quad (19)$$

$$C_{rj} = \frac{r^2}{tEe} \left\{ \frac{\pi}{4} - \frac{2}{\pi} \left( 1 - \frac{e^2}{r^2} \right) + 2 \frac{e}{R} \left[ \frac{2}{\pi} \left( 1 - \frac{e}{r} \right) - \frac{\pi}{8} \right] + \frac{\pi}{4} \frac{\alpha E e}{C} \right\} \quad (20)$$

Subsequent values of  $P_{ij}$  are then:

$$\left( P_{ij} \right)_{p+1} = \left( P_{ij} \right)_p - \left( \delta \epsilon_j / \delta P_{ij} \right)_p \quad (21)$$

Solution of Eq. (18) using corrected values of  $P_{ij}$  from Eq. (21) is rapid and no convergence difficulties have been encountered.

The load carried by each loaded roller is determined by the Radial load solution loop No. 4 of Fig. 4. Eq. (9) is solved by Newton-Raphson iteration using the radial displacement,  $x$  of Eq. (18) as the variable. An initial value of  $x$  is computed using an assumption for the value of  $P_{ij}$ , Eqs. (6, 15, and 16), assuming pure rolling (no slip) for

the maximum loaded roller speed, and cage speed. Subsequent values of  $x$  are:

$$(X)_{p+1} = (X)_p - \left\{ \frac{\partial \epsilon_{LD}}{\partial X} \right\}_p \quad (22)$$

Solution of Eq. (9) using the corrected values of  $x$  is rapid and no convergence difficulties have been encountered.

## FLUID MECHANICS MODEL

Flow models for the (usually) turbulent flow field are briefly discussed, and then applied to calculation of fluid drags acting on roller and cage surfaces. The influence of the mixed component lubricant-air fluid field is treated with respect to definition of wall shear stresses explicit in the calculation of fluid drags. Lastly, the consequences of the fluid drags acting on roller and cage surfaces are described in relation to their influence on bearing behavior.

At least one previous investigator, Poplawski<sup>[4]</sup>, has included the effects of fluid drags in an analytical model of roller bearing performance. This model lumped the effects of fluid drags into a "churning loss" and suggested the use of an effective air-oil density to improve the analytical description. The Poplawski<sup>[4]</sup> model demonstrated significantly better correlation with existing experimental data than did the original Harris<sup>[2]</sup> model. The present work examines in more detail the influence of fluid drag torques acting on individual surfaces, and accounts for the driving influence of such torques on certain cage and roller surfaces as well as the retarding influences of such torques. Both the energy dissipation and the convective heat transfer within the bearings are closely associated with the viscous fluid behavior of the lubricant. The techniques employed in this analysis use a combination of empirical and theoretical treatments to define these effects.

From the standpoint of the dynamic solution of the interacting rollers, races, and cage, the most important factor is calculation of the friction drags on the element surfaces. In general, this effect is described by an equation of the form:

$$T = \tau_w A r \quad (23)$$

where  $T$  is the drag torque acting over the element surface,  
 $A$  is the surface area,  
 $r$  is the reference radius from the center of rotation,  
 $\tau_w$  is the wall shear stress

The description of the wall shear stress is a function of the fluid properties, the motion of the surface with respect to the fluid body, and the proximity of other surfaces influenced by the same fluid. Regarding the last mentioned, close clearances between rotating members of the bearing have especially strong influences.

Fritz<sup>[12]</sup> has investigated the wall shear stress phenomenon in journal bearings with vortex turbulent flow. Examination of typical roller-cage clearance to roller radius ratios, and Reynolds and Taylor numbers representative of  $1 \times 10^6$  DN and higher bearing operation clearly place such fluid flows in the turbulent-vortex regime as defined by Fritz<sup>[12]</sup> and illustrated for a typical case in his Fig. 3. For surface finishes and bearing dimensions typical of  $1 \times 10^6$  DN and higher roller bearings, the flows representative of cage surfaces appears to be in the couette turbulence regime.

Wall shear stress for a surface rotating in a viscous fluid is defined by the relation<sup>[13]</sup>:

$$\tau_w = f(1/2 \rho U^2) \quad (24)$$

where  $U$  = mass average velocity of fluid

$\rho$  = fluid density

$f$  = friction factor

For this correlation,  $U = \frac{r\omega}{2}$

The applicable friction factors from Fritz<sup>[12]</sup>, and curve fitted for computer analysis<sup>1</sup> are:

$$f/f_L = 1.3 \left( \frac{N_{Ta}}{41} \right)^{0.539474} \quad (25)$$

for the vortex-turbulent correlation and

$$f/f_L = 3.0 \left( \frac{N_{Re}}{2500} \right)^{0.85596} \quad (26)$$

for the couette turbulent correlation.

Here,

$$N_{Re} = \frac{r\omega C}{v} \quad \text{is the Reynolds number} \quad (27)$$

$$N_{Ta} = \frac{r\omega C}{v} \sqrt{\frac{C}{r}} \quad \text{is the Taylor number} \quad (28)$$

and

$$f_L = \frac{16}{N_{Re}} \quad \text{is the laminar friction factor} \quad (29)$$

Should calculation yield a Reynolds number less than 2500, or a Taylor number less than 41, a circumstance virtually impossible in high speed roller bearings, the appropriate friction factor then can be taken as the laminar friction factor  $f_L$ .

In addition to the fluid drag acting on the cylindrical surfaces, the roller ends or cage sides provide an additional source of drag. Per Refs. [13] and [14] for a rotating disk wetted on both sides, the total moment resulting from fluid drag about the disk centerline is given by:

$$M_T = \frac{1}{2} \rho \omega^2 r^5 C_n \quad (30)$$

$$\text{where } C_n = \begin{cases} 3.97/(N_{Re})^{1/2} & \text{for laminar flow, } N_{Re} < 300,000 \\ 0.196/(N_{Re})^{1/5} & \text{for turbulent flow, } N_{Re} > 300,000 \end{cases} \quad (31)$$

$$\text{where here } N_{Re} = \left[ \frac{r^2 \omega}{v} \right] \quad (32)$$

For hollow rollers and for the cage, account must be taken of the areas pertinent to the calculations by modifying the radius factor of the disk equation to the form:

$$r^5 = r_{out}^3 (r_{out}^2 - r_{in}^2) \quad (33)$$

where

$r_{out}$  is the outer radius

$r_{in}$  is the inside radius

This is at least true to a good approximation in the case of the roller, since examination of the integral from which a closed form solution of (30) is derived shows that approximately 75% of the total moment contribution comes from the area defined by the outer 50% of the roller radius. In the case of the cage, the "disk" torque acting on the cage side surfaces is less justifiable on theoretical grounds, but the calculated effect has been shown to be small with respect to the cylindrical surface contribution in this instance.

Basic to the above calculations is the realization that high-speed roller bearings never are completely flooded with lubricant, and seldom are more than 15 to 20% full of oil within the bearing for very high speed operation. Indeed, an excess of oil within the bearing has been conclusively shown by Boness to produce adverse effects on bearing operation<sup>[3]</sup>. Motion of the many moving parts within the bearing, in particular the pumping action of the rollers, will tend to induce an air oil mixture within the bearing. Illicitly, it can be argued that for pure viscosity effects in a turbulent regime, this phenomenon will have little tendency to change the fluid behavior from that of a flooded bearing, since in general such effects are confined to relatively thin boundary layers adjacent to the surfaces. Further, the turbulent mechanisms of momentum and energy transfer depends on physical displacement of fluid particles. However, the density or inertia effects of the air oil

mixture can be drastically influenced by comparison to that of a flooded bearing. Hence, it becomes necessary to modify the density of the fluid mixture, choosing a volumetric basis for the calculation:

$$\begin{aligned}\rho_{av} &= (\rho_{oil} \times \text{oil volume} + \rho_{air} \times \text{air volume}) / \text{Total Volume} \\ &= \rho_{oil} \times \frac{\text{oil volume}}{\text{Total volume}}, \text{ defined as } \rho_{oil} \times \text{DECFUL} = \text{DENS}\end{aligned}\quad (34)$$

The apparent density of the fluid is taken as this in roller drag calculations. Recognizing that the land regions and the cage surface on the close clearance land side will be somewhat restrictive to free flow of oil out such regions, the oil density in this region is taken as:

$$\rho_{HIGH} = \frac{\rho_{oil} \times \text{DECFUL}}{0.4 + 0.6 \text{ DECFUL}} \quad (35)$$

The fluid density in other regions is taken as:

$$\rho_{LOW} = \frac{\rho_{oil} \times \text{DECFUL}^2}{0.4 + 0.6 \text{ DECFUL}} \quad (36)$$

These relations derive from flow continuity considerations, assuming 40% of the total flow will be on average confined within the higher density region. While admittedly arbitrary, these assumptions have led to excellent correlation with existing empirical data.

#### Roller Fluid Drag Torque

Consider the drag torque acting on the cylindrical roller surface, as computed from equations (23) through (29),  $T_{rcyl}$ . In this case, careful consideration must be given to the calculation of the characteristic radial clearance required in the calculation. From the close clearance region between the rollers and the cage, and the interrace cage geometry, it is possible to define a characteristic clearance between

the rollers and the surrounding elements. Figure 5 illustrates the geometry. This clearance is defined by:

$$C = C_{CH} = \frac{1}{2\pi} \int_{\text{Circumference}} C(\theta) d\theta \quad (37)$$

Five distinct zones must be considered in the calculation on each semi-cylindrical half of the roller. Rollers are assumed to be in contact with either the leading cage pocket surface (driving roller) or the lagging cage pocket surface (driven roller). Generally, rollers carrying load are driving rollers and unloaded rollers are always cage-driven. Comparing the two roller surfaces, therefore, the only zone not symmetric with respect to the radial ray through the roller center is Zone III, where the entire diametral pocket clearance is taken as 10% of the roller radius. Calculation of the clearance is then straightforward, given dimensions of the cage, rollers, and races.

Similarly, the drag torque acting on the roller ends,  $T_{\text{rend}}$ , is computed directed from Equations (30) through (33). For all roller calculations, the appropriate density is computed from Equation (34).

While not totally fluid mechanical in origin, the sensitive nature of the roller equilibrium solution requires consideration of the influence of the contact between the roller and the guiding shoulders of the cage in the torque equilibrium solution. Computer results show this effect to contribute generally 5 to 10% of total roller drag moment. Further, for a roller guided on the outer race shoulder, this moment can either drive or retard the roller, depending on the distribution of relative local velocities between roller and shoulder. The calculation requires the assumption of a coulomb coefficient of friction between the roller and shoulders, generally taken as 0.05 to 0.08 for a well lubricated contact. While strictly an integral over the contact area, the moment can be closely approximated by dividing the contact area into a number of horizontal and vertical strips or lamina as shown in Figure 6 for a

roller guided on the outer race. A similar situation exists for a roller guided on the inner race, but the appropriate relative kinematics must be used. Further, for the inner race guided roller, the local race speed always exceeds the local roller speed, and hence always produces a net driving torque on the roller. The moment contribution,  $T_{add}$ , of the contact to the roller moment is then given by

$$T_{add} = \mu_c \frac{F_{jG}}{A_G} \left\{ \sum_{i=1}^N \frac{|V_{Ri} - V_{Hji}|}{(V_{Ri} - V_{Hji})} A_{Hji} r_{Hji} - 2 \sum_{k=1}^{S/2} A_{Vjk} r_{Vjk} \right\} \quad (38)$$

The second term always produces a retarding moment, while the sign of the first term, at least for an outer race guided roller, is dependent on the velocity distribution over the contact region.

The resultant vertical force is self-equilibrating, since the velocity distribution is asymmetric with respect to the radial ray through the roller center. However, the horizontal resultant can be either positive or negative, and contributes to the contact force between the roller and the cage, as evidenced in Equation (5). This resultant force is given by

$$F_{add} = \frac{\mu_c F_{jG}}{A_G} \sum_{i=1}^N \frac{|V_{Ri} - V_{Hji}|}{(V_{Ri} - V_{Hji})} A_{Hji} \quad (39)$$

Note that these quantities are functions of velocity, and must be determined at each roller iteration. Since  $F_{jG}$  is constant in any given problem, the derivatives of  $F_{add}$  and  $T_{add}$  are not involved in any of the Newton-Raphson iterations.

The contact force between the roller ends and the guiding race shoulder,  $F_{jG}$ , acts in the direction of the roller axis. Such a force can arise from a variety of sources. Among these are differential pressure acting across the bearing, cage angular misalignments, roller skewing due to gyroscopic moments, and unbalances in the various rotating members which give rise to dynamic forces between the roller and the guiding shoulder.

In this formulation of the problem, the contact force was assumed to arise from differential pressure resulting from crossflow of lubricant through and out the bearing. This axial crossflow was assumed to be superimposed on the swirling turbulent flow pattern existing in the annular spaces between the rollers, cage, and races. In traversing the distance across the bearing, the resistance to flow in the roller axis direction, and hence the differential pressure across the bearing, will depend not only on the axial flow, but also on the flow in the tangential direction. We assume the same turbulent flow mechanism to be operating in both the axial and tangential directions. This leads, after some manipulation, to a differential pressure relation

$$\delta_p = \frac{f_p \ell_p E \omega_c L \bar{V}}{16 A_x} \quad (40)$$

where

$\ell_p$  is the peripheral length of a typical crossflow passage

$E$  is the bearing pitch diameter

$\bar{V}$  is a "length of peripheral surface averaged" circumferential velocity

$\omega_c$  is the cage angular speed

$L$  is the bearing length

$A_x$  is the area of a typical crossflow passage

Calculation of the friction factor uses the Blasius relation<sup>[13]</sup>

$$f = 0.3164 / (4 \sqrt{N_{Re}}) \quad (41)$$

where here

$$N_{Re} = \frac{4 \bar{V} A_x}{\ell_p \nu} \quad (42)$$

It is assumed that this differential pressure acts uniformly on the cage side and the roller disk area exposed to the crossflow. Defining this area as  $A_p$ , finally,

$$F_{jG} = \delta p A_p \quad (43)$$

which is the force appropriate to Equations (38) and (39).

The total fluid drag moment,  $M_{rj}$  acting on the roller in Equation (7) is then calculated as:

$$M_{rj} = T_{rcyl} + T_{rend} \pm T_{add} \quad (44)$$

Note, while the first two terms are always positive in this formulation, the algebraic sign of  $T_{add}$  is determined by the relative velocity distribution, as discussed above.

#### Cage Fluid Drag Torque

The fluid drag torque acting on the cage is composed of the fluid torques acting on the inner and outer cage surfaces, the cage sides, and the cage land surface. Its influence in the equilibrium solution for the cage is indicated in Equation (11) by the quantity  $M_c$ .

Calculation of the four component drag torques proceeds directly from Equations (23) through (29) for the inner and outer cage surfaces and for lands, and from Equations (30) through (33) for the cage sides. The appropriate radii and clearances for these calculations are the local cage surface radii and clearances between adjacent surfaces. Fluid densities in the various regions are computed from Equation (35) and (36). Dimensional changes with speed and thermal effects resulting from dissipation are insignificant in these calculations, except in the case of close land clearances.

The total drag moment acting on the cage is then computed from

$$M_c = T_{cout} - T_{cin} + T_{cside} \pm T_{cland} \quad (45)$$

Note that since the total drag moment positive sense is in the direction of retarding cage motion, the outer surface and side torque terms are always positive. The inner surface drag torque always acts to increase cage speed and is hence always negative. The sign of the land surface torque is positive for an outer land riding cage and negative for an inner land riding cage.

### Influence of Fluid Drag Torques on Solution

Figure 7 compares the predictions of three analytical models with samples of previously published test data of roller bearing cage slip as a function of applied radial load. The present model demonstrates almost exact correlation with this data across the load range for which data is available. Close correlation is shown by the Poplawski<sup>[4]</sup> model, which uses a simplified fluid drag correlation. The Harris<sup>[2]</sup> model matches closely the trend of the test data, but differs significantly in the magnitude of slip predicted across the load range. In addition to the correlation shown for an outer land riding cage, the present model has also accurately predicted the experimentally measured<sup>\*</sup> cage slip of an inner land riding cage bearing.

Power dissipations predicted by the model closely match available rig data.<sup>\*\*</sup> Shaft horsepower dissipation is computed by summing all torques acting on the inner race. The prediction and distribution of these dissipative losses is essential for accurate determination of thermal gradients and operating temperatures. Predictions for two conventional roller bearings analyzed for comparison are summarized below. Operation was approximately  $2.0 \times 10^6$  DN.

<u>Bearing</u>	<u>Experimental Power Dissipation, Hp</u>	<u>Computer Power Dissipation, Hp</u>
130 MM Bore	5.80	6.94
115 MM Bore	4.25	3.89

\* Data courtesy of Boeing Co., Vertol Division, Philadelphia, Pa.

\*\* Data courtesy of Midwest Aero Industries, Div. Pure Carbon Co., St. Marys, Pa.

Both bearings were operated at near synchronous condition. This calculation is extremely sensitive to the amount of lubricant within the bearing, estimated at between 10 to 15% by volume by the test agency. The 100 MM bearing was analyzed for 15% oil-to-air ratio within the bearing, and the 115 MM bearing was analyzed for a 10% oil-to-air ratio. It will be noted that the results bracket the experimental data, being high for the higher oil/air ratio and low for the lower oil/air ratio. A repeat of this analysis taking both bearings at about a 13% oil/air ratio would yield results matching the experimental data.

The foregoing illustrates generally the sensitivity of the solution to fluid drag influences. As further illustration, consider Figure 8 which compares two cage error curves as functions of cage speed for all other conditions the same. For this relatively low speed application, a difference of 10% in oil/air ratio produced a 2% difference in cage slip.

The shape of the cage error curve, of Figure 8, provides a possible further insight into the bi-stable operation of bearings noted by some investigators. Dr. Ehrich [15] noted this phenomenon, and hypothesized its origin as systematic changes in bearing clearances coupled with dynamic phenomenon of shaft rotation. The cage error vs speed curve always has the same characteristic shape, for which three solutions are possible when slip occurs. One root is always close to synchronous, where the steep slope of the error-speed curve requires successive predictions at small slip values to obtain a solutions. Other solutions are possible if the error curve changes sign at less than synchronous speed (two possible additional solutions), or if the error curve is tangent to the abscissa of one point. Since the magnitudes of the errors are strong functions of speed and load, and to a lesser extent of oil/air ratio, it is possible that for some combination of these variables the bearing operation may oscillate between two closely spaced roots. This might occur as thermally induced dimensional changes in internal diametral and close land clearances change the operating

conditions of the bearing. Such operation has been demonstrated using the present model with thermal and dynamic effects considered. One computer run found about 3% slip on the first iteration (without thermal gradients), but sought the synchronous solution when the results of thermal gradients resulting from the first iteration were reflected in the second. While not conclusive at this time, this subject bears extensive further investigation, with comparison to actual test data as it becomes available.

## DIMENSIONAL MODEL

The model accounts for changes which occur during bearing operation as a result of dynamic (centrifugal effects) and thermal deformations. The effects considered to be most significant are:

- Changes in bearing internal diametral clearance (IDC) with dynamic and thermal deformations and with shrink fit between the inner race and the shaft.
- Changes in bearing internal diametral clearance (IDC) due to changes in roller (especially hollow rollers) diameter with dynamic and thermal growth.
- Changes in close clearance guiding cage/race lands with thermal and dynamic deformations, and for an inner land riding cage, changes in the clearance with shrink fit between shaft and inner race.

The use of simple closed form expressions to predict the dynamic and thermal dimensional changes occurring in bearing members is desirable, since this greatly simplifies the system analysis. Predictions of such deformations, on the other hand, must be more than order of magnitude accurate to realistically describe the influence of such operation dependent variables on bearing performance. In the process of model selection, estimates of deformations from available closed form solutions were compared to the results of more sophisticated analyses, using finite element computer solutions of typical bearing element geometries.

### Dynamic Deformations

The dynamic deformation models selected for the races, rollers, and cage are given in Table 1 and are obtained from standard theory of elasticity sources. [16 and 17] Comparison of finite element solutions for a 0.50 "diameter hollow roller with a 0.25" diameter hole showed closest agreement with the generalized plane strain solution. At roller speeds of 150,000 RPM and higher, a  $\pm 4\%$  bulging and contraction of the outer surface near the roller edges was calculated in the finite element solution. This cannot be predicted by any of the closed form solutions, however, since it is common practice to crown rollers, this variation is

not considered significant. For a solid roller, little comparative difference was noted for any of the closed form deformation relations, and hence a plane stress relation was used for simplicity.

Both the inner and outer surface deformations of the inner race, are significant. The deformation of the inner surface contributes to change in the shrink fit between the race and the shaft, and deformation of the outer surface influences both the bearing IDC and the land clearance of an inner land riding cage. The closed form dynamic deformation relation best describing the behavior of both race surfaces was found to be the plane strain relation. These relations generally predict deformation within 5% of the finite element results even at extreme speed, providing race undercuts or other irregularities such as guiding shoulders are small.

The shaft outer surface deformation is also significant in that it contributes to change in shrink fit. While not checked against a finite element model, the shaft conforms to the basic assumptions of the plane strain relation.

The deformations of the cage land surfaces are significant in the determination of clearances required in the calculation of cage land fluid viscous drag. Agreement of closed form predictions with the results of finite element modeling were within 15 to 20% for this deformation for all closed form solutions. However, the calculation of the fluid viscous drag has been determined to be insensitive to this variation, changing only about 2% at maximum speed. This larger deviation is the result of the inability of the closed form solutions to account for the difference in cage surface and land diameters or to account for bending deformations resulting from the additional mass of the land protrusions. Over the relatively narrow land width, the land surface deformation is fortunately quite uniform, as predicted by finite element analysis. The closed form solution best matching the finite element results, within the limitations discussed, was the plane stress formation.

Shrink fit ( $\Delta$ ) between the inner race and shaft acts to decrease the bearing internal diametral clearance (IDC), as compared to

the IDC of an unmounted assembled bearing. Also, for an inner land riding cage bearing, the shrink fit decreases the close land clearance. An extensive treatment of this subject is contained in references [18].

### Thermal Deformations

The model used for calculations [16] of thermal deformations assumes an axisymmetric temperature distribution, uniform end deformations and cylindrical geometry. The radial deformation of the  $i^{\text{th}}$  bearing surface, having inner radius,  $r_I$ , and outer radius,  $r_o$ , is given by:

$$\delta T_i = \frac{2\alpha r_i}{(r_o^2 - r_I^2)} \int_{r_I}^{r_o} T_r dr = \frac{2\alpha r_i}{(r_o^2 - r_I^2)} \left\{ (T_{\text{out}} - T_{\text{ref}}) \left[ \frac{r_o^2}{2} - \frac{(r_o^2 - r_I^2)}{4 \ln \left( \frac{r_o}{r_I} \right)} \right] + (T_{\text{in}} - T_{\text{ref}}) \left[ \frac{(r_o^2 - r_I^2)}{4 \ln \left( \frac{r_o}{r_I} \right)} - \frac{r_I^2}{2} \right] \right\} \quad (46)$$

The above relations are known to be quite accurate within the governing assumptions. No attempt has been made to date to confirm in detail their accuracy for this application. Comparison of thermal growth predictions to the limited empirical data available to the authors shows reasonable agreement of the magnitude of these deformations.

When applying the above to prediction of the thermal growth of the outer race, it must be noted that no radial constraint is included in the formulation. This is typical of the test environment of roller bearings where loading is accomplished through an external yoke, but growth of the outer race is otherwise unconstrained. Other application

of this type of analysis must consider any radial constraint appropriate to the application, particularly because of the possibility of bearing thermal lock-up.

From the above, it follows that when the surface temperatures of all bearing elements are known, the thermal deformations of the bearing members are completely defined.

## THERMAL ANALYSIS

### Problem Formulation

The temperature field within the bearing must be known in order to compute thermal deformations. With the basic assumption of axisymmetric temperature distribution, the techniques of performing such an analysis are well known. Harris [19] has applied heat transfer techniques to the determination of bearing temperature distributions. The technique presented here will basically follow this presentation, with additional emphasis on the calculation and distribution of power dissipation within the bearing, and on calculation of convective conductances or heat transfer coefficients appropriate to the calculation.

All three modes of heat transfer, conduction, convection, and radiation can operate between bearing members and between the bearing and its environment. Conduction is a linear phenomenon. Convection is basically non-linear in that the convective conductance is strongly velocity and temperature dependent. However, in the iterative solution technique used, Fig. 4, velocity is fixed at each step of the iteration. Temperature dependence is mainly reflected in fluid property changes. Since the iterative scheme employs the updated temperatures from the previous temperature iteration solution in the convective conductance calculations for the current temperature solution, the convective mode formulation is linear at each temperature iteration. Radiation heat transfer depends on differences of fourth powers of surface temperatures, and is hence always non-linear. The forms of the conductive, convective,

and radiation heat transfer equations respectively are:

$$H_{\text{cond}_{ij}} = \begin{cases} \frac{2\pi k l}{\ln\left(\frac{r_o}{r_i}\right)} \Delta T_{ij}; & \text{hollow cylindrical body of length } l_s, \text{ in radial direction} \\ k A_T \frac{\Delta T_{ij}}{\Delta L}; & \text{axial direction, through area } A_T \text{ over distance } \Delta L \end{cases} \quad (47)$$

$$H_{\text{conv}_{ij}} = h_k A_{s_k} \Delta T_{ij} \quad (48)$$

$$H_{\text{rad}_{ij}} = \frac{\sigma \left[ (T_i + 460)^4 - (T_j + 460)^4 \right]}{\frac{(1-\epsilon_m)}{\epsilon_m A_{s_m}} + \frac{1}{\bar{F}_{m,n} A_{s_m}} + \frac{(1-\epsilon_n)}{\epsilon_n A_{s_n}}} \quad (49)$$

where

$\sigma$  = Boltzmann radiation constant

$\epsilon_m$  and  $\epsilon_n$  are the emissivities associated with the  $m^{\text{th}}$  and  $n^{\text{th}}$  surfaces, respectively.

$\bar{F}_{m,n}$  = view factor of  $n^{\text{th}}$  surface seen from  $m^{\text{th}}$  surface

These equations are basic, and are derived in any standard heat transfer text, such as reference [20].

The radiation mode of heat transfer becomes significant only for temperature differences of the order of 100°F and higher. For normal bearing operation, such conditions do not exist within the bearing. However, heat transfer by this mode can be significant between the bearing and its environment, and must be included.

Formulation of the heat transfer problem requires discretizing the bearing elements into a set of nodes, and writing a Kirchhoff energy balance at each node. The power dissipation occurring within the bearing

acts as the driving potential, and must be computed and distributed among the nodes. Fig. 9 defines the nodal pattern used in this analysis. In this model, provisions are made for coolant flow through the outer race and through the shaft, and for lubricant to be flowing both through the bearing and under the inner race. Any of these flows except the flow through the bearing may be set to zero. The coolant through the outer race, and the lubricant flows under the race and through the bearing are assumed to mix external to the bearing, and to wash the inner surface of the chamber, the shaft, and the exterior of the bearing. The environment external to the bearing assumes the assembly to be enclosed in a test chamber, and to be loaded through an external yoke extending through the chamber. The governing equations are then of the form, for nodes  $i = 1$  to 21,

$$\sum_{j=1}^{21} H_{ij} + \sum_{k=1}^{N_i} Q_k = \epsilon_i \quad (50)$$

Here  $H_{ij}$  is the energy transfer between nodes  $i$  and  $j$ , and the  $Q_k$  are the dissipations, external energy inputs, energy transfer to coolant or lubricant flows, or losses from a typical node  $i$ .  $N_i$  is the total number of  $Q_k$  at node  $i$ . Table 2 illustrates the flow of energy between all nodes, and defines the  $Q_k$  quantities at each node. The explicit forms of the equations defined generally by (50) are derivable directly from Table 2. Note that all energy fluxes other than losses are assumed to enter each node. The temperature differences of equations (47), (48) and (49) may thus be uniformly taken at  $(T_j - T_i)$  at each node  $i$ .

The energy balances of equations (50) are equated to the error functions  $\epsilon_i$ , where  $\epsilon_i$  approaches zero for the steady state equilibrium set of temperatures. At each temperature iteration, Fig. 4, in the bearing solution, this non-linear set of equations is solved by Newton-Raphson iteration techniques. As an initial guess of the temperature field to start the iterative process, setting all temperatures equal to the previous

value of bearing oil temperature,  $T_{11}$ , has been found to produce rapid convergence. To implement the Newton-Raphson solution scheme, the set of equations (50), with the  $H_{ij}$  quantities expressed in terms of equations (47), (48), and (49) must be rewritten in the form

$$\sum_{j=1}^{21} \left( A_{ij} T_j + A_{ij}^* T_j^4 \right) + \sum_{k=1}^{N'_i} Q_k + \sum_{k=1}^{(N_i - N'_i)} B_k = c_i \quad (51)$$

Here the  $A_{ij}$  are thermal admittances for terms originating from convection and conduction, and  $A_{ij}^*$  are thermal admittances for terms originating from radiation.  $N'_i$  is the total number of quantities,  $Q_k$  at node  $i$  not explicitly containing temperature, and  $B_k$  are constants originating from such sources as products of lubricant mass flow rates, specific heats, and inlet temperatures. The non-linear set of equations (51) for  $i = 1$  to 21 is then directly solvable for the temperature field using the Newton-Raphson solution technique.

### Power Dissipation

As previously stated, the driving potentials which result in thermal deformations are the power dissipations occurring within the bearing. These arise from fluid boundary layer and coulomb friction phenomenon. The distribution of the component dissipations is shown in Table 2. The total power expended within the bearing must appear at the shaft surface, since this is the driven member, and is easily calculated as the sum of all roller to inner race tractions and the sum of the fluid drags acting on the inner race and shaft surfaces (including land torques for an inner land riding cage). Shaft power loss is an important design factor and one that until now could only be estimated empirically based upon test experience.

Power dissipations at specific nodes, shown in Table 2, are also easily calculated. Roller to race contact dissipation is the product of the EHD traction and the sliding velocity in the contact. Fluid drag

moments are described by the fluid mechanics model.

External energy input such as energy dissipations by slave bearings supporting the shaft in test apparatus, other supporting bearings in an engine, energy input from turbine gasses, etc., must be calculated separately and introduced as heat sources or sinks at the appropriate nodes of Table 2.

### Heat Transfer Coefficients

Correct values of the heat transfer coefficients, or more properly the convective conductances, used in the thermal analysis are essential to obtaining a representative solution. While standard techniques of determining these quantities can be used for non-rotating surfaces, the shaft, cage, and roller surfaces pose a special problem. Bjorklund<sup>[21]</sup> has investigated the problem for the case of concentric rotating cylinders. The techniques and correlations of this source will be used here.

For two concentric rotating cylinders, with the annular space between them containing a viscous fluid, the critical Taylor number for both is given by

$$N_{Ta_{cr_n}} = \left[ \frac{48.7 \left( 2 + \frac{C}{r_5} \right)}{(1-\eta) \left[ 1 - \eta \left( 1 + \frac{C}{r_5} \right) \right] \left[ 0.0571 \left( \frac{1+\eta}{1-\eta} - 0.625 \frac{C}{r_5} \right) + \frac{.00056}{\frac{1+\eta}{1-\eta} - 0.625 \frac{C}{r_5}} \right]} \right] \quad (52)$$

where

$$\eta = \frac{\omega}{\Omega} \quad \text{Speed ratio} \quad (53)$$

C = radial clearance between inner race and inner cage surfaces or between inner race surface and cage land surface for an inner land riding cage.

The Taylor number for this condition is given by

$$N_{Ta} = \sqrt{\frac{C}{R}} (R\omega_c/\beta) \quad (54)$$

where

$\beta$  = kinematic viscosity of fluid

$R$  = radius of inner rotating member

$\omega = \begin{cases} \Omega & \text{for inner race to cage condition,} \\ \omega_c & \text{for outer race to cage condition} \end{cases}$

The Nusselt number for pure conductance through the fluid is given by

$$N_{Nu_{cond}} = \left(\frac{C}{R}\right) / \ln \left(1 + \frac{C}{R}\right) \quad (55)$$

and the ratio of the local Nusselt number to the conduction Nusselt number is given by

$$\frac{N_{N_i}}{N_{Nu_{cond}}} = 1.1 \left[ \frac{N_{Ta} - \left( N_{Ta_{cr\eta}} - N_{Ta_{cr\eta=0}} \right) \left( 1 - 3.5 \frac{C}{r_5} \right)}{41.1 + \left( N_{Ta_{cr\eta}} - N_{Ta_{cr\eta=0}} \right) \left( 3.5 \frac{C}{r_5} \right)} \right]^{1/2} \quad (56)$$

Finally, the convective conductance is given by

$$h = \frac{k_f}{C} N_{Nu} \quad (57)$$

where  $k_f$  = thermal conductivity of the fluid.

For the inner cylinder rotating only,

$$\frac{N_{Nu}}{N_{Nu_{cond}}} = 0.175 N_{Ta}^{1/2} \quad (58)$$

applies as an alternate to equation (53).

Here the appropriate  $C$  is the radial clearance between the outer race and cage outer surface or cage lands for an outer land riding cage. Equations (52) through (58) can be used directly to obtain the appropriate coefficients for the race and cage cylindrical surfaces. Over the vertical cage surfaces, an average of the coefficients of the bounding cylindrical surfaces is recommended. These relations also define the coefficient values on the roller surfaces, using equation (58) and the average roller clearance defined by equation (37). In all of the above calculations, the fluid density used for the calculation of the kinematic viscosity should be computed as discussed in equations (34-36). The variation of fluid properties with temperature must also be considered, updating the fluid properties at each step of the iterative solution.

Coefficients for the outer bearing surfaces and the chamber inner and outer surfaces are computed from a correlation suggested by Jakob<sup>[22]</sup> for natural convection of fluids in contact with horizontal cylinders

$$h = 0.525 \frac{k_f}{D_r} \left( \frac{D_r^3 \gamma g \Delta t}{\beta^2} \cdot \frac{\beta}{\alpha_d} \right)^{0.25} \quad (59)$$

where

$D_r$  = diameter of cylinder

$\gamma$  = coefficient of volumetric expansion

$g$  = gravitational acceleration

$\alpha_d$  = thermal diffusivity

$\Delta t$  = absolute value of temperature difference between surface and bulk fluid temperature

For condition inside the chamber, the fluid properties appropriate to the calculation are those of the lubricant, since the bearing outer surface, the shaft, and the inner chamber wall are assumed to be washed with the mixed oil. The temperature difference should be taken between

the surface temperature in question and the mixed lubricant temperature, which is computed from

$$T_{ave} = \frac{\dot{m}_6 c_{p6} T_6 + \dot{m}_{11} c_{p11} T_{11} + \dot{m}_{16} c_{p16} T_{16}}{(\dot{m}_6 c_{p6} + \dot{m}_{11} c_{p11} + \dot{m}_{16} c_{p16})} \quad (60)$$

where

$\dot{m}_i$  is the mass flow rate of the  $i^{th}$  lubricant

$c_{pi}$  is the specific heat of the  $i^{th}$  lubricant at Temperature  $T_i$

For the outer chamber surface, the appropriate fluid properties are those of air, and the temperature difference is taken between the chamber wall and the external ambient. For external circulation of air over the chamber, forced convection relations must be used, for which standard formulations can be obtained from Kays [23].

The shaft surface coefficients can be obtained from equations (52) through (58), using equation (58) rather than equation (56), if care is taken to use mass averaged fluid properties. The resulting prediction will be higher than the actual coefficient value. The clearance required here is the difference between shaft and chamber radii. This result should be checked against the prediction of equation (59), which provides a lower bound on the coefficient value, and engineering judgement used to choose the proper value of the coefficient.

The heat transfer coefficient for the external surface of the loading yoke depends on the geometry of the member. Generally, this can be treated as a fin heated at the root, and standard correlations applied, such as those of reference [20].

### Sample Thermal Analysis Results

The results of the thermal analysis of a conventional inner land riding roller bearing operating at  $2 \times 10^6$  DN are summarized in Table 3. The guiding shoulders for the rollers were on the outer race. Two cases

are compared, for conditions with and without under race cooling. This analysis was accomplished using specified operating values of IDC and land clearances, and hence the results are quite comparable for cage slips and power dissipations. The original conditions necessary to achieve the specified operating conditions were computed from the results of the thermal analysis and considering dynamic influences, and are summarized in Table 3 along with results pertinent to the thermal analysis.

The results shown in Table 3 are consistent, showing generally lower temperatures for the case with additional cooling, and a higher oil temperature rise for the reduced cooling case. Also, with under race cooling the temperature difference from the inner to the outer race is 13.7°F, as compared to a temperature difference of 34.7°F for the case of no under race cooling. These results are in general agreement with measured values for comparable bearing operating conditions.

#### DISCUSSION OF APPLICATION OF EXPERIMENTAL TRACTION DATA AND ROLLER KINEMATICS

Typical traction values for several roller bearings from 65mm bore to 140mm bore and for shaft speeds from  $1.0 \times 10^6$  DN through  $4.0 \times 10^6$  DN with MIL-L-7808 oil are presented in Table 4, for unloaded and the maximum loaded roller contacts. All tabulated values were computed with the full EHD, fluid mechanics, dimensional, and thermal models described in this paper.

A roller always rotates near a pure rolling condition (low sliding velocity) at the outer race contact of a roller bearing with inner race or shaft rotation. Sliding velocities from near zero to 3 in/sec are typical as shown in Tables 4a and 4b for outer-race contact.

An unloaded roller, Table 4a, rotates about its own axis at an angular speed slightly less than the angular speed required for pure rolling at the outer race contact. Positive sliding (outer race relative surface velocity is greater than the roller surface velocity) always occurs and is in the range of near zero to 3 in/sec. The rolling portion.

of the total traction value is significant and cannot be ignored. Indeed the rolling portion can even predominate as shown by the ratio of rolling traction to total traction in Table 4a.

A loaded roller which produces a cage driving force rotates about its own axis at an angular speed slightly greater than the angular speed required for pure rolling at the outer race contact. Negative sliding occurs and is in the range of near zero to -3 in/sec as shown in Table 4b. The maximum loaded roller and most of the loaded rollers in the bearing have negative sliding at the outer race. Occasionally a lightly loaded roller or rollers near the entry and exit from the radial load zone will have positive sliding at the outer race contact. Such rollers result in a net drag on the cage similar to completely unloaded rollers. In all cases the rolling portion of the total traction is significant and cannot be ignored.

A loaded roller always has positive sliding at the inner race contact. Typical values are shown in Table 4c. A bearing operating at essentially epicyclic cage speed (no cage slip) has very low values of sliding velocity ( $< 3$  in/sec) at the inner race contact and the rolling portion of the total traction is significant. A bearing operating with measureable cage slip can develop high values of positive sliding velocity at the inner race contact as shown in Table 4c. In these cases the sliding portion of the traction reaches a ceiling value and again the rolling portion of the total traction value is significant and cannot be ignored.

A high speed roller bearing with elastohydrodynamic oil films cannot operate under a pure rolling condition. An examination of the traction formulation of Eq. (3) shows that for zero sliding velocities the traction at both inner and outer races would be negative and no equilibrium solution can occur as shown in Fig. 2. Some cage slip (however small) must occur.

## RECOMMENDATIONS

1. Experimental data defining the rolling portion of the total traction force in an EHD contact is needed. The accuracy and usefulness of a complete systems analysis of a high speed roller bearing is very dependent upon good rolling friction data.

Archard and Crook<sup>[1]</sup> have stated that for loads which develop essentially parallel surfaces in the Hertzian contact and at speeds of sliding above a few centimeters per second, the sliding component of traction predominates and the rolling component can be ignored. This assumption has been generally accepted and has led to an emphasis upon obtaining twin disk traction data only for sliding conditions by current researchers.

Typical twin disk machines (with equal size disks) measure only the sliding contribution to the total traction in an EHD contact. Because of disk symmetry the data is also symmetric about zero sliding speeds, i.e., the traction value vanishes at zero sliding and reversal of the relative sliding direction reverses the direction of the traction. The rolling portion of the total traction is very small compared to maximum traction values. The instrumentation of existing traction machines is not designed to measure small magnitudes of rolling traction, indeed the contribution of rolling traction is calibrated-out along with disk support bearing friction. Symmetry of test machine geometry leads to symmetry of results. Special attention to non-symmetrical bench rig design and instrumentation is required.

2. Cage dynamics need to be explored and better defined both experimentally and analytically. Bi-stable<sup>[15]</sup> operation is shown to be possible by the present analysis.

## ACKNOWLEDGEMENT

The authors express their thanks to The Franklin Institute Research Laboratories for sponsoring development of the computer program and preparation of this paper.

FIGURES

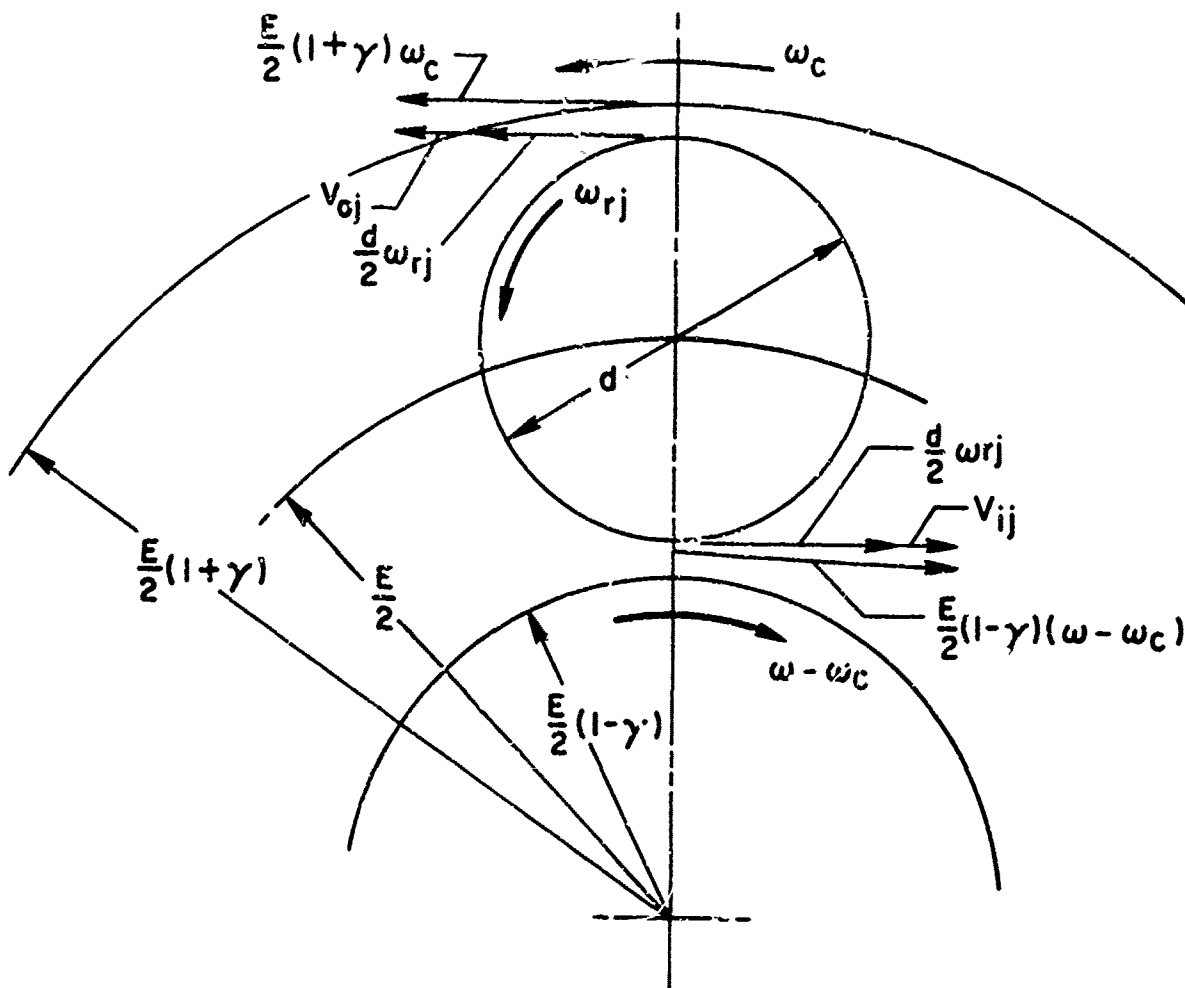


Figure 1. Surface Velocities and Relative Rotational Speeds of Raceways and Rollers Including Slip at Each Contact as a Result of Cage Slip

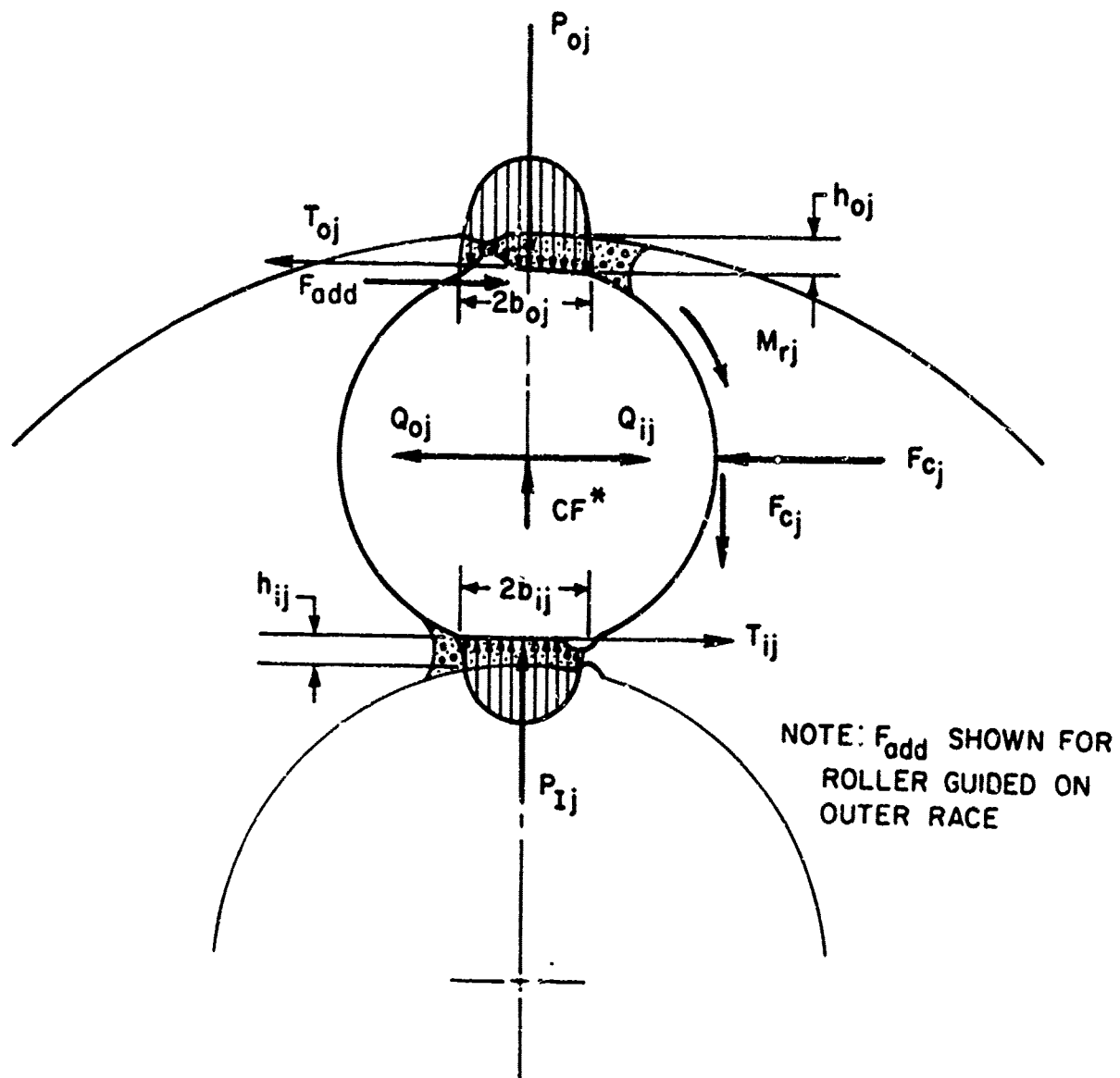


Figure 2. Forces and Moments Acting on a Loaded Roller

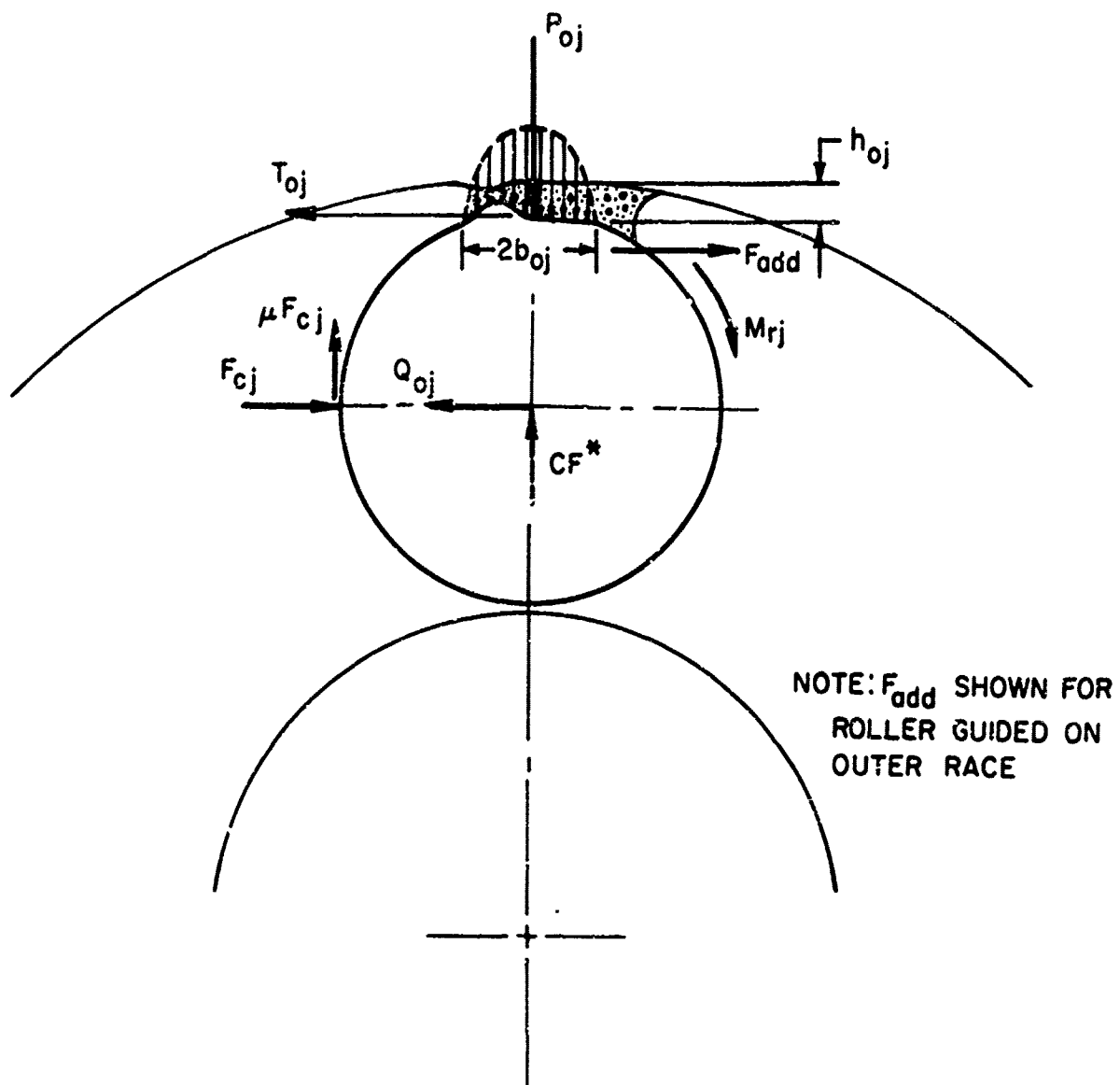


Figure 3. Forces and Moments Acting on an Unloaded Roller

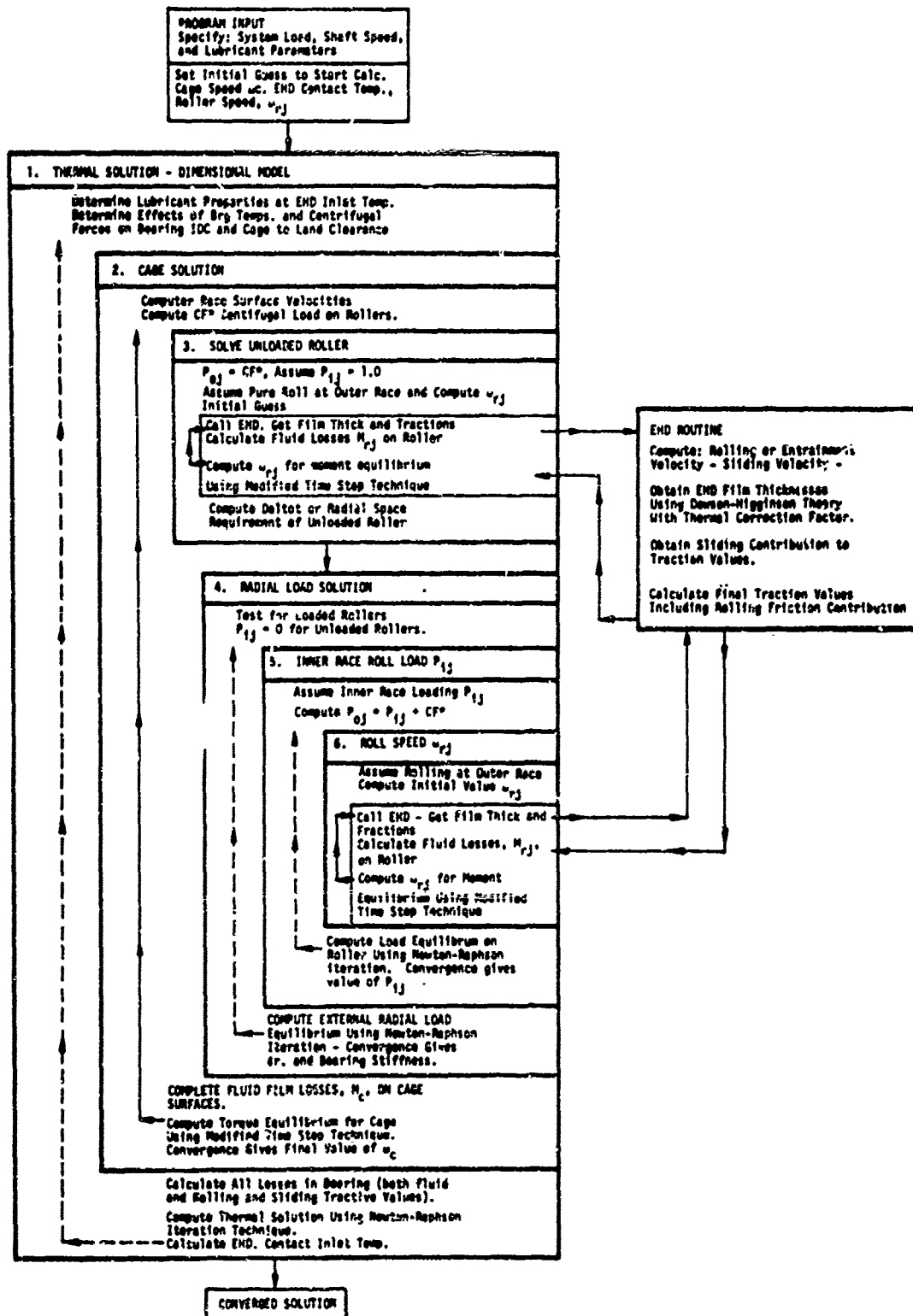


Figure 4. Solution Techniques Flow Chart

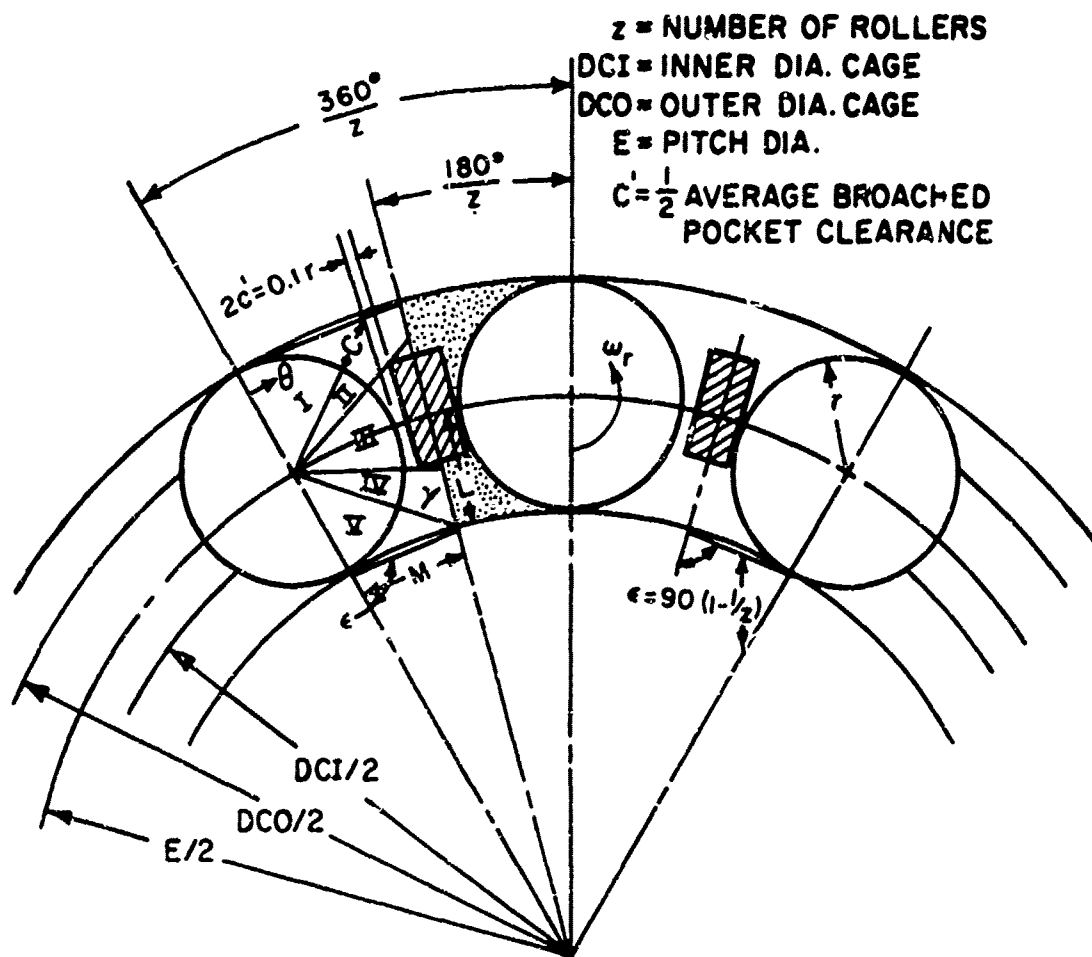


Figure 5. Roller Clearance Distribution in Cage

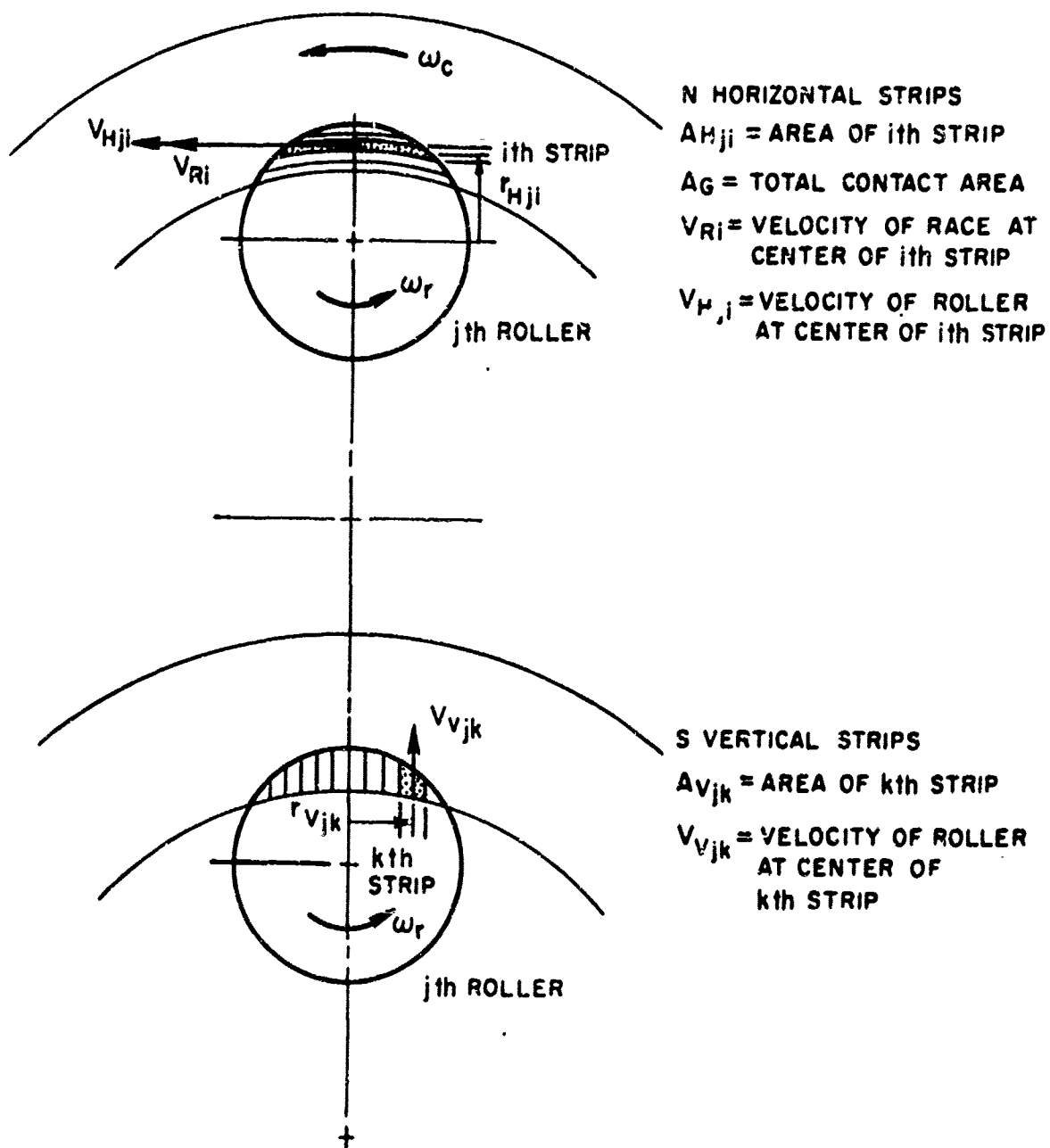
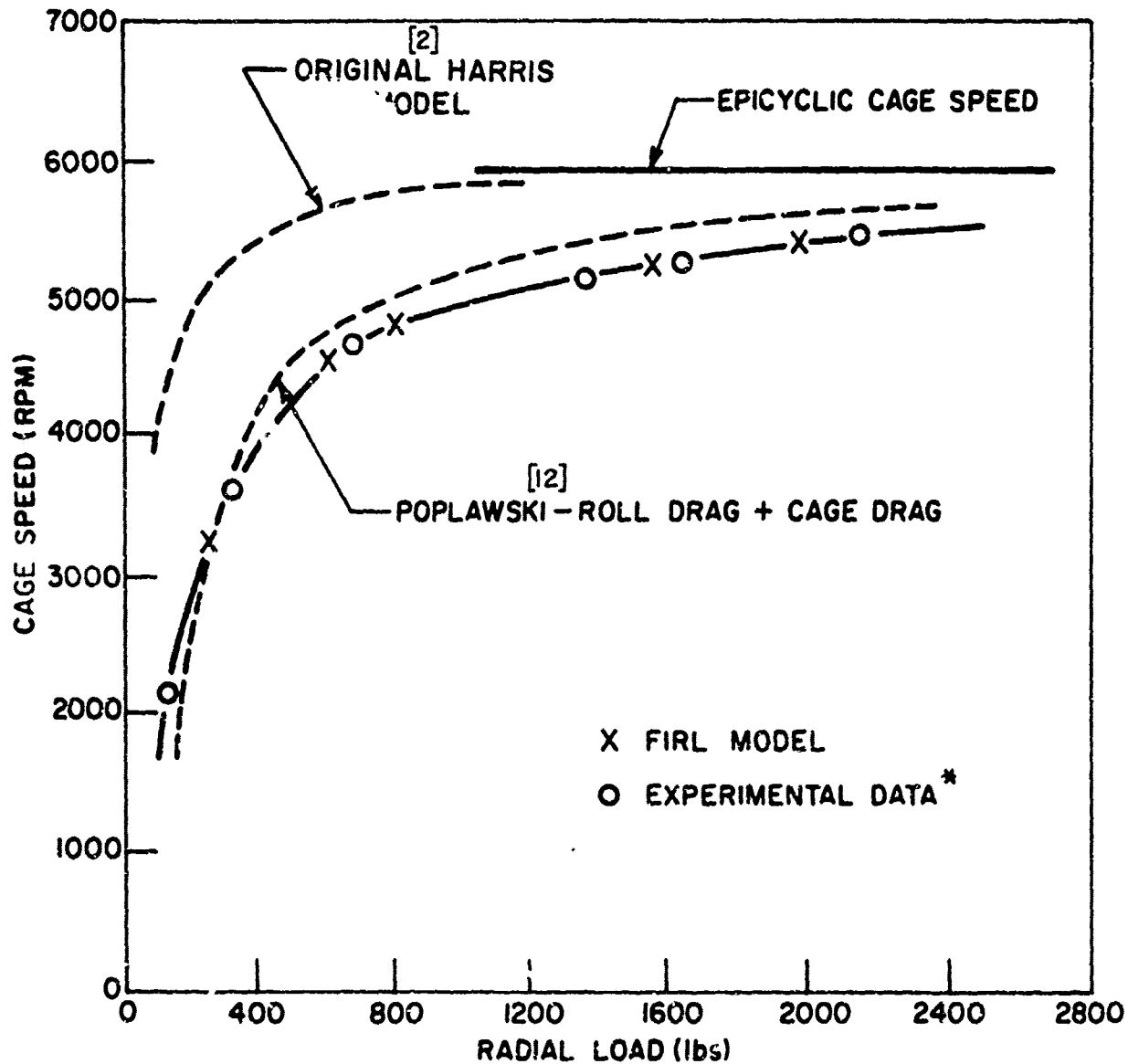


Figure 6. Mathematical Model of Horizontal and Vertical Relative Velocity Distributions in Roller-Shoulder Contact

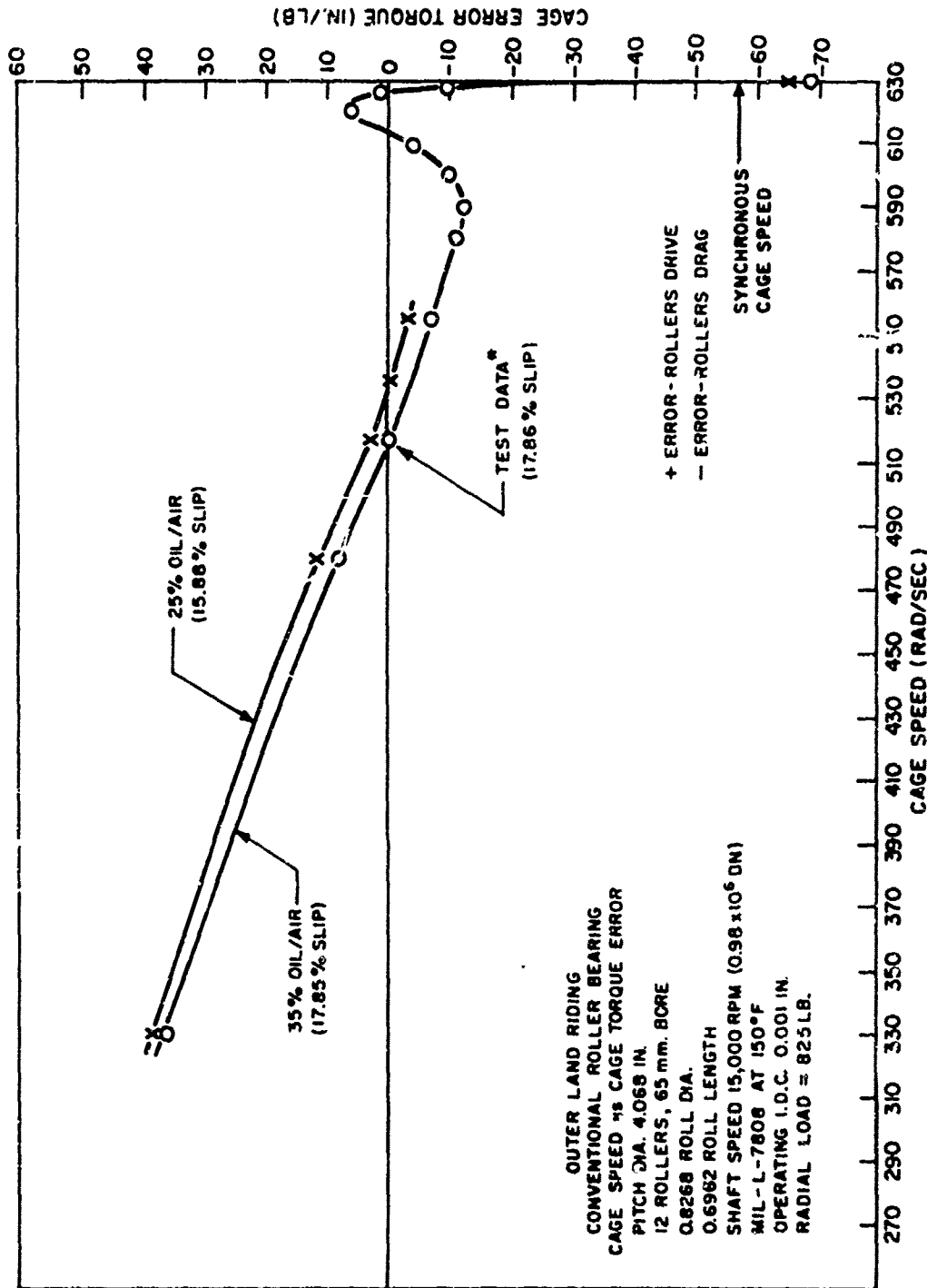
# ROLLER BEARING CAGE SPEED CORRELATION

MIL-L-7808D  
15,100 RPM  
.0010" MOUNTED INTERNAL CLEARANCE  
OUTER RACE RIDING CAGE



\*DATA - Courtesy of BOEING COMPANY  
VERTOL DIVISION  
PHILADELPHIA, PA.

Figure 7. Roller Bearing Cage Speed Correlation



\* COURTESY OF BOEING VERTOL DIVISION

Figure 8. Influence of Oil/Air ratio on Each Solution

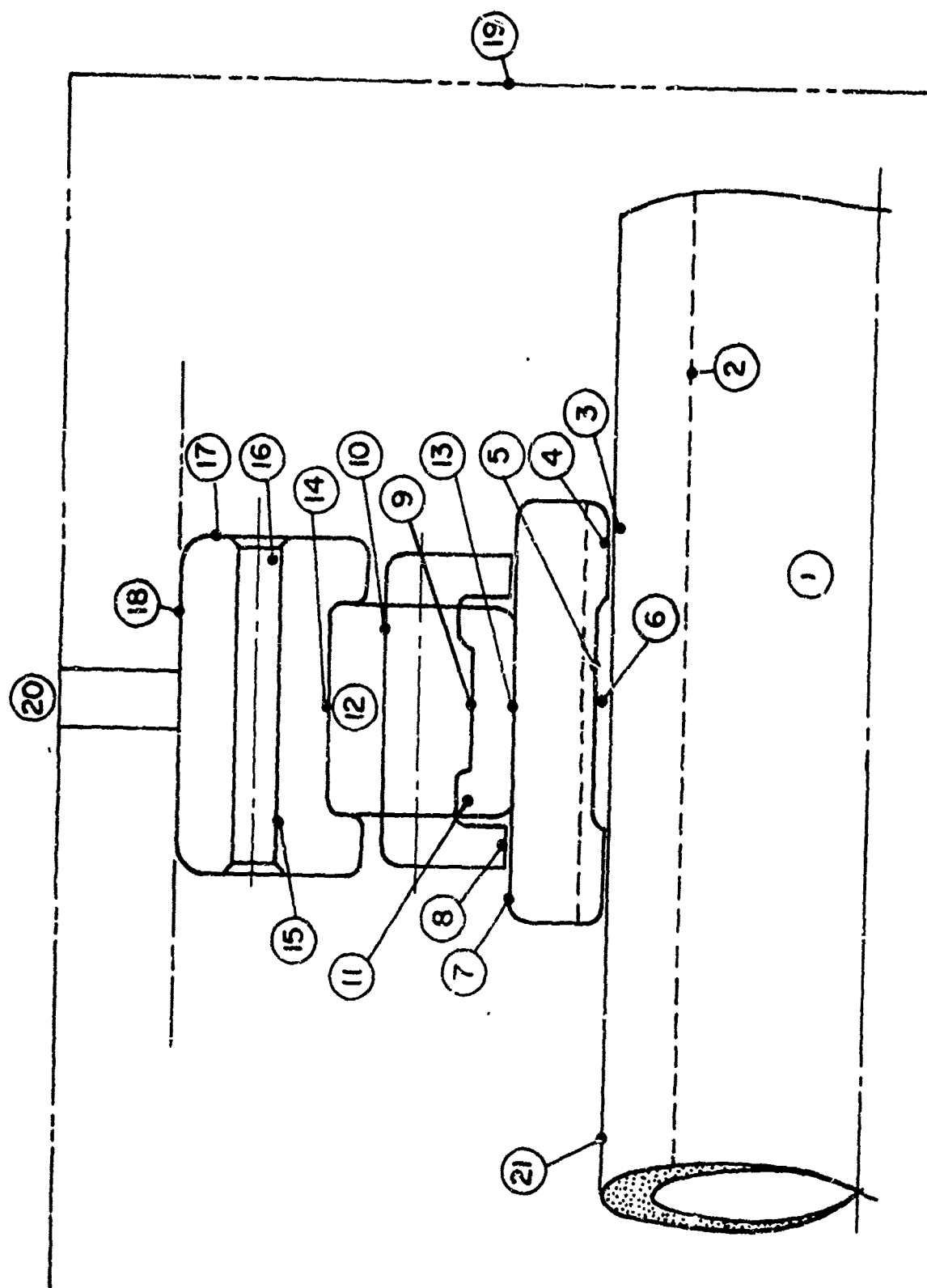


Figure 9. Nodes used in Thermal Analysis

TABLES

Table 1  
DIMENSIONAL MODELS  
DIAMETER GROWTH DUE TO CENTRIFUGAL EFFECTS

Location	Model	Formula
Hollow Roller Outer Surface	Generalized Plain Strain	$\delta_{rot} = \frac{\rho_r \omega_r^2 r_o (1+\sigma_r) (3-2\sigma_r)}{2 E_r (1-\sigma_r)} \left[ (1-\sigma_r) r_i^2 + \frac{(1-2\sigma_r)}{(3-2\sigma_r)} r_o^2 \right] + \frac{\rho_r \omega_r^2 r_o^2}{E_r} (r_i^2 + r_o^2)$
Solid Roller Outer Surface	Plane Stress	$\delta_{rot} = \frac{\rho_r \omega_r^2 r_o^2}{2 E_r} (1-\sigma_r)$
Inner Race & Hollow Shaft Outer Surface	Plane Strain	$\delta_{IR_o} = \frac{\rho_{IR} \omega_{IR}^2 r_o (1+\sigma_{IR}) (3-2\sigma_{IR})}{2 E_r (1-\sigma_{IR})} \left[ (1-\sigma_{IR}) r_i^2 + \frac{(1-2\sigma_{IR})}{(3-2\sigma_{IR})} r_o^2 \right]$
Inner Race Inner Surface	Plane Strain	$\delta_{IR_i} = \frac{\rho_{IR} \omega_{IR}^2 r_i (1+\sigma_{IR}) (3-2\sigma_{IR})}{2 E_r (1-\sigma_{IR})} \left[ \frac{(1-2\sigma_{IR})}{(3-2\sigma_{IR})} r_i^2 + (1-\sigma_{IR}) r_o^2 \right]$
Inner Land Riding Cage - Land Diameter	Plane Stress	$\delta_{CL} = \frac{\rho_{CL} \omega_{CL}^2 r_L (3+\sigma_{CL}) (1-\sigma_{CL})}{2 E_C} \left[ \frac{r_L^2}{(3+\sigma_{CL})} + \frac{r_o^2}{(1-\sigma_{CL})} \right]$
Outer Land Riding Cage - Land Diameter	Plane Stress	$\delta_{CL} = \frac{\rho_{CL} \omega_{CL}^2 r_L (3+\sigma_{CL}) (1-\sigma_{CL})}{2 E_C} \left[ \frac{r_i^2}{(1-\sigma_{CL})} + \frac{r_L^2}{(3+\sigma_{CL})} \right]$
<p><math>\rho</math>, mass density (lb-sec<sup>2</sup>/in.<sup>4</sup>)  <math>\Omega</math>, shaft angular velocity (rad/sec)  <math>\omega_{CL}</math>, cage angular velocity (rad/sec)  <math>\sigma</math>, Poisson's ratio</p>		<p><math>E</math>, Youngs Modulus, (lb/in.<sup>2</sup>)  <math>r_i</math>, innermost radius (in.)  <math>r_o</math>, outermost radius (in.)  <math>r_L</math>, cage land radius (in.)</p>

Table 2  
DESCRIPTION OF THERMAL ANALYSIS BY NODES

Node	Location and Description	Heat Transfer Path		Dissipative and External Energy Assignments	Remarks
		With Nodes	Type		
1	Inner Shaft Coolant	2,21	CV	$Q_1 = A_1 C_{p1} (T_{1H_1} - T_1)$	Coolant flow through hollow shaft.
2	Inner Shaft Surface	1 3,4(a),21(b)	CV C		a) for $\Delta \leq 0$ interference fit b) use average of $T_2$ & $T_3$
3	Outer Shaft Surface	4(a) 2,4(b),21(b)	CV C		c) for $\Delta > 0$ loose fit on shaft
4	Outer Edges of Underside of Inner Race (In Contact with Shaft)	5(c),6(d) 2(a),3(a),3,21(a)	CV C		d) use average of $T_4$ & $T_5$
5	Middle Section of Underside of Inner Race	6(a)(d),6 4,7,13	CV C		a) sides of undercut
6	Under Race Coolant	3,4(a),5,10,19, 21	CV	$Q_6 = A_6 C_{p6} (T_{1H_6} - T_6)$	Oil flow cooling under inner race.
7	Outer Edges of Top Side of Inner Race	11 5,13 8(f)	CV C R	$1/6 Q_{q15}$ -Cage-Inner Surface $1/3 Q_{c13}$ -Lands(f)	f) for inner land riding cage
8	Lands of Cage	11,11(h),11(i) 9 7(f),14(g)	CV C R	$1/3 Q_{q15}$ -Lands(f or g)	g) f. outer land riding cage h) use average of $T_8$ & $T_9$ inner side surface i) use average of $T_8$ & $T_9$ outer side surface
9	Inner Surface of Cage	11,11(h) 8,10 12,12	CV C R	$1/3 Q_{q15}$ -Cage-Inner Surface $1/2 Q_{COUL} \left( \frac{V_C}{V_C + V_R} \right)$	j) dissipation due to Coulomb friction between roller and cage pockets. $V_C$ = Cage Volume $V_R$ = Roller Volume (Total)
10	Outer Surface of Cage	11(i),11 9 12,12	CV C R	$1/2 Q_{COUL} \left( \frac{V_C}{V_C + V_R} \right)$ $1/2 Q_{q15}$ -Cage-Outer Surface	
11	Oil Within Bearing	7,8,9,10,12,13,14 8(a)(h),8(a)(i) 10,13,21	CV CV CV	$Q_{11} = A_{11} C_{p11} (T_{1H_{11}} - T_{11})$ $1/3 Q_{q15}$ -Cage-Inner Surface $1/3 Q_{q15}$ -Cage-Outer Surface $1/3 Q_{q15}$ -Lands $1/2 Q_{q15}$ -Rollers $1/3 Q_{SLIDE}$ -Inner Race $1/2 Q_{SLIDE}$ -Outer Race $Q_{q15}(h)$	Oil flow through bearing b) $Q_{q15}$ is internal fluid energy dissipation not attributable to particular surfaces and = Shaft Power - Sum of Surface Dissipations. $Q_{SLIDE}$ = $\mu$ D N Traction x Sliding Velocity
12	Rollers	11 3,10,13,14	CV R	$1/2 Q_{q15}$ -Rollers $Q_{COUL} \left( \frac{V_R}{V_C + V_R} \right)$ (j) $1/4 Q_{SLIDE}$ -Inner Race $1/4 Q_{SLIDE}$ -Outer Race	
13	Middle Section of Top Side of Inner Race (Roller Path)	11 5,7 9,12	CV C R	$1/4 Q_{SLIDE}$ -Inner Race $1/6 Q_{q15}$ -Cage-Inner Surface	
14	Inner Surface of Outer Race (Roller Path)	11 15 8(b),10,12	CV C R	$1/4 Q_{SLIDE}$ -Outer Race $1/3 Q_{q15}$ -Lands(b)	
15	Inner (Canted) Surface of Outer Race	16 14,17	CV C		
16	Outer Race Cooling Fluid	15,17,18,19,21	CV	$Q_{16} = A_{16} C_{p16} (T_{1H_{16}} - T_{16})$	Oil flow through outer race
17	Outer (Canted) Surface of Outer Race	16 15,18	CV C		
18	Outer Surface of Outer Race	6,11,16,21 17,19,20 19	CV C R		
19	Chamber Walls	6,11,16 18 18	CV C R	$Q_{EXT19}$ (i) $Q_{LOSS}$ -CVSH-Ambient Air	i) external energy input from other bearings, seals, etc.
20	Load Yoke Heat	18	C	$Q_{LOSS}$ -CV-Ambient Air.	
21	Outer Shaft Surface Remote From Bearing	1,6,11,16(h),18 2(a)(b),4(a)	CV C	$Q_{EXT21}$ (i)	a) assumes all cooling oil flows min at node 21 on way to common sump.

CV - Convection  
C - Conduction  
R - Radiation

Table 3  
TYPICAL THERMAL ANALYSIS

Bearing & Lubricant Data

Pitch diameter - 6.512 in.  
Roller diameter - 0.5 in.  
Operating IDC - .002 in.  
Operating radial land clearance - 0.015 in.  
Lubricant - MIL-L-7808D  
Lubricant flow rates - 6 lb/min through bearing (both runs)  
6 lb/min under race (2nd run only)  
Lubricant inlet temperature - 250°F  
Radial load - 333 lb  
Shaft speed - 14,280 rpm  
Oil/air ratio in bearing - 15%

Temperature Distribution (Ref. Fig. 9)

Node	Location	Temperature, °F	
		No Under-Race Cooling	Under Race Cooling
1	Inner shaft coolant	--	--
2	Inner shaft surface	361.5	295.8
3	Outer shaft surface at bearing	361.7	293.6
4	Inner race at shaft	361.8	310.7
5	Under-cut surface of inner race	362.5	314.6
6	Under race coolant	--	265.9
7	Inner race beyond roller contact	361.7	317.1
8	Cage at the land	380.8	370.3
9	Cage inner surface	393.1	383.1
10	Cage outer surface	392.9	383.0
11	Internal lubricant to bearing	330.7	318.3
12	Rollers	351.3	339.2
13	Inner race at rollers	367.5	324.8
14	Inner surface of outer race	329.9	307.2
15	Inner cooled surface outer race	329.9	307.1
16	Outer race lubricant	--	--
17	Outer cooled surface outer race	329.8	306.2
18	Bearing outer diameter	329.4	302.6
19	Chamber wall (inner side)	309.0	273.7
20	Loading bolt (strut) root	281.8	260.1
21	Shaft (external to bearing)	335.3	293.1
		No Under-Race Cooling	With Under-Race Cooling
Percent cage slip		32.5	33.7
Power dissipation, H <sub>p</sub>		7.09	7.15
Initial shrink fit, in.		0.0082	0.0088
Machined IDC, in.		0.0097	0.0089
Mounted IDC, in.		0.0024	0.0011
Machined diametral land clearance, in.		0.0037	0.0035
Mounted diameter land clearance, in.		0.0029	0.0027
Mixed lubricant temperature at sump, °F		330.7	292.3

Table 4  
TYPICAL EHD FILM THICKNESS AND TRACTION VALUES

4a  
OUTER RACE CONTACT OF UNLOADED ROLLERS

Sig. No.	S Cap Size	$V_{ej}$ in/min	$V_{ej}$ in/min	$V_{ej}$ in/min	$f(T_e)$	Sliding Portion		Rolling Portion		Traction $T_{ej}$ lb	Oil Film Thick- ness $h$ in	SMD Contact Temp $T_c$ °F	Roller					Ratio [Rolling] $T_{ej}$
						$\frac{ V_{ej} }{V_{ej}}$	$f(T_e)$	$\frac{ V_{ej} }{V_{ej}}$	$f(T_e)$				Size in	Ball Size in	Cage Rolling Load lb	Radial Load lb	Ratio [Rolling] $T_{ej}$	
1.5	10.0	1263	2.31	172.37	0.0098	1.968	-0.001	0.007	22.2	130	HEL-L-7000	65	0.0200	Outer	815	0.10		
1.20	0.007	1653	1.075	69.0	0.010	0.007	-0.265	0.232	19.7	250	HEL-L-7000	115	0.200	Inner	2075	1.15		
2.0	0.006	1332	2.123	34.71	0.016	0.267	-0.130	0.435		250	HEL-L-7000	140	0.250	Inner	215	7.20		
3.0	19.00	2023	2.623	66.0	0.0060	0.710	-0.323	0.430		250	HEL-L-7000	140	0.150	Inner	215	0.75		
4.0	0.0003	3113	1.000	130.07	0.0093	1.332	-0.112	1.120	6.7	250	HEL-L-7000	140	0.250	Inner	215	0.10		
0.2	20	2302	2.375	70.23	0.012	0.947	-0.172	0.720	5.4	250	HEL-L-7000	140	0.250	Inner	215	0.23		
0.0	0.006	3113	0.010	130.07	0.0070	0.947	-0.123	0.004	7.5	200	3048	150	0.250	Inner	215	0.10		

4b  
OUTER RACE CONTACT OF MAXIMUM LOADED ROLLER

Seq. No.	S Cap Size	$V_{ej}$ in/min	$V_{ej}$ in/min	$V_{ej}$ in/min	$f(T_e)$ in	Sliding Portion		Rolling Portion		Total Traction $T_{ej}$ lb	Oil Film Thick- ness $h$ in	SMD Islet Temp $T_c$ °F	Roller					Ratio [Rolling] $T_{ej}$
						$\frac{ V_{ej} }{V_{ej}}$ in/min	$f(T_e)$ in	$\frac{ V_{ej} }{V_{ej}}$ in/min	$f(T_e)$ in				Size in	Ball Size in	Cage Rolling Load lb	Radial Load lb		
1.0	10.0	1263	-2.10	274.0	0.0001	-0.000	-0.000	-0.002	-0.000	-0.002	10.7	150	HEL-L-7000	65	0.0200	Outer	815	0.13
1.20	0.027	1653	-0.08	552.0	0.010	-0.004	-0.264	-0.264	-0.264	-0.264	11.2	250	HEL-L-7000	115	0.200	Inner	2075	0.90
2.0	0.006	1330	-0.46	247.0	0.010	-0.262	-0.130	-0.071	0.7	250	HEL-L-7000	140	0.250	Inner	215	0.03		
3.0	10.00	2023	-1.725	100.1	0.0042	-0.701	-0.323	-1.103	13.0	250	HEL-L-7000	140	0.200	Inner	215	0.20		
4.0	0.0003	3113	-0.0003	715.1	0.0030	-0.770	-0.112	-2.040	7.7	250	HEL-L-7000	140	0.250	Inner	215	0.07		
0.0	20	2302	-0.0010	130.5	0.010	-0.001	-0.172	-0.172	0.9	250	HEL-L-7000	140	0.250	Inner	215	0.90		
0.0	0.006	3113	-0.0010	275.0	0.0030	-1.007	-0.223	-1.222	2.1	200	3048	150	0.225	Inner	215	0.13		

4c  
INNER RACE CONTACT OF MAXIMUM LOADED ROLLER

Sigsbee No.	S Cap Size	$V_{ej}$ in/min	$V_{ej}$ in/min	$V_{ej}$ in/min	$f(T_e)_{11}$	Sliding Portion		Rolling Portion		Total Traction $T_{11}$ lb	Oil Film Thick- ness $h$ in	SMD Islet Temp $T_c$ °F	Roller					Ratio [Rolling] $T_{11}$
						$\frac{ V_{ej} }{V_{ej}}$	$f(T_e)_{11}$	$\frac{ V_{ej} }{V_{ej}}$	$f(T_e)_{11}$				Size in	Ball Size in	Cage Rolling Load lb	Radial Load lb	Ratio [Rolling] $T_{11}$	
1.0	10.0	1263	654.5	307.2	0.0100	1.000	-0.007	7.170	12.0	150	HEL-L-7000	65	0.0200	Outer	815	0.10		
1.20	0.027	1653	7.720	652.2	0.0023	1.000	-0.265	0.002	11.2	250	HEL-L-7000	115	0.200	Inner	2075	0.90		
2.0	0.006	1332	43	215.2	0.010	0.000	-0.165	3.073	11.0	250	HEL-L-7000	140	0.20	Inner	215	0.04		
3.0	19.00	2003	3	99.0	0.0113	2.130	-0.300	1.723	13.0	250	HEL-L-7000	140	0.20	Inner	215	0.70		
4.0	0.0000	6130	0.004	570.0	1.0047	1.000	-0.260	4.732	9.9	250	HEL-L-7000	140	0.20	Inner	215	0.04		
0.0	20	4630	730	50.4	0.010	1.003	-0.174	2.700	11.4	250	HEL-L-7000	140	0.20	Inner	215	0.31		
0.0	0.0000	6130	0.02	100.0	0.010	2.732	-0.104	2.520	2.3	200	Polyphenyl Ether	150	0.20	Inner	215	0.20		

## NOMENCLATURE

### Load & Speed Equilibrium

- b           = semi-width of Hertzian contact - in.
- $C_r$        = hollow roller ring deflection constant - in/lb.
- $CF^*$       = centrifugal force acting on roller - lb.
- d           = roller diameter - in.
- E           = pitch diameter of bearing - in.
- $E_{YM}$      = Modulus of elasticity - lb./in<sup>2</sup>
- $E'$        = reduced Modulus =  $E_{ym}/(1-\sigma^2)$
- $f(T_e)$    = coefficient of traction at temperature  $T_e$
- Fddd       = contact force on roller from guiding race shoulder (lb.)
- $F_c$        = cage to roller force - lb.
- $F_x$        = radial external load - lb.
- G           = material parameter =  $\alpha E'$
- $G_1, G_2, G_3$  = parameters to determine  $f(T_e)$
- $G_1 = \frac{\eta_e V}{P_{hz} h}$    (Shear Rate Effects)
- $G_2 = \frac{\beta_1 \eta_e V^2}{8K_f}$    (Thermal heating effects)
- $G_3 = \alpha P_{hz}$    (Pressure viscosity effect)

$h$	= lubricant average film thickness - in.
$I_r$	= roller polar moment of inertia lb-in-sec <sup>2</sup>
$I_c$	= cage polar moment of inertia lb-in-sec <sup>2</sup>
$I$	= bending moment of inertia for hollow roller - in <sup>4</sup>
$K$	= roller to race deflection constant
$K_f$	= thermal conductivity of lubricant, BTU/o <sub>F</sub> -hr.-ft.
$\ell$	= effective length of roller contact - in.
$m_r$	= roller mass - lb-sec <sup>2</sup> /in.
$M_c$	= cage fluid drag moment - lb-in.
$M_r$	= roller fluid drag moment - lb-in.
$P$	= roller load - lb
$p$	= order of iteration
$P_{HZ}$	= maximum Hertz contact stress - lb./in <sup>2</sup>
$P_d$	= diametral clearance - in.
$Q$	= hydrodynamic pressure force - lb.
$\bar{Q}$	= dimensionless form of $Q = Q/(\ell E'R)$
$Q_m$	= dimensionless heating parameter = $2\eta_e U^2/(K_f T_e)$
$r$	= mean radius of hollow roller - in.
$R$	= radius of an equivalent cylinder and plane - in.
$t$	= thickness of hollow roller - in.
$T$	= traction in an EHD contact - lb.
$T_e$	= temperature of lubricant at entrance to EHD contact - °F
$U$	= fluid entrainment velocity - in./sec.
$\bar{U}$	= dimensionless form of $U = \eta_e V/(E'R)$

$V$	= sliding velocity - in./sec.
$\bar{V}$	= dimensionless form of $V = \eta_e V / (E'R)$
$\bar{W}$	= dimensionless load = $P / (2E'R)$
$X$	= radial displacement of inner race - in.
$X_\phi$	= deviation of races from true circular form - in.
$Z$	= total number of rollers
$\alpha$	= pressure viscosity exponent - in <sup>2</sup> /lb.
$\beta$	= temperature viscosity coefficient - °F
$\gamma$	= ratio of roller diameter to bearing pitch diameter
$\phi_j$	= angular location of roller, deg.
$\phi_T$	= thermal reduction factor for EHD film thickness
$\Omega$	= angular velocity of inner race, rad/sec.
$\omega_c$	= angular velocity of cage, rad/sec
$\omega_r$	= angular velocity of roller, rad/sec.
$\eta$	= lubricant absolute viscosity - lb.-sec/in. <sup>2</sup>
$\mu$	= coulomb coeff of sliding friction
$\delta_o$	= roller - outer race deflection - in.
$\delta_i$	= roller - inner race deflection - in.
$\delta_{CF}$	= hollow roller deflection from $CF^*$ - in.
$\delta_{ROT}$	= roller diametral expansion from $\omega_r$ - in.
$\delta_{TOTAL}$	= total deflection of an unloaded roller - in.
$\delta_{\phi_j}$	= relative movement of races at $\phi_j$ - in.
$\sigma$	= poisson's ratio

## SUBSCRIPTS

i	= inner race contact
o	= outer race contact
j	= roller number or location
u	= an unloaded roller
e	= entrance region of EHD contact

### Fluid Mechanics

A	Surface Area in. <sup>2</sup>
A <sub>G</sub>	Total contact area between roller and guiding shoulders in. <sup>2</sup>
A <sub>Hji</sub>	Area of i <sup>th</sup> horizontal lamina in. <sup>2</sup>
A <sub>P</sub>	Roller and cage surface area within typical crossflow passage exposed to crossflow in. <sup>2</sup>
A <sub>Vjk</sub>	Area of k <sup>th</sup> vertical lamina in. <sup>2</sup>
A <sub>x</sub>	Cross sectional area of a typical crossflow passage in. <sup>2</sup>
C	Radial clearance, in.
C'	Clearance of cage pocket and roller, in.
C <sub>N</sub>	Laminar or turbulent correlation factor for disk rotating in a viscous fluid
F <sub>jG</sub>	Contact force between roller and race guiding shoulder lb
f	Friction factor
f <sub>L</sub>	Laminar friction factor
L	Bearing length
l <sub>p</sub>	Peripheral length of a typical crossflow passage in.
M <sub>T</sub>	Moment about center line of a disk rotating in a viscous fluid in-lb.

$N$  Number of horizontal lamina  
 $N_{Re}$  Reynold's number (Defined in Text)  
 $N_{Ta}$  Taylor number (Defined in Text)  
 $r$  Reference radius in.  
 $r_{Hji}$  Distance from roller center to  $i^{th}$  horizontal lamina in.  
 $r_i$  Inner radius  
 $r_o$  Outer radius  
 $r_{Vjk}$  Distance from radial ray through roller center to  $k^{th}$  lamina in.  
 $S$  Number of vertical lamina  
 $\delta_p$  Crossflow differential pressure lb/in.<sup>2</sup>  
 $T$  Drag torque in.-lb  
 $T_{add}$  Moment contribution of contact force to roller drag moment in.-lb  
 $T_{cland}$  Fluid drag moment on cage lands in.-lb  
 $T_{cside}$  Fluid drag moment on cage sides in.-lb  
 $T_{rend}$  Moment contribution of roller ends to roller drag moment in.-lb  
 $T_{rcyl}$  Moment contribution of roller surface to roller drag moment in.-lb  
 $U$  Mass average velocity of fluid in./sec  
 $\bar{V}$  Peripheral crossflow surface average velocity in./sec  
 $V_{Hji}$  Velocity of roller at  $i^{th}$  horizontal lamina in./sec  
 $V_{Ri}$  Velocity of race at  $i^{th}$  horizontal lamina in./sec  
 $V_{Vjk}$  Velocity of roller at  $k^{th}$  vertical lamina in./sec  
 $\mu_c$  Coulomb coefficient of friction between roller and race guiding shoulder  
 $\nu$  Fluid Kinematic viscosity in.<sup>2</sup>/sec  
 $\rho$  Fluid mass density lb sec<sup>2</sup>/in.<sup>4</sup>  
 $\tau_w$  Wall shear stress, lb/in.<sup>2</sup>

## Thermal Analysis and Dimensional Model

$a$	roller inner radius, in.
$B_k$	energy rate constants in formulation of thermal problem, ref. equation (48), Btu/sec.
$b$	roller outer radius, in.
$C$	radial clearance between cylindrical surface - in.
$c_{p_i}$	specific heat of lubricant or coolant associated with $i^{\text{th}}$ thermal node - Btu/lb $^{\circ}$ F.
$\bar{F}_{m,n}$	Radiation view factor between $m^{\text{th}}$ and $n^{\text{th}}$ surface
$g$	gravitational acceleration, 386.4 in./sec $^2$
$H_{ij}$	energy transfer between nodes $i$ and $j$ Btu/sec
$h_k$	convective conductance associated with $k^{\text{th}}$ surface Btu/sec - in. $^2$ $^{\circ}$ F
IDC	bearing internal diametral clearance - in.
$k$	thermal conductivity - Btu/sec in. $^{\circ}$ F
$k_f$	thermal conductivity of fluid - Btu/sec in. $^{\circ}$ F
$l_s$	generic length of cylindrical surface - in.
$m_i$	lubricant or coolant flow rate of $i^{\text{th}}$ thermal node - lb/sec.
$N_i$	total number of component dissipations, external energy inputs, energy transfer to coolant or lubricant flows, and losses at $i^{\text{th}}$ thermal node.
$N'_i$	total subset of $N_i$ not explicitly containing temperature.
$N_{Ta_{\text{cond}}}$	Taylor Number for pure conduction through a fluid.
$N_{Ta_{cr_n}}$	critical Taylor number at speed ratio $n$ .
$r_L$	radius of inner race at land for an inner land riding cage or radius of outer race at land for an outer land riding cage - in.
$T_{\text{ave}}$	mixed lubricant temperature - $^{\circ}$ F

$T_i$	temperature of $i^{\text{th}}$ thermal node - °F.
$T_{\text{ref}}$	initial uniform reference temperature of all bearing elements - °F
$\alpha$	coefficient of thermal expansion - in./in. °F.
$\alpha_d$	thermal diffusivity - in. <sup>2</sup> /sec.
$\nu$	kinematic viscosity of fluid - in. <sup>2</sup> /sec.
$\gamma$	coefficient of volumetric expansion - 1/°F.
$\Delta T_{ij}$	Temperature difference between $i^{\text{th}}$ and $j^{\text{th}}$ thermal nodes, $T_j - T_i$ , - °F.
$\Delta t$	absolute temperature difference between surface and fluid.
$\delta_{T_i}$	thermal deformation of the $i^{\text{th}}$ surface of a bearing member, (see Figure 1) - in.
$\epsilon_i$	energy error function at $i^{\text{th}}$ temperature node for Newton-Raphson solution of temperature field in bearing - Btu/sec.
$\epsilon_m$	emissivity of $m^{\text{th}}$ surface.
$\mu$	coulomb coefficient of friction between rollers and cage.
$\eta$	ratio of cage to shaft angular velocities.
$\nu$	Poisson's ratio
$\sigma$	Boltzmann radiation constant - Btu/sec. in. <sup>2</sup> °R <sup>4</sup> .

12. Fritz, R. J., *Friction Factors for Use in Analysis of Journal Bearings with Vortex Turbulent Flow*, KAPL-M-6546, G. E. Knolls Atomic Power Laboratory, U. S. Atomic Energy Commission, Contract No. W-31-109 Eng-52.
13. Schlichting, Dr. H., *Boundary Layer Theory*, Fourth Edition, McGraw Hill Book Co., Inc., 1960.
14. Goldstein, S., *Modern Developments in Fluid Dynamics*, Vol. I and II, Dover Publications, Inc., 1965.
15. Ehrich, F. F., *Bistable Vibration of Rotors in Bearing Clearance*, presented at the winter annual meeting, ASME Machine Design Division, Chicago, Ill., Nov. 7-11, 1965.
16. Timoshenko and Goodier, "Theory of Elasticity," McGraw Hill Book Co. Inc., 1956.
17. Wang, "Applied Elasticity," McGraw Hill Book Co. Inc., 1953.
18. "New Departure Analysis of Stresses and Deflection," Vol. I, 1946. New Departure Division of G.M. Corp. Bristol, Conn.
19. Harris, T. A., "Rolling Bearing Analysis," John Wiley and Sons, Inc., 1966.
20. Eckert, E. R. G. and Drake, R. M., "Heat and Mass Transfer, Second Edition, McGraw Hill Book Co. Inc., 1959.
21. Bjorklund, I. S. and Kays, W. M., "Heat Transfer Between Concentric Rotating Cylinders," ASME Journal of Heat Transfer, Aug. 1959, Pages 175-186.
22. Jakob, M., Hawkins, G. A., "Elements of Heat Transfer and Insulation," John Wiley & Sons Inc., Second Edition, 1950.
23. Kays, W. M., "Corrective Heat and Mass Transfer," McGraw Hill Book Co. Inc., 1966.

## SECTION VIII

### REFERENCES

1. Rumberger, J. H., et.al., Gas Turbine Engine Mainshaft Roller Bearing - Systems Analysis", Submitted to Lubr. Div. ASME for publication in Trans. ASME, Jrnl. of Lubr. Tech. 1973.
2. Dowson, D. and Higginson, G. R., "Elastohydrodynamic Lubrication - The Fundamentals of Roller Gear Lubrication", Pergamon Press, New York, 1966.
3. Palmgren, A., "Ball and Roller Bearing Engineering", S. H. Borbank and Company, Third Edition, 1959.
4. McGrew, J. M., et. al., "Elastohydrodynamic Lubrication - Preliminary Design Manual", Technical Report AFAPL-TR-70-27, Air Force Aero Propulsion Laboratory, Air Force Systems Command, Wright Patterson Air Force Base, November 1970.
5. Nypan, L. J., et.al., "Optimal Speed Sharing Characteristics of a Series Hybrid Bearing", Trans. ASME, Jrnl. of Lub. Tech., Vol. 95, Series F, No. 1, January 1973, pp. 76-81.
6. Peacock, L. A., and Rhodes, W. L., "High Temperature Lubricant Screening Tests", SKF Industries, NASA CR 72615, September 1969, for NASA Lewis Research Center, Cleveland, Ohio.
7. Parker, R. J., Bamberger, E. N., and Zaretsky, E. V., "Bearing Torque and Fatigue Life Studies with Several Lubricants for Use in the Range 500° to 700°F", NASA Technical Note, TN-D-3948, May 1967.
8. Bamberger, E. N., Zaretsky, E. V., and Anderson, W. J., "Effect of Three Advanced Lubricants on High Temperature Bearing Life", ASME Jrnl. of Lub. Tech. Vol. 92, Series F, No. 1, January 1970, pp. 23-33.
9. Chasman, M. R., "Latest Available 5P4E High Pressure Viscometry Data", telephone conversation 10/1/71, Aero Propulsion Laboratory, WPAFB, Ohio.
10. Bamberger, E. N. - "Unpublished Information (1955) on reversed bending fatigue properties of Air Melt M-50 at 500°F" - Telephone Conversation - Nov. 1972.

## SECTION VIII (Cont'd)

### REFERENCES

11. *FIRL Computer Program, FEBOR, Finite Element Analysis Program for Bodies of Revolution Subjected to Axisymmetric Loading - Program No. 52-4.*